SYNTHESIS AND CHARACTERIZATION OF Fe (IRON), Co (COBALT), Ni (NICKEL) CONTAINING METAL ORGANIC FRAMEWORKS (MOFs)

by

Çağla GALIN

B.S., Chemistry, Boğaziçi University, 2019

Submitted to the Institute for Graduate Studies in

Science and Engineering in partial fulfillment of

the requirements for the degree of

Master of Science

Graduate Program in Chemistry

Boğaziçi University

2022

ACKNOWLEDGEMENTS

First of all, I would like to express my sincere gratitude my thesis supervisor Assoc. Prof. Oktay DEMİRCAN for giving me the opportunity to do research, for his encouragement, valuable advices, and the continuous support. His guidance helped me in all time of research and writing of this thesis.

I would like to thank my committee members; Prof. Amitav SANYAL and Prof. Emren NALBANT, for allocating their precious time and reviewing my thesis.

Also, I would like to thank my lab mates, Eslem, Hüseyin, Müşerref, and Furkan for their help and motivational support during my thesis study.

I am also grateful to Asu ZİYLAN YAVAŞ for her advices, helps and encouragement.

Finally, I would like to thank my family, my mother Gülay, my father Yahya, and especially my sisters Beyza and Umut Ela for their understanding, love, and endless support.

ABSTRACT

SYNTHESIS AND CHARACTERIZATION OF Fe (IRON), Co (COBALT), Ni (NICKEL) CONTAINING METAL ORGANIC FRAMEWORKS (MOFs)

In recent years, scientists and industries have been interested in metal organic frameworks (MOFs), a class of porous materials. Metal organic frameworks are formed by connecting metal clusters or ions with organic linkers. In addition to porous structures of MOFs, they have high surface areas, structural diversity, adjustable chemical functionality, high thermal stability, and easy synthesis. MOF can be used in many applications such as gas storage (e.g., hydrogen, methane, acetylene, and carbon dioxide), catalysts, and energy applications (e.g., batteries and supercapacitors). In this study, cheaper starting materials (metal salts of iron (Fe), cobalt (Co), and nickel (Ni)) based MOFs were synthesized via sonochemical synthesis method due to its fast, energy-efficient, and environment friendly method, and fumaric acid and terephthalic acid were used as organic linkers. The effects of temperature, pH, concentration, and solvent on MOF material were investigated. X-Ray Diffraction Analysis (XRD), Scanning Electron Microscope/Energy Dispersive X-Ray Analysis (SEM/EDX), and Infrared (IR) Spectroscopy, were used for characterization of synthesized compounds. In this thesis, the synthesis conditions for Fe (iron) with fumaric acid-based MOFs are optimized for the first time by using 1 mmol starting materials at 75 ºC and pH=natural (2.57) in 90 minutes sonication. Fe, Co, and Ni containing MOFs are synthesized for the first time by using terephthalic acid as organic linker and DMF as solvent, successfully by exploiting 90 minutes sonication. When pH of organic ligands solutions increased for faster deprotonation of organic ligands, iron oxide nanoparticles, cobalt (II) hydroxide and nickel (II) hydroxide were obtained instead of MOF structures.

ÖZET

Fe (DEMİR), Co (KOBALT), Ni (NİKEL) İÇEREN METAL ORGANİK KAFES YAPILARIN (MOFs) SENTEZİ VE KARAKTERİZASYONU

Son yıllarda, gözenekli malzemeler sınıfından olan metal organik kafes yapıları (Metal Organic Frameworks, MOFs) birçok bilim insanının ve endüstrinin dikkatini çekmektedir. Metal organik kafes yapılar, metal kümeleri veya iyonları ile organik bağlayıcıların birleştirilmesi sonucu oluşur. Gözenekli yapılarına ek olarak, MOF yapılar yüksek yüzey alanlarına, yapısal çeşitliliğe, ayarlanabilir kimyasal işlevselliğe, yüksek ısıl kararlılığa ve kolay sentezlenebilirlik gibi özelliklere sahiptirler. MOF yapılar, gaz depolama (örneğin hidrojen, metan, asetilen ve karbon dioksit), katalizörler ve enerji uygulamaları (örneğin piller ve süper kapasitörler) gibi birçok uygulamada kullanılabilir. Bu çalışmada, hızlı, enerji verimli ve çevre dostu bir yöntem olması nedeniyle sonokimyasal sentez yöntemi kullanılmıştır. Daha ucuz başlangıç malzemeleri olan demir (Fe), kobalt (Co), nikel (Ni) bazlı metal organik kafes yapılar sentezlemiş ve organik bağlayıcılar olarak fumarik asit ve tereftalik asit kullanılmıştır. Bu çalışmada sıcaklık, pH, konsantrasyon ve çözücünün MOF yapıları üzerindeki etkileri araştırıldı. Sentezlenen örneklerin karakterizasyonu için X-Işını Kırınım Analizi (XRD), Taramalı Elektron Mikroskobu/Enerji Dağılımlı X-Işını Analizi (SEM/EDX) ve Kızılötesi (IR) spektroskopisi yöntemleri kullanılmıştır. Bu tez çalışmasında, Fe (demir) ve fumarik asit içeren MOF yapıların sentez koşulları, ilk kez 1 mmol başlangıç maddeleri kullanılarak, 75 ºC'de ve doğal pH'de 90 dakika sonikasyon ile optimize edildi. Fe, Co, Ni içeren MOF yapılar, organik bağlayıcı olarak tereftalik asit ve çözücü olarak DMF kullanılarak ve 90 dakika sonikasyon ile ilk kez başarılı bir şekilde sentezlendi. Organik bağlayıcı çözeltilerinin pH'si arttırılınca, MOF yapılar yerine demir oksit nanoparçacıklar, kobalt (II) hidroksit ve nikel (II) hidroksit elde edildi.

TABLE OF CONTENTS

LIST OF FIGURES

LIST OF ACRONYMS/ABBREVIATIONS

1D	1-Dimensional
2D	2-Dimensional
3D	3-Dimensional
BDC	1,4-benzenedicarboxylate
BET	Brunauer-Emmett-Teller
bpy	2,2'-bipyridine
BTC	1,3,5-benzenetricarboxylate
DEE	Diethyl Ether
DEF	N,N-Diethylformamide
DEP	Diethyl Phthalate
DMA	N,N-Dimethylacetamide
DMF	N,N-Dimethylformamide
DMP	2,2-Dimethoxypropane
DMSO	Dimethyl sulfoxide
DOE	Department of Energy
DPE	Dipropylene Glycol Monoethyl Ether
DPP	Propylene Glycol Propyl Ether
DUT	Dresden University of Technology
EDCLs	Electrochemical Double-Layer Capacitors
EDX	Energy Dispersive X-Ray Analysis
EtOH	Ethanol

FA	Fumaric Acid
H_2BDC	Benzene-1,4-dicarboxylic acid
H_2BPB	1,4-bis(4-pyrazo-lyl)benzene
H_2BPDC	Biphenyl-4,4'-dicarboxylic acid
H_2O	Water
H_3BTC	1,3,5-benzenetricarboxylic acid
H_3BTE	4,4',4''-(benzene-1,3,5-triyltris(ethyne-2,1-diyl)tribenzoic acid)
H6BHB	3,3',3'',5,5',5''-benzene-1,3,5-triyl-hexabenzoic acid
HKUST	Hong Kong University of Science and Technology
IR	Infrared
IRMOF	IsoReticular Metal Organic Framework
IUPAC	International Union of Pure and Applied Chemistry
MeOH	Methanol
MIL	Material Institut Lavoisier
MOF	Metal Organic Framework
PET	Polyethylene terephthalate
pyz	Pyrazine
pzdc	Pyrazine-2,3-dicarboxylate
SEM	Scanning Electron Microscope
TEA	Triethanol amine
TPA	Terephthalic Acid
UiO	Universitetet i Oslo
UTSA	The University of Texas at San Antonio
w %	Weight Percent

XRD	X-Ray Diffraction Analysis
ZIF	Zeolitic Imidazolate Framework
λ	Wavelength

1. INTRODUCTION

1.1. Porous Materials and Metal Organic Frameworks (MOFs)

Porous materials can be defined as any material containing regions of empty space that other molecules can be selectively adsorbed or had chemical transformations into some other materials [1]. According to International Union of Pure and Applied Chemistry (IUPAC) are classified as micropores those of width less than 2 nm, as mesopores those ranging from 2 to 50 nm, and as macropores those wider than 50 nm [2]. Zeolites, one of the porous materials, have only inorganic molecules. On the contrary, activated carbons have only organic molecules. Also, metal organic frameworks have both inorganic and organic units. Porous materials are used in energy conversion and storage, gas separation and storage, catalysis, adsorption, and biochemistry [3-6].

Zeolites, porous hydrated aluminosilicates, has tetrahedral crystal structure that contains water and cations [7]. Figure 1.1 shows a 2D zeolite structure with extra-framework cations (Me^{n+}), and a chemical model of a zeolite structure. The name of zeolite that was invented by the Swedish mineralogist Alex F. Cronstedt (1722-1765) came from boiling stone [8]. When zeolite is heated, it releases water in its pores as water vapor. As zeolites can be occurred naturally, they can be made synthetically [9]. Zeolites can be classified according to their pore sizes and containing Si/Al ratio [10]. Since zeolites have ion exchange capacity, low cost and toxicity, biocompatibility, there are many application areas, zeolites used in, such as agriculture, food, water and wastewater treatment, protection of environment and ecology, civil engineering [10-15]. Figure 1.1 shows a 2D zeolite structure with extra-framework cations (Me^{n+}), and a chemical model of a zeolite structure.

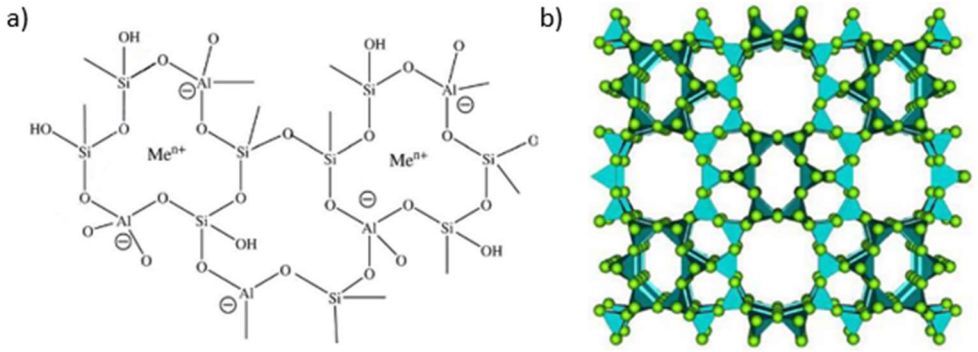

Figure 1.1. a) An image of 2D zeolite structure, and b) a model of zeolite structure [16].

Activated carbons, amorphous and porous carbon-based materials, have high surface area and porosity, good adsorption capacity and mechanical strength [17]. Figure 1.2. shows irregular pore structure of activated carbon and relation with various sized molecules. As activated carbons can be prepared from non-renewable materials, such as petroleum coke, lignite, and coal, agricultural wastes, such as oil palm fiber, coconut shell, orange peel, apple peel, rise husk, and among others can be used to produce activated carbons [18-20]. The nature of the raw material used, carbonization and activation processes affect the properties of activated carbons. Wastewater treatment, catalysis, gas adsorption, dye adsorption are some application areas of activated carbons [21-23].

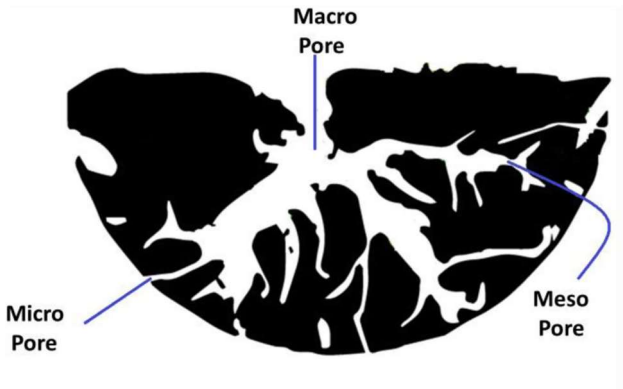

Figure 1.2. The presentation for irregular pore structure of activated carbon [24].

Metal organic frameworks (MOFs), hybrid porous materials, are formed by connecting metal clusters or ions with organic linkers (as seen in the Figure 1.3.). The starting point of metal organic frameworks is based on research made by Hoskins and Robson in 1989 [25-26]. The neutral porous network, $CoC_6H_3(COOH_{1/3})_3(NC_5H_5)2.2/3(NC_5H_5)$, which was synthesized by Yaghi and Li in 1995 [27]. Moreover, the term "metal organic framework" was used first time in this publication. 1,3,5-benzenetricarboxylate (BTC) and $Co(NO_3)_2$ were chosen as the building block and metal source, respectively. Since MOFs have ordered structure, high thermal stability, adjustable chemical functionality, high porosity, they can be used in various applications, such as energy storage, drug delivery, cancer therapy, greenhouse gas capture, heterogeneous catalysis, gas/vapor separation, luminescent and fluorescent materials [28-29].

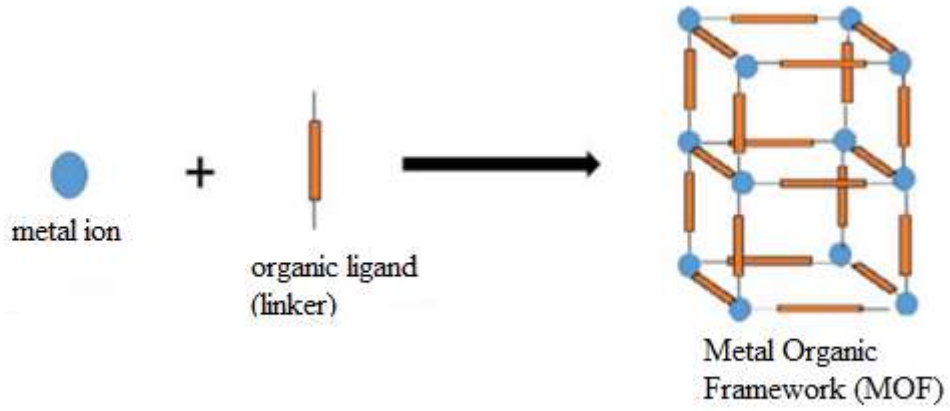

Figure 1.3. Schematic presentation for MOF formation.

MOFs contain metal ion nodes, linked by at least ditopic organic ligands (linkers), making network with permanent 1D, 2D or 3D microporosity. The transition metal or d-block elements, such as Ti^{4+}, Zr^{4+}, V^{3+}, Cr^{3+}, Mn^{2+}, Fe^{3+}, Ni^{2+}, Co^{2+}, Cu^{2+}, Zn^{2+}, Cd^{2+}, main group metals such as Mg^{2+}, Al^{3+}, or Ga^{3+} are metal ions usually used as MOF materials [30]. Organic linkers are generally rigid, multitopic ligand molecules that belong to the group of bi-, tri-, or tetra-topic carboxylates, amines, phosphonates, or sulfonates [31]. Free coordination sites of metal ions or metal-ligand fragments, examples of possible structures

for metal organic frameworks, and multidentate organic linkers (bi-dentate, tri-dentate, tetra-dentate, respectively) are shown in the Figure 1.4. Examples of 1D, 2D, and 3D MOFs are given in the Figure 1.5. First synthesis of MIL-53 was made in 2002 from $Cr(NO_3)_3$ and 1,4-benzenedicarboxylic acid [32]. MIL-53 can be used in several applications such as catalyst, removal of pharmaceutical pollutant, adsorption of heavy metals [33-35]. MIL-71 synthesized from vanadium(III) dicarboxylate and 1,4-benzene dicarboxylic acid [36]. According to authors, it is the first porous hybrid oxyfluorinated vanado(III)carboxylate. [36] MIL-73 refers as nickel succinate, and it has magnetic and sorption properties [37].

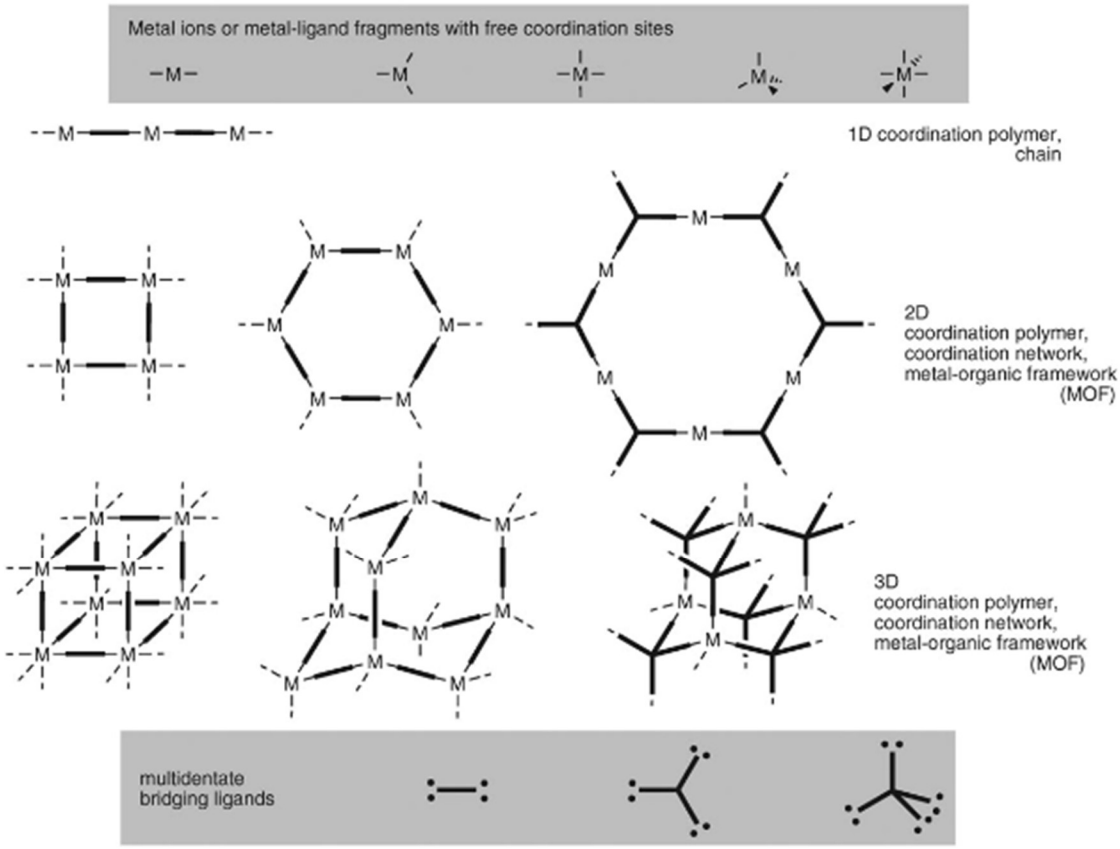

Figure 1.4. Schematic representation for the metal ion or metal ligands, the structure of MOFs (in 1D, 2D, 3D), and multidentate organic linkers [31].

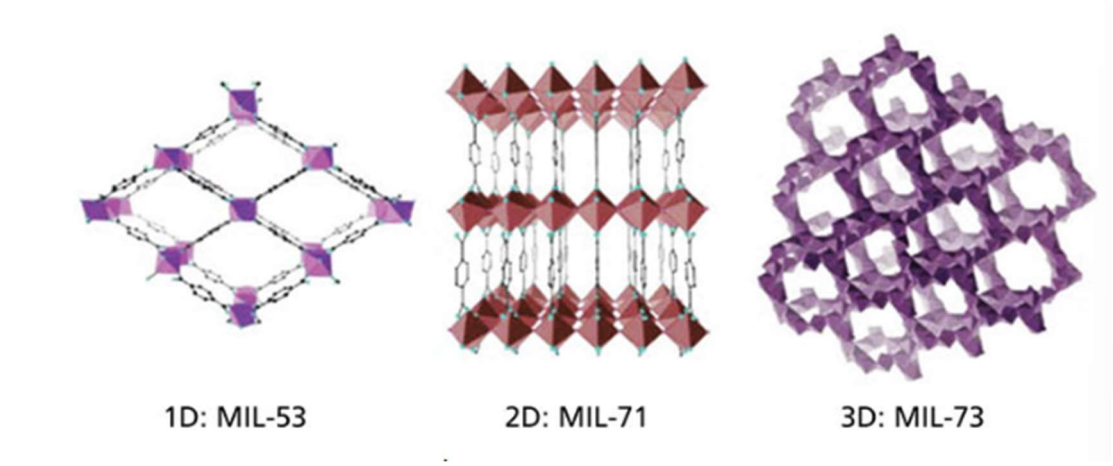

Figure 1.5. Examples for 1D, 2D and 3D MOFs [38].

MOFs are a subset of coordination polymers according to IUPAC (International Union of Pure and Applied Chemistry). Terminological nomenclature of MOF materials changes according to different conditions. It is categorized as the metal source used in synthesis (Fe-MOF, Cu-MOF), institute where MOF materials are synthesized in (MIL; Material Institut Lavoisier, DUT; Dresden University of Technology, HKUST; Hong Kong University of Science and Technology, UiO; Universitetet i Oslo), the organic ligand used in the structure or structure similarities (ZIF; Zeolitic Imidazolate Framework, IRMOF; IsoReticular Metal Organic Framework), the numbers after the MOF-term according to order of the synthesis (MOF-5, MOF-74, MIL-88, MIL-53, ZIF-8) [39].

1.2. Synthesis Methods of Metal Organic Frameworks

Generally, MOFs are synthesized via solvothermal or hydrothermal synthesis routines. The reaction can be varied from several hours to days. Different synthesis methods were tried to decrease synthesis time, such as electrochemical, mechanochemical, microwave-assisted, and sonochemical methods. Figure 1.6. shows summary of most used synthesis methods of metal organic frameworks. Different synthesis methods may affect not only the synthesis time, but also crystal size, uniformity of crystals, and yields. Also, the ratio of starting materials (metal salt/organic ligand), the type of solvent and amount of

solvent, reaction temperature and time, pH of the reaction medium affect the crystal structure of the MOF materials and synthesis yield [40,41].

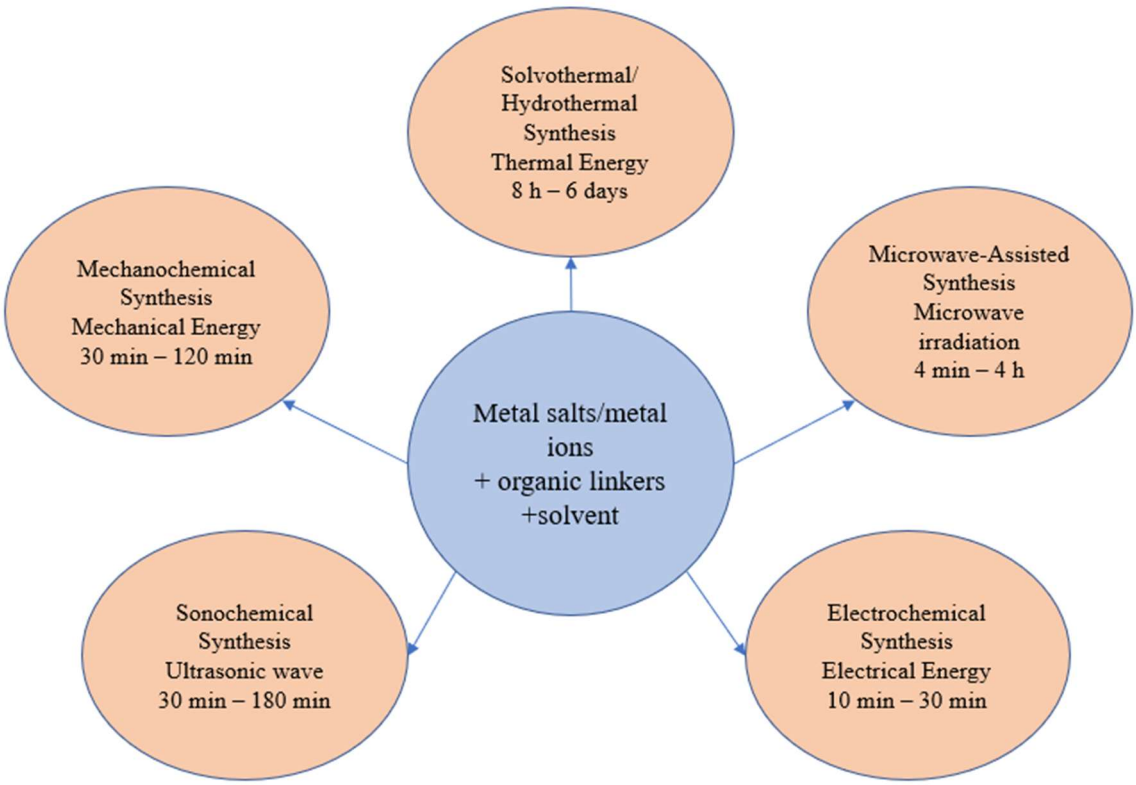

Figure 1.6. Most used synthesis methods of metal organic frameworks.

1.2.1. Solvothermal/Hydrothermal Synthesis

The most widely used methods in the synthesis of the MOF structures are solvothermal or hydrothermal synthesis methods by conventional electrical heating. The methods are based on the reaction between metal salts and organic ligands in the solvent medium (as seen in the Figure 1.7.), and the synthesis time changes from 8-h to 6-days. If the reaction occurs at the lower temperatures, sealed glass vials can be used or if the reaction occurs at temperatures above 130 ºC, the Teflon-lined autoclaves can be used. In solvothermal synthesis, high-solubility organic solvents, such as dimethyl formamide,

diethyl formamide, acetonitrile, acetone, ethanol, or methanol, are employed. In hydrothermal synthesis, water is used instead of organic solvents [42-44].

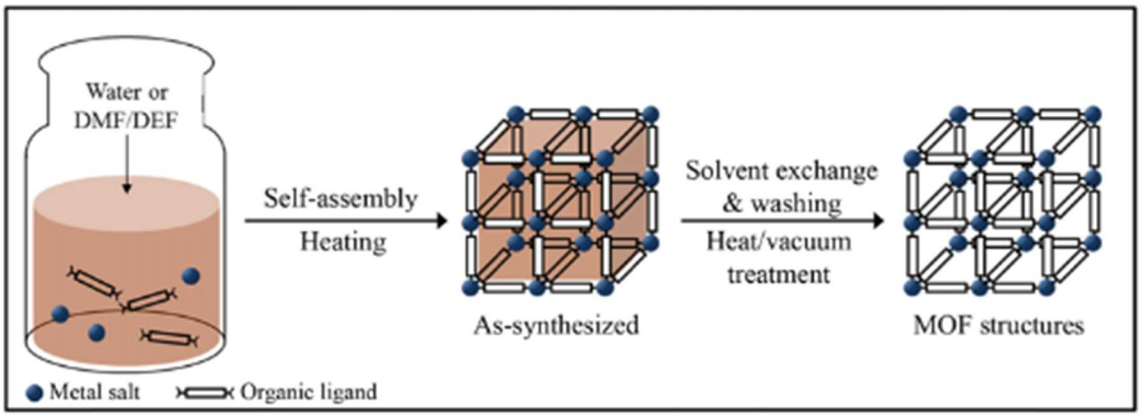

Figure 1.7. Solvothermal/Hydrothermal synthesis of MOFs [45].

1.2.2. Electrochemical Synthesis

The main idea of electrochemical synthesis of MOFs is based on anodic dissolution of metal ions which react with the organic linkers and electrolytes in the reaction medium. Illustration of electrochemical synthesis is shown in the Figure 1.8. Metal ions are used instead of metal salts. Since anions from metal salts do not involve into the reaction medium, it is possible to obtain high-purity MOF structures [46]. Also, MOFs can be synthesized at lower temperature and faster compared to solvothermal synthesis route. Electrochemical synthesis route has the possibility to run continuous process and obtain higher yields, therefore the method is suitable for industrial process. Electrochemical synthesis of MOFs was first reported for HKUST-1 in 2005 by Mueller and co-workers [47]. Solvent, electrolyte, voltage-current density, and temperature are possible parameters for the yields, structure, and morphology of the MOF materials [48].

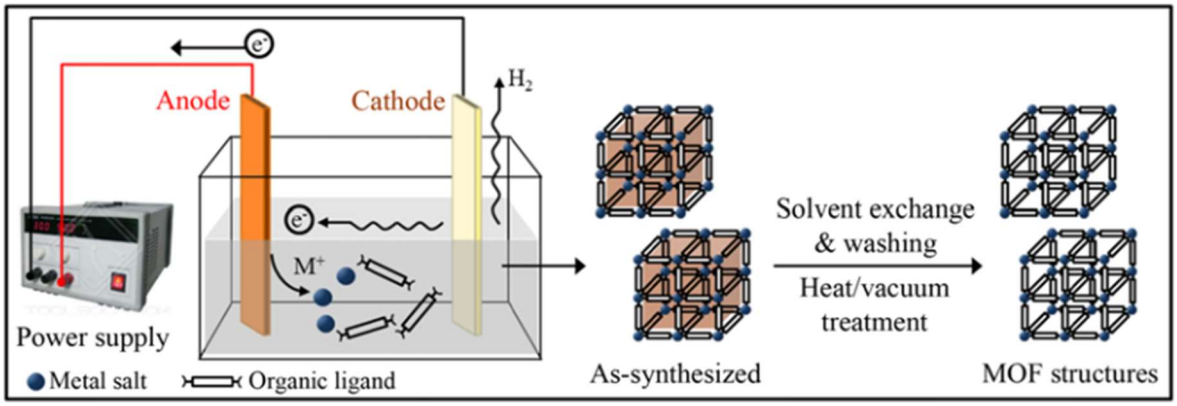

Figure 1.8. Electrochemical synthesis of MOFs [45].

1.2.3. Mechanochemical Synthesis

Intramolecular bonds are broken mechanically in ball-mill grinder then, a chemical transformation takes place in mechanochemical synthesis (as seen in the Figure 1.9.) [49]. Since reactions usually occur at lower temperature under solvent-free conditions, mechanochemical synthesis is environment-friendly method. Metal oxides can be preferred as starting material instead of metal salts in some cases, water forms as only side product [50]. Use of mechanochemical synthesis for MOFs was first reported in 2006 by Pichon and co-workers [51]. In this study, cooper acetate and isonicotinic acid were grinded together for 10-min without heating. After mechanical process, the material was kept under 200 ºC for 3 hours in order to get rid of water and acetic acid in purification process. Mechanochemical reactions can be accelerated by adding small amount of solvent which increases mobility of the reactants. Also, the addition of solvent can affect morphology of MOFs. In the study of Yang and co-workers for mechanochemical synthesis of HKUST-1, BET surface area increased with the addition of 100µl of MeOH [52].

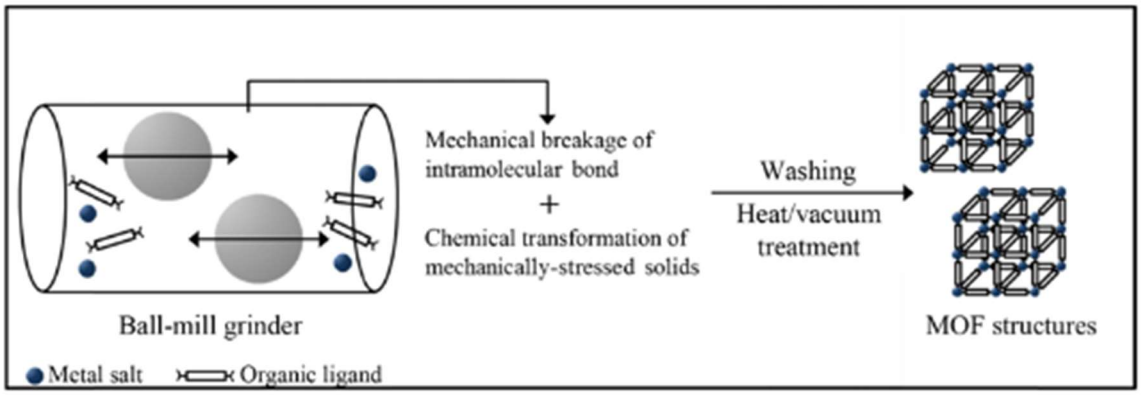

Figure 1.9. Mechanochemical synthesis of MOFs [45].

1.2.4. Microwave-assisted Synthesis

Microwave-assisted synthesis route is preferred due to shorter synthesis time of MOFs, fast crystallization, phase selectivity, narrow particle size distribution, facile morphology control [53]. In microwave synthesis, a Teflon vessel, contains starting materials and solvent, is sealed, and put into the microwave unit. Representative microwave-assisted synthesis was shown in the Figure 1.10. Microwave irradiation causes dipole rotation and ionic conduction for molecules in the reaction mixture. Dipole rotation and ionic conduction provide local heating, therefore rapid synthesis is achieved [54]. Microwave irradiation time, power level, temperature, concentration of starting materials are some parameters affect the morphology of MOFs and synthesis time. Cr-MIL-100 was the first reported MOF for microwave-assisted synthesis [55]. When the compound was synthesized in 4 days at 220 ºC by hydrothermal synthesis, it was synthesized in 4 hours at 220 ºC with similar physicochemical and textural properties compared with the conventional method. MOF-5 was synthesized by both microwave synthesis and conventional synthesis by Choi and co-workers in order to compare effect of synthesis method [56]. When the compound was synthesized in 12 hours by conventional method, it was synthesized in 15 minutes by microwave-assisted synthesis. Increase in irradiation power and synthesis temperature caused reduction of synthesis time with increasing crystal quality.

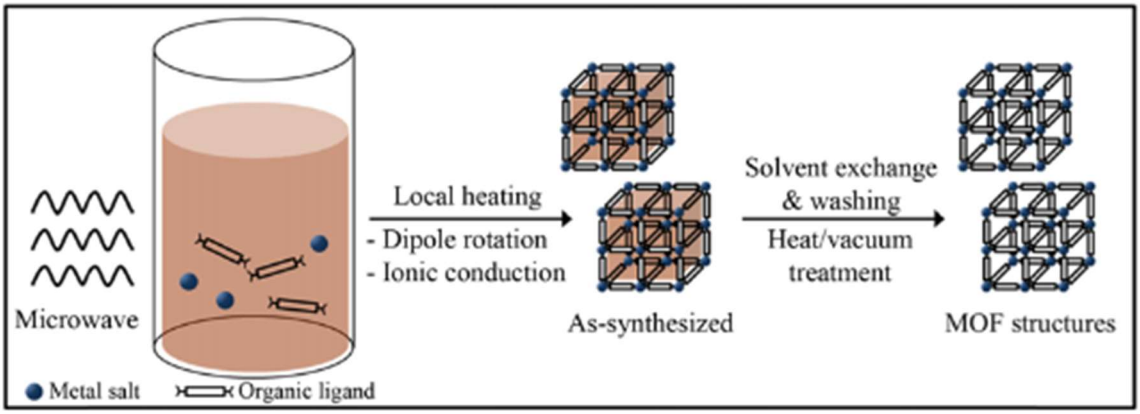

Figure 1.10. Microwave-assisted synthesis of MOFs [45].

1.2.5. Sonochemical Synthesis

Sonochemical synthesis methods provides a decrease in crystallization time and smaller particle size when compared to conventional methods. Ultrasound is sound waves with a frequency between 20 kHz and 10 MHz [57]. Direct interaction does not occur between ultrasound and molecules to make chemical reactions because the wavelength is much larger than molecular dimensions [58]. Ultrasound interacts with liquids and creates small bubbles. Formation, growth, and collapse of the bubbles are called as acoustic cavitation (as seen in the Figure 1.11). Acoustic cavitation produces hot spots with very high temperatures (~5000 K), pressures (~1000 atm), and heating and cooling rates (above 10^{10} K/s) [59]. The extreme conditions can cause the excitation of molecules, bond breakage, and the formation of radicals. Ultrasonic horn (or probe) and ultrasonic bath are used as ultrasonic experimental equipment. The acoustic frequency and intensity, change depending on the equipment used, affect cavitation [60]. In addition, vapor pressure, viscosity, and chemical reactivity of chosen liquid, the temperature, solvents are important parameters for chemical reactions [61].

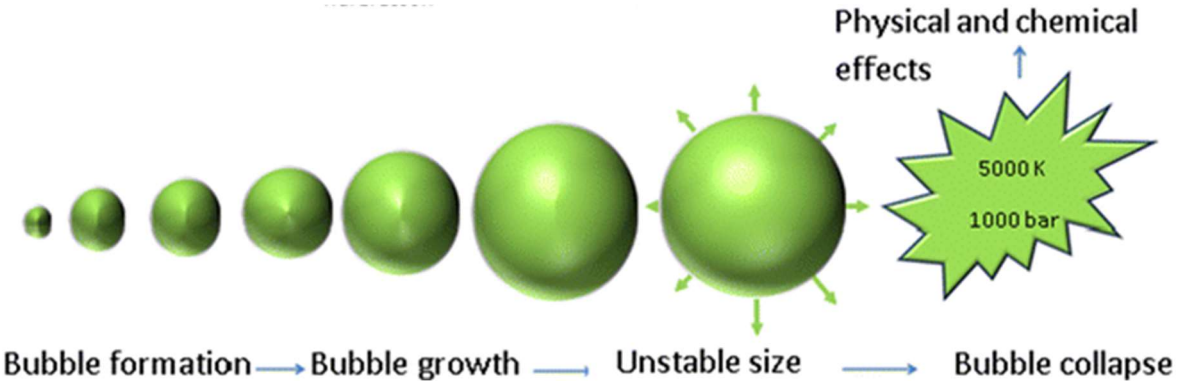

Figure 1.11. Schematic presentation of formation, growth, and collapse of bubbles, acoustic cavitation [62].

Researchers have been interested in sonochemical synthesis of MOFs due to a fast, energy-efficient, environment-friendly, low-temperature method. Illustration of sonochemical synthesis of MOFs is shown in the Figure 1.12. Sonochemical synthesis method has been used since 2008 for synthesis of MOFs. A fluorescent microporous MOF, from zinc acetate dihydrate and benzene-1,3,5-tricarboxylic acid (H_3BTC) was synthesized for different reactions times of 5, 10, 30 and 90 min by Qui and co-workers [63]. Increase in size of nanoparticles with increasing reaction times was observed. Another research was made by Son and co-workers in 2008 for sonochemical synthesis of MOF-5 [64]. MOF-5 was synthesized from zinc (II) nitrate hexahydrate and terephthalic acid in 30 min via sonochemical method. When synthesis time was compared with conventional solvothermal synthesis (24 hours), decrease in synthesis time was observed. Chalati and co-workers synthesized Fe-MIL-88A from iron (III) chloride hexahydrate and fumaric acid with using an ultrasonic bath [65]. Effect of different parameters, concentration, reaction time, temperature, and pH, on particle size of MOF was investigated in this study. Depend on the equipment, used in synthesis, larger or smaller increase in temperature may be observed during synthesis. Therefore, the reaction temperature can be monitored or kept under same starting temperature by using external cooling.

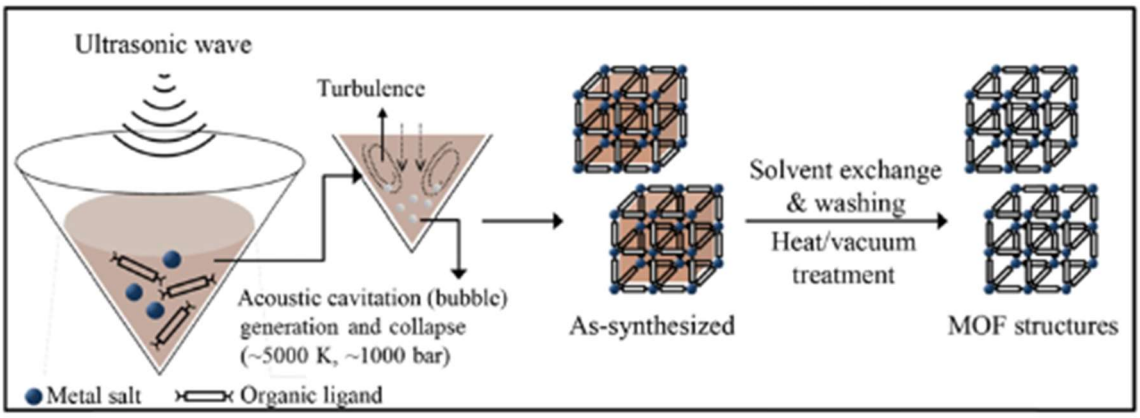

Figure 1.12. Sonochemical synthesis of MOFs [45].

1.3. Factors Effecting Synthesis and Structure of Metal Organic Frameworks

The crystallization, structure, and morphology of MOFs do not only depend on type of synthesis, but also many compositional parameters such as solvent, pH of reaction mixture, molar ratio of starting materials, concentration, and process parameters such as pressure, time, and temperature [66].

1.3.1. Solvent-effect

Choice of solvent is an important parameter in the synthesis of MOFs, because solvent may affect the behaviour of metal and ligand. The solvents may coordinate with metal ions or behave as a guest molecule in MOF structure. H_2O, DMF, DMSO, DEF, DMA, DEE, DPE, DPP, DEP are the main solvents used in MOF synthesis [67]. As solvent choice can control deprotonation of carboxylate ligands; the basicity of solvent medium can also control deprotonation of carboxylate ligands. In Cheng and co-workers' study, the DMF/EtOH mixture and anhydrous methanol media were used as solvents [68]. When the mixture of DMF and ethanol was used in synthesis, 3D pillar-layered framework was obtained and when anhydrous methanol media was used, 1D zig-zag chain structure was obtained. So, chance in solvent polarity affects the dimensionality of MOF structures. Huang and co-workers selected DMF, DMA, and DMP as solvent in cobalt-based MOF synthesis

[69]. Pore sizes of the complexes were decrease with decreasing the sizes of the solvent molecules.

1.3.2. pH-effect

Acidity or basicity of the reaction medium has a significant impact on crystallization and growth of metal organic hybrid materials. pH of the reaction medium affects the deprotonation of an organic ligand, the connectivity behaviour of organic ligand to metal ion, and formation of OH-ligand. In Luo and co-workers' study, effect of pH on cobalt-based metal organic frameworks was studied [70]. The final structures of complexes were varied as 2D framework for pH=5, 2D-double-layer framework for pH=7, and 3D framework for pH=9. Also, compounds had different colours with changing pH of the reaction medium. Pink-coloured crystals at pH=5, purple-coloured crystals at pH=7, and brown-coloured crystals at pH=9 were observed. Wang and co-workers, and Chen and co-workers used NaOH for changing pH [71-72]. According to these studies, as NaOH makes basic medium for deprotonation of an organic ligand, it can take part in the structure of the framework.

1.3.3. Temperature-effect

In addition to solvent and pH, reaction temperature is also one of the important factors in the synthesis of metal organic frameworks. Solubility of organic ligands, the coordination modes of organic ligands can be affected to the reaction temperature. Forster and co-workers synthesized cobalt-based MOFs from cobalt hydroxide and succinic acid at different temperatures (60 ºC, 100 ºC, 150 ºC, 190 ºC, and 250 ºC) and change in temperature was the only parameter changed. 1D chains at 60 ºC and 100 ºC, 2D networks at 150 ºC, and 3D frameworks at 190 ºC and 250 ºC was observed [73]. Also, density of the MOFs in this study increased with increasing the reaction temperature. In Deng and co-workers' study, 2 different coloured nickel-based MOFs were synthesized in the similar synthesis process at 120 ºC and 180 ºC [74]. The green block crystalline Ni-MOF at 120 ºC had a 2D layered structure and the orange block crystalline Ni-MOF at 180 ºC had 2-fold interpenetrating 3D framework.

1.4. Applications of Metal Organic Frameworks

Since metal-organic frameworks have porous structure, high surface area, adjustable chemical functionality, thermal stability, they are used in various applications such as gas storage, catalysis, batteries, and supercapacitors.

1.4.1. Gas Storage

Gases are highly used in industry and daily life for energy demand. H_2, CH_4, and C_2H_2 gases are used as energy resources, but there are some problems on storage of gases. In addition to energy resources, concentration of CO_2 gas in atmosphere is an important global concern because the global climate system is affected by increase in CO_2 concentration in the atmosphere. Therefore, metal organic frameworks have potential in gas storage because of their tunable pore sizes, chemical functionalities, good thermal and mechanical properties.

1.4.1.1. Hydrogen (H_2) Storage in MOFs. Alternative energy sources are highly attracted attention by scientists because of many reasons: (i) fossil fuel supply is limited in the earth, (ii) burning of fossil fuels causes carbon dioxide emission and increase in carbon dioxide concentration in the atmosphere causes climate change. Hydrogen is an alternative energy resource. When hydrogen is burned, water is produced as a result of the reaction. Also, hydrogen provides 3 times more energy compared to gasoline. However, there are challenges for storage of hydrogen because of a low density of hydrogen (0.0899 kg/m^3) [75]. First study of hydrogen storage in MOFs was done with MOF-5 of composition $Zn_4O(BDC)_3$ (BDC= 1,4-benzenedicarboxylate) in 2003 by Rosi and co-workers [76]. Hydrogen was stored 4.5 weight % in MOF-5 at 78 K and 1 atm and 1 weight % in MOF-5 at room temperature and pressure of 20 bar which was considered as up limit of safe pressure. MOF-210 from solvothermal reaction of H_3BTE (4,4',4''-(benzene-1,3,5-triyltris(ethyne-2,1-diyl)tribenzoic acid), H_2BPDC (biphenyl-4,4'-dicarboxylic acid) and zinc(II) nitrate hexahydrate had 6240 m^2/g BET surface area and hydrogen storage capacity of 17.6 weight % at 77 K and 80 bar [77].

1.4.1.2. Methane (CH_4) Storage in MOFs. Methane, is the main component of natural gas, has highest hydrogen/carbon ratio in order hydrocarbon-fuels. Natural gas can be used as alternative fuel instead of fossil fuels. Natural gas is much environment-friendly when compared to fossil fuels since it releases less CO_2 which has greenhouse gas effect [78]. A tank that contains MOFs provides more gas storage than an empty tank thanks to the large surface area of MOFs [79]. First study of methane storage in MOFs was done by Kondo and co-workers in 1997 [80]. Cobalt based MOF was prepared from $Co(NO_3)_2.6H_2O$ and 4,4'-bipyridine and methane adsorption capacity of the Co-MOF was found as 52 cm^3/g at 30 atm and 298 K. Guo and co-workers synthesized UTSA-20 from H_6BHB (3,3',3'',5,5',5''-benzene-1,3,5-triyl-hexabenzoic acid) and $Cu(NO_3)_2.2.5H_2O$ for methane storage at room temperature [81]. Methane storage capacity of UTSA-20 was found as 195 v/v at room temperature and 35 bar and this value is higher than DOE methane storage target (180 v/v at room temperature and 35 bar).

1.4.1.3. Acetylene (C_2H_2) Storage in MOFs. Acetylene is the one of the compounds in organic chemistry. As acetylene is used as starting material in the industry, it can be alternative energy source. Since acetylene has explosive nature, it should be stored at under 2 atm [82]. Matsuda and co-workers studied C_2H_2 storage in microporous $Cu_2(pzdc)_2(pyz).2H_2O$ (pzdc=pyrazine-2,3-dicarboxylate and pyz=pyrazine). The material stored 42 cm^3/g C_2H_2 at room temperature and 1 atm [83]. The acetylene storage capacity of HKUST-1 was found as 201 cm^3/g at 295 K and 1 atm [84]. Since open Cu^{2+} sites in HKUST-1 provided binding sites for acetylene, uptake of acetylene in HKUST-1 was high.

1.4.1.4. Carbon Dioxide (CO_2) Storage in MOFs. Level of carbon dioxide, which has the biggest portion in greenhouse gases, in the atmosphere is increasing day by day. Increase in concentration of greenhouse gases in the atmosphere causes increase in global temperature and climate change. Therefore, carbon dioxide capture and storage systems are needed to keep the global temperature approximately constant. Metal organic frameworks are promising candidate for carbon dioxide capture and storage systems thanks to their open metal sites, high surface areas, and tunable pore sizes. Carbon dioxide storage in MOFs is based on adsorption of carbon dioxide with MOFs. So, adsorption capacity and enthalpy of

adsorption are important parameters [85]. Millward and Yaghi worked with various MOFs for capacity of metal organic frameworks for carbon dioxide storage [86]. MOF-177 had 4508 m^2/g surface area and its CO_2 capacity was 33.5 mmol/g at room temperature and 35 bar. The amount of CO_2 storage capacity of MOF-177 was 9 times higher than empty pressurized container and 2 times higher than zeolites. In another work made by Kim and co-workers, MOF-177 was pyrolyzed at 1000 ºC and porous carbon materials were obtained [87]. After pyrolysis, the amount of carbon dioxide uptake for MOF-177 was approximately 3 times higher than before.

1.4.2. Catalysis

Catalyst makes the chemical reactions faster with decreasing activation energy of the chemical reaction. In the end of the reaction, catalysts are not consumed, and their chemical structures do not change. Since metal organic frameworks may be similar to behaviour of metal complex catalysts, they can take advantages of homogeneous catalysts. Also, they can take advantages of heterogeneous catalysts because they can separate from the reaction medium easily and they are recyclable [88]. MOFs can be used in catalysis reactions due to their properties such as their controllable pore size, high surface area, acid sites and basic sites, stability [89]. The use of MOFs for catalyst was first reported in 1994 by Fujita and co-workers [90]. $[Cd(4,4'\text{-}Bpy)_2](NO_3)_2$ (Bpy=bipyridine) was used for cyanosilylation of aldehydes. The reaction was catalysed by the Cd-MOF because there was no reaction with $Cd(NO_3)_2$ and 4,4'-bpy alone. MIL-53 (Fe) was prepared from $FeCl_3.6H_2O$ and H_2BDC (1,4-benzenedicarboxylic acid) in DMF by Liang and co-workers [91]. MIL-53 (Fe) was used as bifunctional photocatalyst for reduction of Cr(VI) in this study. After 40 min of visible light irradiation, the MIL-53 (Fe) photocatalyst reduced Cr(VI) at a rate of about 100% and catalytic activity of Fe-MIL-53 was found more efficient than N-doped TiO_2 under the same experimental conditions. In another study, $[Co^{II}(BPB)]_3DMF$ was synthesized from Co^{II} nitrate and 1,4-bis(4-pyrazolyl)benzene (H_2-BPB) in DMF [92]. Since the MOF contained redox activity Co^{II} atoms, it was used as catalyst for the oxidation of cyclohexene with tert-butyl hydro-peroxide as oxidant. When catalyst did not present in the reaction medium, the reaction did not occur under the same conditions.

1.4.3. Energy Applications

The need for energy in modern life constantly increasing, and one of the biggest problems for humanity is dealing with the energy crisis. Mostly, fossil fuels are used for the energy needs. However, the world has limited fossil fuel resources and the use of fossil fuels has harmful effects on the environment and human health. Therefore, there is an urgent need for efficient, clean, and sustainable resources. Electricity can be generated from renewable energy sources such as wind and solar energy but produces electricity from wind and solar energy needs energy storage systems. Supercapacitors and batteries are important technologies for applications such as portable electronics and electric vehicles. However, they have some limitations. Capacitors show high-rate performance, but the energy density is not enough for electric vehicles and batteries have high energy density, but their power density is low [93-94]. Metal organic frameworks have attracted attention for electrochemistry since they have high porosity, large surface areas, and tunable structural properties. Figure 1.13. shows usage of MOFs and MOF-derived materials in electric energy storage and applications.

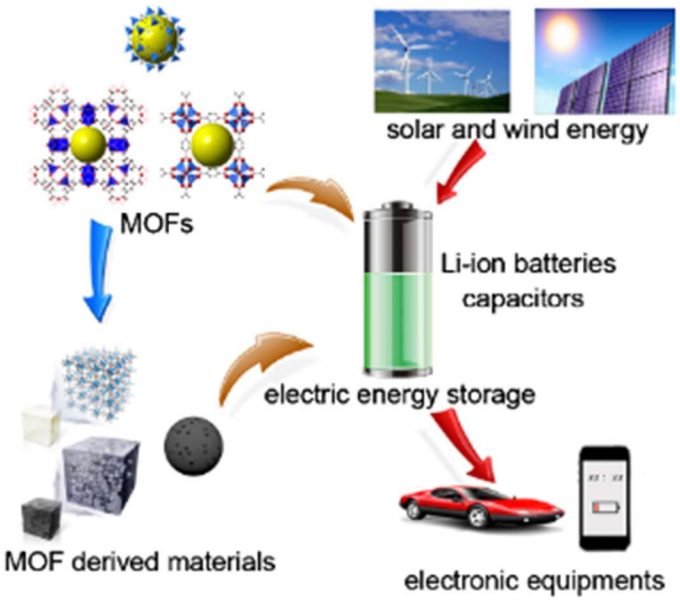

Figure 1.13. Usage of metal organic frameworks in energy applications [95].

Supercapacitors, also called electrochemical capacitors are energy storage devices. Despite their high-power density and long cycle life, the energy density of supercapacitors needs further improvements. There are two types of supercapacitors: electrochemical double-layer capacitors (EDLCs) and pseudo-capacitors. Carbon based active materials with high surface areas such as graphene and carbon nanotube are used in EDLCs. Pseudo-capacitors are based on fast and reversible redox reactions on the surface of the electrode materials. Transition metal oxides and conductive polymers are used as pseudo-capacitors [95,96]. MOFs are candidates for supercapacitors due to their high surface area and excellent pore sizes. In Lee and co-workers' study, cobalt-based MOF from $Co(NO_3)_2.6H_2O$ and terephthalic acid had pseudo-capacitor behaviour [97]. As pristine MOFs are used as supercapacitors, MOF-derived materials are also used as supercapacitors. In Meng and co-workers' study iron-based MOF was used as template to prepare porous Fe_3O_4/carbon composite electrode [98]. A specific capacitance of 139 F/g was found and 83.3% of capacitance of the electrode remained after 4000 cycles.

There are many types of batteries such as ion batteries, metal-air batteries, and metal-sulphur batteries. These batteries work with different mechanism, but they have same units: the electrodes (cathode and anode), and the electrolytes. The chemical reactions occur at the part of cathode and anode. Electrolyte make ion transportation and prevents electronic conduction. Since metal ions and metal oxides have redox active sites and metal organic frameworks contain metals as inorganic unit, they can be used in batteries [99]. In 2007, use of Fe-based MOF was first reported by Ferey and co-workers [100]. Fe-MIL-53 was chosen cathode material for lithium-ion batteries. Also, nickel and cobalt-based MOFs are promising candidates as anodes of lithium-ion batteries [101-103].

2. SCOPE OF THESIS

Metal organic frameworks (MOFs) are classified in porous materials and formation of MOFs is based on connection between metal clusters or ions and organic linkers. MOFs are used in various applications such as energy storage, drug delivery, gas capture and storage, heterogeneous catalysis, luminescent and fluorescent materials since they have high surface area, tunable pore size, tunable chemical functionality, high porosity. This study is aimed to synthesize iron (Fe), cobalt (Co), and nickel (Ni) based metal organic frameworks, and investigate effects of temperature, pH, concentration, and solvent on synthesized compounds. In this thesis study, metal salts of iron (Fe), cobalt (Co), and nickel (Ni) are selected as metal source of different MOFs due to their abundance and cost for different types of applications such as gas storage, and energy conversion. Fumaric acid and terephthalic acid are preferred as organic linkers due to their stability at different conditions and their lab scale synthesis easily.

Chapter 1 gives a brief introduction about porous materials, especially for MOFs. Synthesis methods of MOFs, factors (solvent, pH, and concentration) effecting synthesis and structure of MOFs, and some applications (gas storage, catalysis, and energy applications) of MOFs are explained in the Chapter 1. Chapter 2 includes aim of this thesis and summarizes this thesis, briefly. Materials used in the experiments are given in Chapter 3 and structure and properties of ligands used in the synthesis of Fe, Co, Ni based MOFs are explained in this chapter. Also, Chapter 3 includes process of synthesis of fumaric acid and selected MOFs and explanation about characterization techniques. MOFs were synthesized via Sonochemical synthesis method that was fast, energy-efficient, and environment friendly method. Results and discussion are presented in Chapter 4. Effects of varied parameters (temperature, pH, concentration, metal ion, and solvent) on Fe, Co, Ni based MOFs were studied. Synthesized materials were characterized by X-Ray Diffraction Analysis (XRD), Scanning Electron Microscope/Energy Dispersive X-Ray Analysis (SEM/EDX), Infrared (IR) Spectroscopy. Conclusion of this study is given in Chapter 5 and possible future work for this study is commented in Chapter 6.

3. EXPERIMENTAL

3.1. Materials

Iron (III) chloride hexahydrate (98%, Alfa Aesar), cobalt (II) chloride hexahydrate (98%, Alfa Aesar), nickel (II) chloride (98%, Acros Organics, maleic anhydride (98%, Merck), terephthalic acid (98+%, Thermo Scientific), triethanol amine (98%, Merck), sodium hydroxide (99%, Sigma-Aldrich), and ultra-pure water (obtained from Millipore, Milli-Q) were used in the experiments. Mercury Ultrasonic Cleaner with 40 kHz for sonochemical synthesis and Domel Centric 260 R for centrifuge were used in the experiments.

3.2. Structure and Properties of Ligands

Fumaric acid was synthesized from maleic anhydride (as seen in section 3.3.1.). Fumaric acid also known as trans-butenedioic acid that is a carboxylic acid has the chemical formula $HO_2CCH=CHCO_2H$. Structure of fumaric acid is shown in the Figure 3.1.

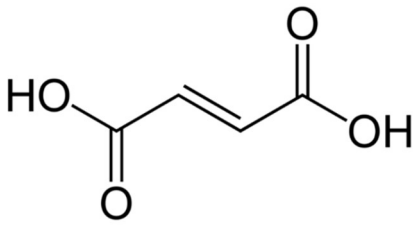

Figure 3.1. Structure of fumaric acid.

Terephthalic acid with chemical formula C_6H_4-1,4-$(COOH)_2$ also known as benzene-1,4-dicarboxylic acid. Structure of terephthalic acid is shown in the Figure 3.2. Terephthalic acid has different coordination modes with metals (as seen in the Figure 3.3.) [104].

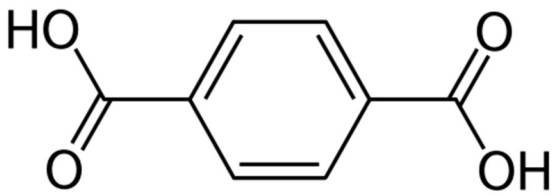

Figure 3.2. Structure of terephthalic acid.

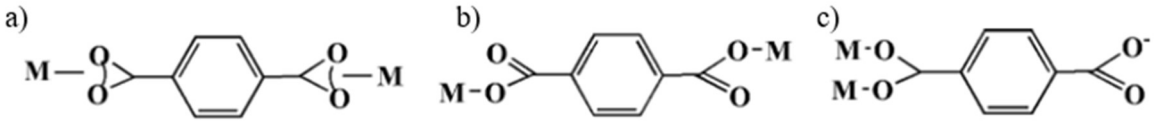

Figure 3.3. Various coordination modes of terephthalate ion, a) bidentate, b) monodentate, c) bis-monodentate.

3.3. Synthesis

3.3.1. Synthesis of Fumaric Acid

Fumaric acid synthesis was made according to textbook in reference 105. 11 g of maleic anhydride was dissolved in 15 ml of hot water at 80 ºC in a round bottom flask. The solution was allowed in order to cool to room temperature. When temperature of the solution reached room temperature, 15 ml of concentrated HCl was added slowly into the solution. The mixture was put into the reflux set-up. After boiling of the mixture, reflux was done for 10 min. Then, the mixture was kept under fume hood in order to cool to room temperature. Vacuum filtration was applied to obtain white crystalline precipitate. The precipitate was washed several times with cold water. Then, the wet solid material was left in order to dry. After 2 days, dry white crystals were collected and stored in a glass bottle for subsequent uses.

3.3.2. Synthesis of MOFs

Iron and fumaric acid-based compounds were synthesized according to modification of synthesis process in reference article [65]. Modified synthesis processes were given in the below.

$Fe^{III}(FA).H_2O$-1: 10 mM $FeCl_3.6H_2O$ solution was prepared from 0.2703 g of $FeCl_3.6H_2O$ and 100 ml of distilled water. 10 mM fumaric acid (FA) solution was prepared from 0.1161 g of fumaric acid and 100 ml of distilled water. The two solutions were mixed into a 250 ml beaker. Then, the mixture was put in ultrasonic bath (as seen in the Figure 3.4.) at 20 ºC for 90 min. Temperature was checked for every 15 min and when increase in temperature was observed, the temperature was kept constant by adding ice into the ultrasound bath. After 90 min sonication, centrifuge was done to the mixture for 10 min at 6000 rpm. Brown coloured precipitate was washed 3 times with distilled water and 3 times with ethanol. Then, precipitate was allowed to dry and brown coloured crystals were collected after 2 days and kept in a glass bottle for subsequent uses.

$Fe^{III}(FA).H_2O$-2: Same procedure in $Fe^{III}(FA).H_2O$ at 20 ºC was applied for 50 ºC instead of 20 ºC. Brown coloured precipitate was observed.

$Fe^{III}(FA).H_2O$-3: Same procedure in $Fe^{III}(FA).H_2O$ at 20 ºC was applied for 75 ºC instead of 20 ºC. Lighter brown coloured precipitate than the ones at 20 ºC and 50 ºC was observed.

$Fe^{III}(FA).H_2O$-4: 1.352 g (5 mmol) of $FeCl_3.6H_2O$ was dissolved in 100 ml of distilled water and 0.580 g (5 mmol) of fumaric acid was dissolved in 90 ml of distilled water and 10 ml of ethanol Then, two solutions were mixed into a 250 ml beaker and put in ultrasound bath at 75 ºC for 90 min. Temperature was checked for every 15 min and kept constant by adding ice when temperature increased. After 90 min, the mixture was cooled at

room temperature and transferred into 50 ml of centrifuge tubes and centrifuged for 10 min at 6000 rpm. Light-brown coloured precipitate was washed 3 times with distilled water and 3 times with ethanol. Precipitate was dried for 2 days. Then, crystals were kept in a glass bottle for subsequent uses.

Fe^{III}(FA).H_2O-5: 2.703 g (10 mmol) $FeCl_3.6H_2O$ was dissolved in 100 ml of distilled water and 1.161 g (10 mmol) of fumaric acid was dissolved in 90 ml of distilled water and 10 ml of ethanol. They were mixed into a 250 ml beaker. Then, the mixture was put in ultrasonic bath at 75 ºC for 90 min. Temperature was controlled for every 15 min and kept constant at 75 ºC by adding ice. After sonication, the mixture was cooled at room temperature and transferred into 50 ml of centrifuge tube in equal portions. The mixture was centrifuged for 10 min at 6000 rpm. Light-brown coloured precipitate was washed 3 times with distilled water and 3 times with ethanol. After washing precipitate was allowed to dry and crystals were collected after 2 days and kept in a glass bottle for subsequent uses.

Fe^{III}(FA).H_2O-6: 0.2703 g (1 mmol) of $FeCl_2.6H_2O$ was dissolved in 100 ml of distilled water. 0.1161 g (1 mmol) of fumaric acid was dissolved in 100 ml of distilled water and adjusted to pH~7 by addition of 1 M NaOH solution. Then, the two solutions were mixed into a 250 ml beaker and the mixture was put in ultrasonic bath at 75 ºC for 90 min. The mixture was cooled to room temperature at the end of 90 min sonication. Then, the mixture was transferred into 50 ml of centrifuge tubes and centrifuged for 10 min at 6000 rpm. Washing process (3 times with distilled water and 3 times with ethanol) was applied and the precipitate was allowed to dry. Black coloured crystals were collected after 2 days and kept in glass a bottle for subsequent uses.

Fe^{III}(FA).H_2O-7: The same procedure that for Fe^{III}.H_2O-0.01 M at 75 ºC (pH=7) was used except that pH was adjusted to 10. Black coloured crystals were obtained.

Iron, cobalt, and nickel containing compounds with terephthalic acid were prepared with respect to modified synthesis process in reference article [106] and these synthesis processes were given in the below.

Fe^{III}(TPA).DMF: 0.2027 g (0.75 mmol) $FeCl_3.6H_2O$ and 0.1246 g (0.75 mmol) terephthalic acid were added into the mixture of 32 ml DMF, 2 ml ethanol, and 2 ml distilled water. The mixture was stirred and 0.8 ml of triethanol amine (TEA) was added into the mixture. The yellow-coloured mixture was put in ultrasonic bath at 75 ºC for 90 min. Temperature was checked for every 15 min and when increase in temperature was observed, the temperature was kept constant by adding ice into the ultrasound bath. After 90 min sonication, the dark-orange-coloured mixture was cooled to room temperature and transferred into 50 ml centrifuge tubes and centrifuged for 10 min at 6000 rpm. The precipitate was washed 3 times with distilled water and 3 times with ethanol and allowed to dry. Dark-orange-coloured crystals were collected after 2 days and kept in a glass bottle for subsequent uses.

Co^{II}(TPA).DMF: 0.1784 g (0.75 mmol) $CoCl_2.6H_2O$ and 0.1246 g (0.75 mmol) terephthalic acid were added into the mixture of 32 ml DMF, 2 ml ethanol, and 2 ml distilled water. The mixture was stirred, and blue coloured solution was observed. 0.8 ml TEA was added into the mixture and colour of the mixture changed to purple. The mixture was put into ultrasonic bath at 75 ºC for 90 min. Temperature was checked every 15 min and kept constant at 75 ºC. After 90 min sonication, Light-pink coloured mixture was obtained, and the mixture was cooled to room temperature. The mixture was transferred into 50 ml centrifuge tubes and centrifuges for 10 min at 6000 rpm. Precipitate was washed 6 times with ethanol because the compound was found as soluble in water. The precipitate was dried in 2 days and collected. Light-pink compound was kept in a glass bottle for subsequent uses.

Ni^{II}(TPA).DMF: 0.0972 g (0.75 mmol) nickel (II) chloride and 0.1246 g (0.75 mmol) terephthalic acid were added into the mixture of 32 ml DMF, 2 ml ethanol, and 2 ml distilled water. The mixture was stirred, and light-yellow-coloured mixture was obtained. 0.8 ml TEA was added into the mixture and colour of the mixture did not change. The mixture was put in ultrasonic bath at 75 ºC for 90 min and temperature kept constant with controlling temperature for every 15 min. After sonication, light-blue-coloured mixture was obtained. The mixture was cooled to room temperature and transferred into 50 ml centrifuge tubes and centrifuged for 10 min at 6000 rpm. Washing 3 times with distilled water and 3 times with

ethanol was applied and precipitate was allowed to dry. Light-blue coloured compound was collected after 2 days and kept in a glass bottle for subsequent uses.

Co^{II}/Ni^{II}(TPA).DMF: 0.75 mmol metal salt mixture (0.0486 g nickel (II) chloride and 0.0892 g $CoCl_2.6H_2O$) and 0.75 mmol terephthalic acid (0.1246 g) were added into the mixture of 32 ml DMF, 2 ml ethanol, and 2 ml distilled water. After the mixture was stirred, blue coloured solution was observed. 0.8 ml TEA was added into the mixture and colour of the mixture changed to pink. The mixture was put in ultrasound bath at 75 ºC for 90 min and temperature was controlled for every 15 min. When temperature increased, temperature kept constant at 75 ºC by addition of ice into the ultrasound bath. After sonication, light-blue coloured mixture was obtained and transferred into the 50 ml centrifuge tubes and centrifuged for 10 min at 6000 rpm. The mixture was washed 6 times with ethanol because the compound was soluble in water. Then, precipitate was allowed to dry, and light-blue crystals were collected after 2 days. The compound was kept in a glass bottle for subsequent uses.

Fe^{III}(TPA).H_2O: 0.75 mmol terephthalic acid (0.1246 g) was added into 50 ml of distilled water and adjusted to pH~7 by addition of 1 M NaOH. 0.75 mmol $FeCl_3.6H_2O$ (0.2027 g) was dissolved in 50 ml of distilled water and two solutions were mixed in 250 ml beaker. The mixture was put in ultrasonic bath for 30 min and 90 min at 75 ºC by controlling of the temperature and ice was added when temperature increased. After sonication, the mixtures were cooled to room temperature and transferred into 50 ml of centrifuge tubes and centrifuged for 10 min at 6000 rpm. The precipitates were washed with 3 times with distilled water and 3 times with ethanol and dried. Brown coloured crystals for 30 min and orange-coloured crystals for 90 min and were collected after 2 days and kept in a glass bottle for subsequent uses.

Co^{II}(TPA).H_2O: 0.75 mmol terephthalic acid (0.1246 g) was added into 50 ml of distilled water and adjusted to pH=10 by addition of 1 M NaOH. 0.75 mmol $CoCl_2.6H_2O$ (0.1784 g) was dissolved in 50 ml of distilled water and they were mixed in 250 ml beaker. 0.8 ml of triethanol amine (TEA) was added into the reaction mixture to increase

deprotonation of terephthalic acid. Then, the mixture was put in ultrasonic bath at 75 ºCfor 90 min and cooled to room temperature after sonication. The mixture was transferred into 50 ml centrifuge tubes and centrifuged for 10 min at 6000 rpm. Washing process 6 times with ethanol was applied and precipitate was allowed to dry. Dark-green coloured crystals were collected after 2 days and kept in a glass bottle for subsequent uses.

Ni^{II}(TPA).H_2O: 0.75 mmol terephthalic acid (0.1246 g) was added into 50 ml of distilled water and adjusted pH=10 by addition of 1 M NaOH. 0.75 mmol $NiCl_2$ (0.0972 g) was dissolved in 50 ml of distilled water and mixed with terephthalic acid solution in 250 ml beaker. 0.8 ml TEA was added into the reaction mixture and put in ultrasonic bath at 75 ºC for 90 min. Then, it was cooled to room temperature and transferred into 50 ml centrifuge tubes and centrifuged for 10 min and 6000 rpm. The precipitate was washed 3 times with distilled water and 3 times with ethanol and dried. After 2 days, light-green coloured crystals were collected and kept in a glass bottle for subsequent uses.

3.4. Characterization Techniques

The characterizations of MOF materials were completed by SEM/EDX, XRD, and IR spectroscopy. SEM was used to determine particle size, surface morphology of materials, and EDS was used to determine elemental composition of materials. XRD was used to obtain information about crystallinity and purity of materials. IR spectroscopy was used to determine intermolecular bonds of organic molecules.

3.4.1. X-Ray Diffraction Analysis (XRD)

Crystallinity of materials can be obtained by using X-ray diffraction technique. X-rays are diffracted into many specific directions due to the crystalline structure of sample. A spectrum is obtained by the diffracted X-rays and the spectrum is like fingerprint for the materials. If sample has low crystallinity, broaden peaks are obtained in the spectrum.

XRD spectrums were collected with Rigaku D/MAX-Ultima+/PC Diffractometer with Cu-Kα radiation (λ=1.54 Å) at Boğaziçi University Advanced Technologies Research and Development Center.

3.4.2. Scanning Electron Microscope/Energy Dispersive X-Ray Analysis (SEM/EDX)

SEM is a characterization technique to determine particle size, microscopic surface structures, and EDX gives information about elemental composition of the sample. In SEM, high-energy electrons across the surface of the sample. Reflected electron signal is detected by detector and the signal forms an image.

SEM/EDX analyses of this thesis were carried out using FEI-Philips XL30 instrument (equipped with EDAX-energy dispersive X-ray analysis unit) at Boğaziçi University Advanced Technologies Research and Development Center.

3.4.3. Infrared (IR) Spectroscopy

The sample interacts with infrared radiation and infrared radiation can be absorbed, emitted, or reflected due to intermolecular motions. IR spectrums are made as intensity versus wavelength (cm^{-1}) graphs. Functional groups (-OH, C=O, N-H, CH_3, etc.) are seen at 4000-1500 cm^{-1} and the region of 1500-400 cm^{-1} is called as fingerprint region. Peaks in this region are generally specific for the material.

IR spectrums of the compounds were received from Thermo Fisher Scientific Nicolet 380 FT-IR spectroscopy with ATR-Diamond and 32 scans were applied.

4. RESULTS AND DISCUSSION

4.1. Characterization of Fumaric Acid

In the spectrum (in Figure 4.1.), broad peak between 3000 and 2500 cm^{-1} comes from O-H stretch of carboxylic acid, The C=O stretching band and C=C stretching band give broadband at 1634 cm^{-1}. C-OH bend is also observed at 1420 cm^{-1}. Peak at 1272 cm^{-1} refers to C-O stretching and broad peak at 884 cm^{-1} refers to OH wag vibrations. Peaks in the infrared spectrum of fumaric acid that synthesized in the lab are consistent with the literature [107-109].

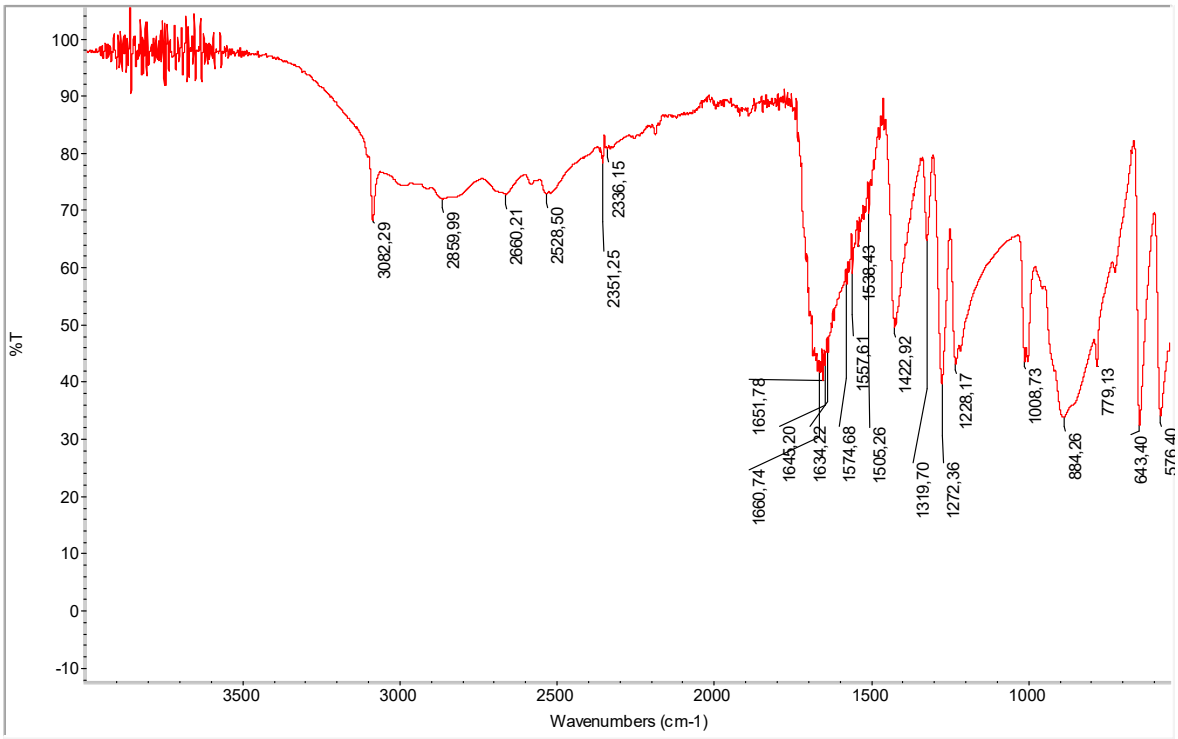

Figure 4.1. IR spectrum of fumaric acid synthesized in the lab.

4.2. Characterization of Fe, Co, Ni Based Metal Organic Frameworks

Results and discussion of Fe, Co, Ni based metal organic frameworks are given according to effect of parameters: temperature, concentration, pH, metal ion. SEM images and XRD patterns of Fe, Co, Ni based MOFs are given in the following subheadings.

4.2.1. Effect of Temperature on $Fe^{III}(FA).H_2O$

In this part of the study, temperature effect on the synthesis of $Fe^{III}(FA).H_2O$ was investigated. $Fe^{III}(FA).H_2O$ was synthesized via sonochemical synthesis method at 20 ºC, 50 ºC, and 75 ºC. The compounds were named as $Fe^{III}(FA).H_2O$-1 for synthesis at 20 ºC, $Fe^{III}(FA).H_2O$-2 for synthesis at 50 ºC, and $Fe^{III}(FA).H_2O$-3 for synthesis at 75 ºC. $Fe^{III}(FA).H_2O$-1 and $Fe^{III}(FA).H_2O$-2 had brown colour while $Fe^{III}(FA).H_2O$-3 had lighter brown colour.

SEM images of the compounds were given in the Figure 4.2., Figure 4.3., and Figure 4.4. Hexagonal rod-like structures were obtained at all three temperatures and with increasing temperature, particles became more monodispersed. In addition, particle size of $Fe^{III}(FA).H_2O$-3 was found as approximately 4 μm with respect to its SEM images. In EDX analysis, C (27.8 w %), O (50.3 w %), Fe (20.0 w %) and Cl (1.9 w %) for $Fe^{III}(FA).H_2O$-1, C (29.4 w %), O (50 w %), Fe (15.3 w %), and Cl (5.2 w %) for $Fe^{III}(FA).H_2O$-2, and C (24. 7 w %), O (42.9 w %), Fe (32.4 w %), and Cl (0.45 w %) for $Fe^{III}(FA).H_2O$-3 were detected. Cl peaks probably came from impurity in fumaric acid.

XRD patterns of the compounds were not matched with database of Boğaziçi University Advanced Technologies Research and Development Center therefore, XRD peaks were compared with literature [65, 110]. Peaks at nearly 10º (2θ) were characteristic peaks of iron fumarate and peaks were observed at 10.2º and 10.8º (2θ) for $Fe^{III}(FA).H_2O$-1, 10.2º and 10.8º (2θ) for $Fe^{III}(FA).H_2O$-2, and 10.9º and 11.8º (2θ) for $Fe^{III}(FA).H_2O$-3 (Figure 4.5., Figure 4.6.,and Figure 4.7.). Also, comparison of XRD patterns for the

compounds was given in the Figure 4.8. for clear observing of similar peaks. The peak shift in $Fe^{III}(FA).H_2O$-3 was considered because of growing crystal at higher temperature. Since peaks were sharper with increasing temperature, crystallinity of the compounds increased with increasing temperature.

O-H stretch of fumaric acid did not appear between 3000 and 2500 cm^{-1}, C-OH bend (at 1420 cm^{-1}) and OH wag vibrations (at 884 cm^{-1}) of fumaric acid were not observed, peaks at nearly 1590 cm^{-1} came from C=C stretching band, and peaks at nearly 1390 cm^{-1} came from C-O stretching band in the IR spectrums of $Fe^{III}(FA).H_2O$-1, $Fe^{III}(FA).H_2O$-2, and $Fe^{III}(FA).H_2O$-3 (Figure 4.9.).

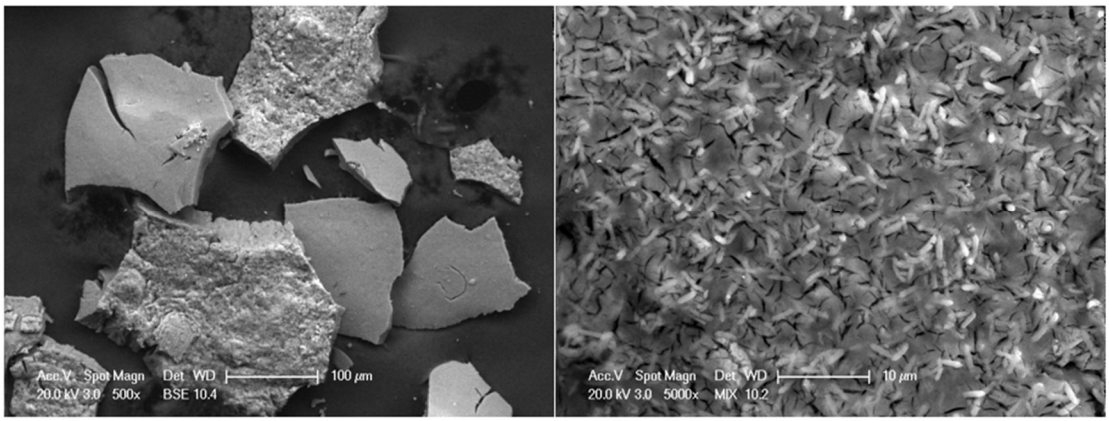

Figure 4.2. SEM images of $Fe^{III}(FA).H_2O$-1 synthesized at 20 ºC.

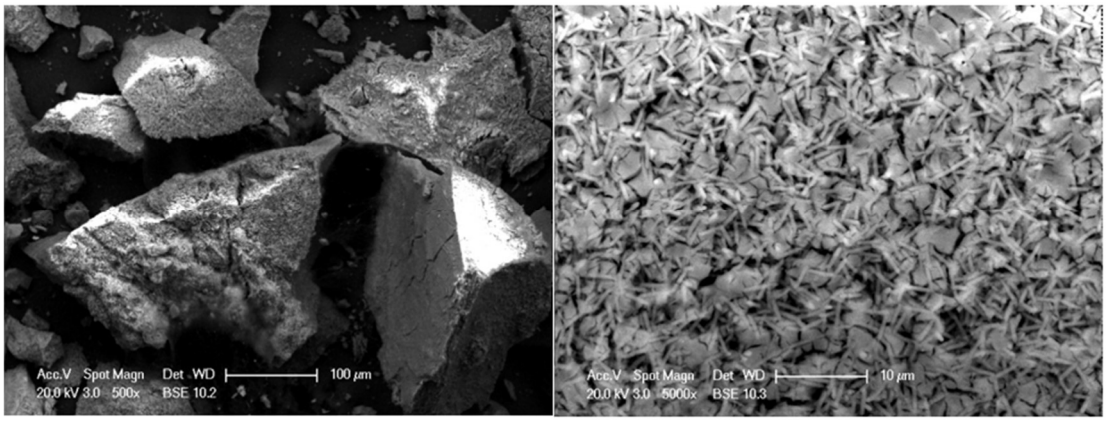

Figure 4.3. SEM images of $Fe^{III}(FA).H_2O$-2 synthesized at 50 ºC.

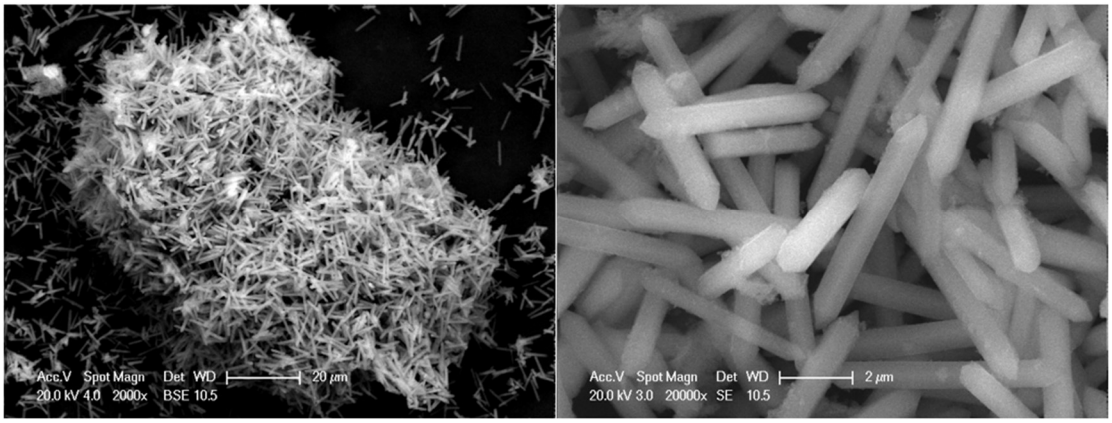

Figure 4.4. SEM images of $Fe^{III}(FA).H_2O$-3 synthesized at 75 ºC.

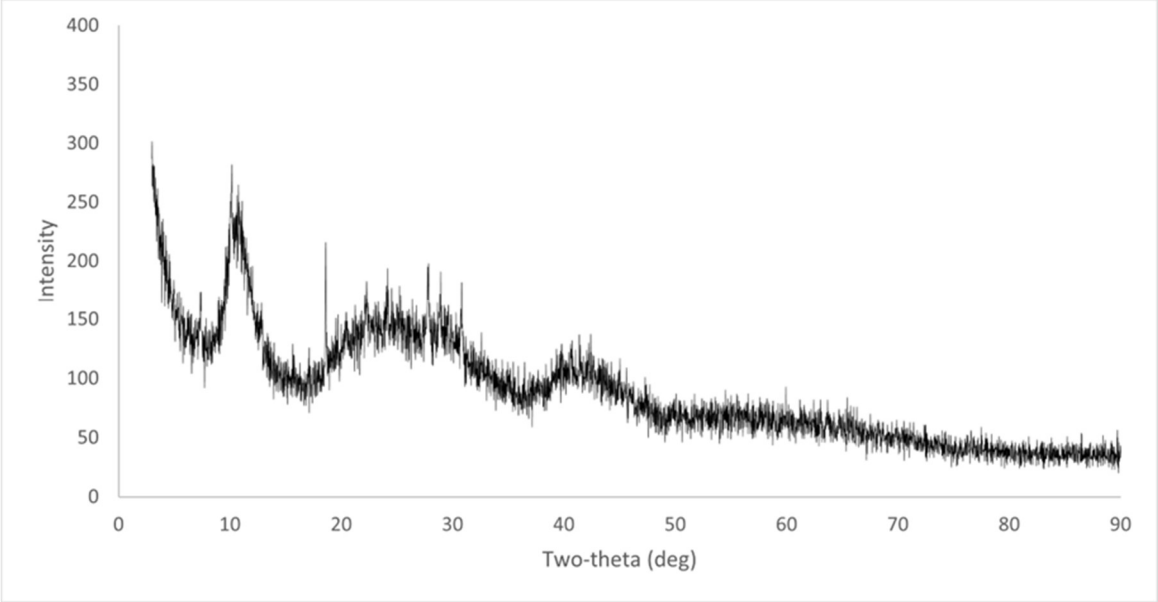

Figure 4.5. XRD pattern of $Fe^{III}(FA).H_2O$-1 synthesized at 20 ºC.

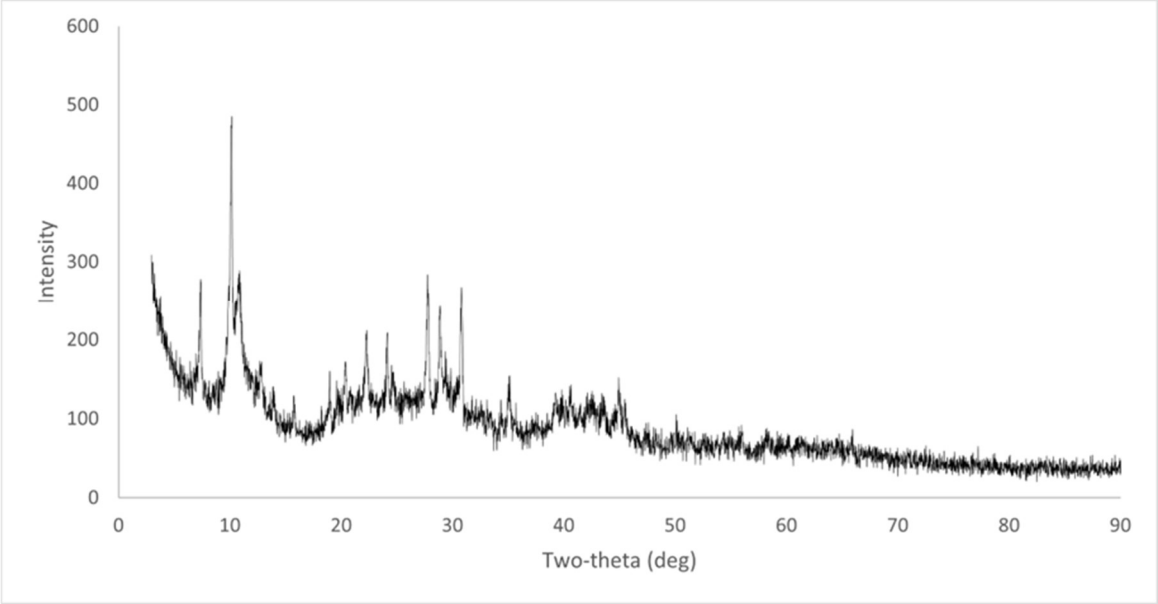

Figure 4.6. XRD pattern of $Fe^{III}(FA).H_2O$-2 synthesized at 50 ºC.

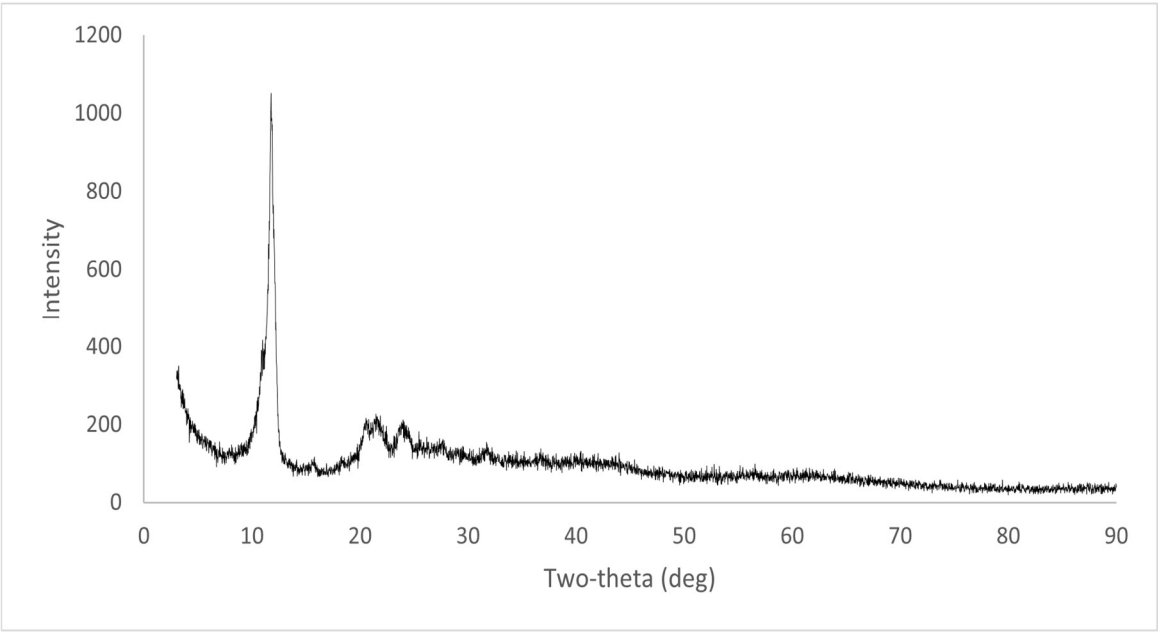

Figure 4.7. XRD pattern of $Fe^{III}(FA).H_2O$-3 synthesized at 75 ºC.

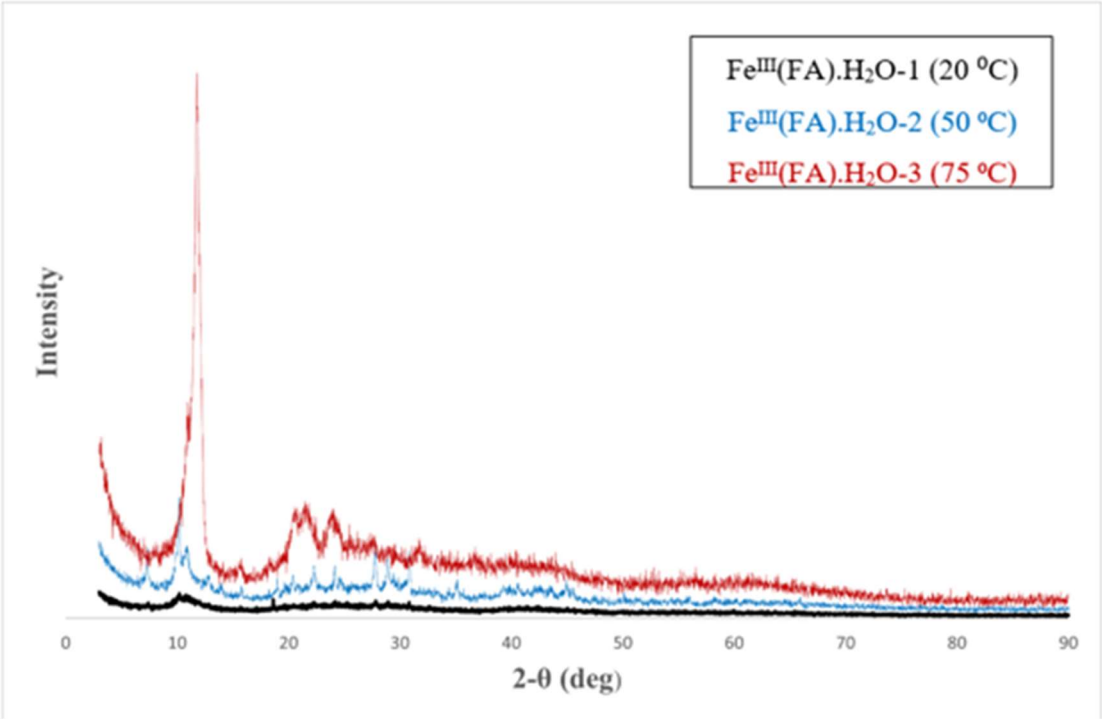

Figure 4.8. Comparison of XRD patterns for Fe^{III}(FA).H$_2$O-1 (20 ºC) in black, Fe^{III}(FA).H$_2$O-2 (50 ºC) in blue, Fe^{III}(FA).H$_2$O-3 (75 ºC) in red.

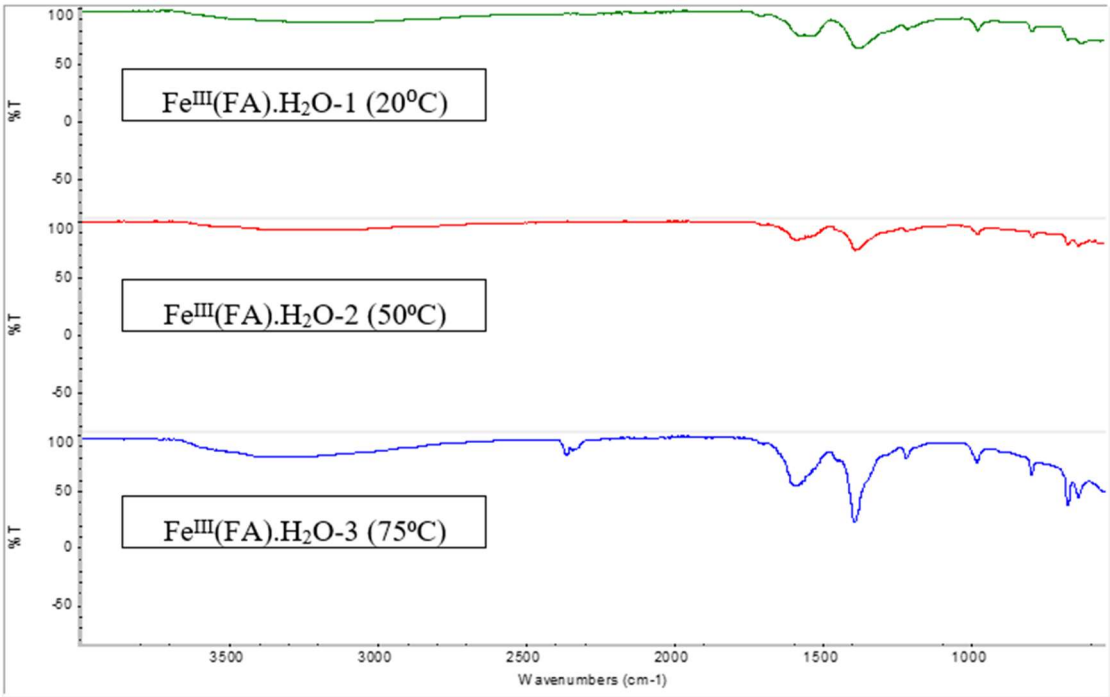

Figure 4.9. IR spectrums for Fe^{III}(FA).H$_2$O-1 (20 ºC) in green, Fe^{III}(FA).H$_2$O-2 (50 ºC) in red, Fe^{III}(FA).H$_2$O-3 (75 ºC) in blue.

As a result of all these analysis in this part, Fe-MOF can be synthesized from iron (III) chloride hexahydride and fumaric acid via sonochemical synthesis method in 90 min at various temperatures (20 ºC, 50 ºC, and 75 ºC). As seen in the SEM results, MOFs synthesized at all three temperatures had hexagonal rod-like structures, but monodispersity of particles increased when temperature was increased. All three XRD patterns had characteristic peaks of iron fumarate at nearly 10º (2θ) and crystallinity of the compounds was increased with increasing temperature. In addition, deprotonation of fumaric acid was seen in all three IR spectrums. Increase in temperature provided faster motions of metal ions and organic ligand molecules and they found each other in shorter time. Therefore, the best crystallization and monodispersed particles were obtained for the synthesis at 75 ºC.

4.2.2. Effect of Concentration on $Fe^{III}(FA).H_2O$

Effect of concentration was studied for 1 mmol, 5 mmol, and 10 mmol starting materials (equivalent amount of metal salts and organic ligands) in 100 ml solvent. Sonochemical synthesis method was used, and synthesis was performed at 75 ºC. Temperature of 75 ºC was selected because high crystallinity was observed at 75 ºC (as seen in section 4.1.1.). The compounds were called as $Fe^{III}(FA).H_2O$-3 for 1 mmol starting materials, $Fe^{III}(FA).H_2O$-4 for 5 mmol starting materials, and $Fe^{III}(FA).H_2O$-5 for 10 mmol starting materials. Since fumaric acid had low solubility in water, ethanol was used as auxiliary solvent to dissolve fumaric acid in $Fe^{III}(FA).H_2O$-4 and $Fe^{III}(FA).H_2O$-5. Although 5 mmol fumaric acid could be soluble in 100 mol water, no precipitate was observed when synthesis performed in only water. All three compounds had same colour of light brown.

Uniform particle distributions were not observed in SEM images of $Fe^{III}(FA).H_2O$-4 and $Fe^{III}(FA).H_2O$-5 (Figure 4.10. and Figure 4.11.). Result for the SEM image of $Fe^{III}(FA).H_2O$-3 was explained in section 4.1.1. According to SEM images, the compound had porous structure.

Characteristic XRD peaks at 10.2º and 10.8º (2θ) were observed for $Fe^{III}(FA).H_2O$-4 and $Fe^{III}(FA).H_2O$-5 (Figure 4.12. and Figure 4.13.). Peaks at between 20º and 30º (2θ) probably came from impurities like iron oxide because oxygen in the air could react with iron ions in the reaction mixture. XRD patterns for $Fe^{III}(FA).H_2O$-4 and $Fe^{III}(FA).H_2O$-5 were seemed very similar except intensity numbers. Comparison of XRD patterns for $Fe^{III}(FA).H_2O$-3, $Fe^{III}(FA).H_2O$-4, and $Fe^{III}(FA).H_2O$-5 were given in the Figure 4.14. and decrease in crystallinity of the compounds with increasing the concentration of starting materials were noted in the XRD patterns.

IR spectrums of $Fe^{III}(FA).H_2O$-4 and $Fe^{III}(FA).H_2O$-5 were similar IR spectrums in Section 4.1. Peaks at nearly 1550 cm^{-1} were related C=C stretching band, and peaks at nearly 1380 cm^{-1} were related C-O stretching band in the IR spectrums of $Fe^{III}(FA).H_2O$-4 and $Fe^{III}(FA).H_2O$-5 (Figure 4.15.).

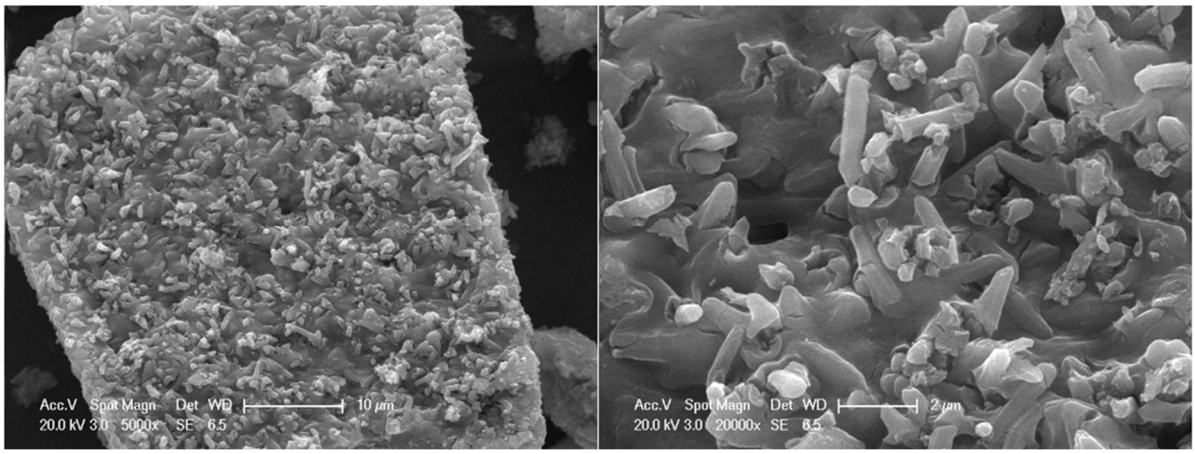

Figure 4.10. SEM images of $Fe^{III}(FA).H_2O$-4 with 5 mmol starting materials.

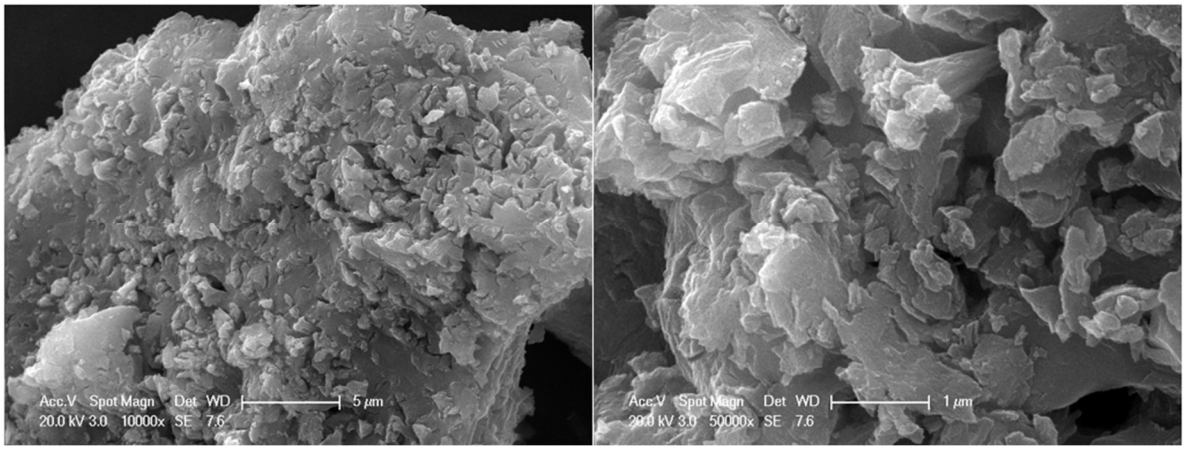

Figure 4.11. SEM images of $Fe^{III}(FA).H_2O$-5 with 10 mmol starting materials.

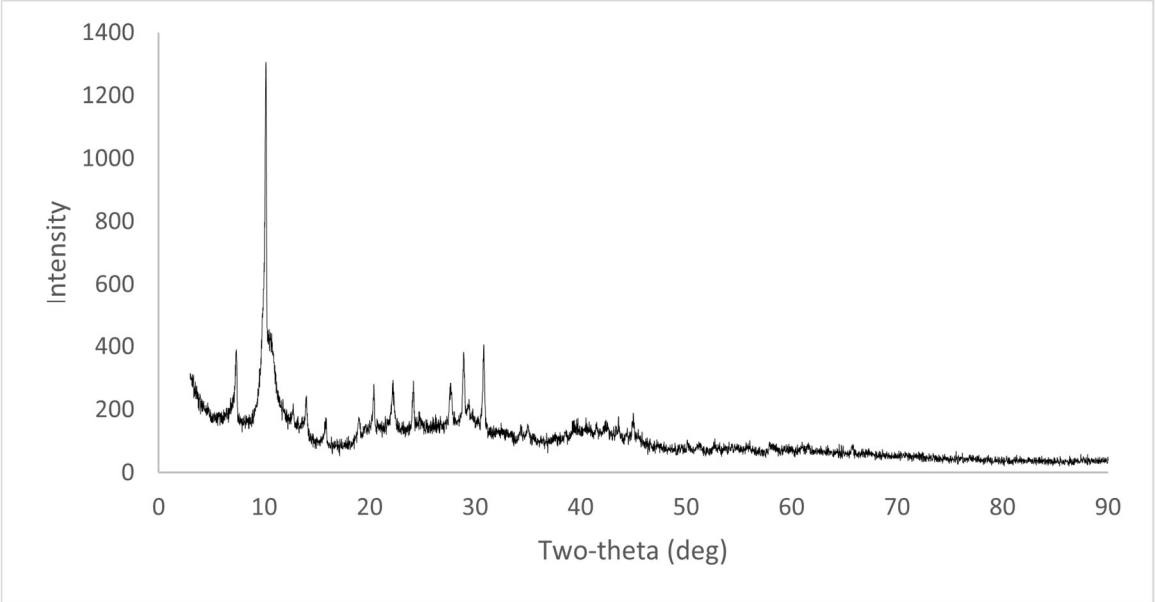

Figure 4.12. XRD pattern of $Fe^{III}(FA).H_2O$-4 with 5 mmol starting materials.

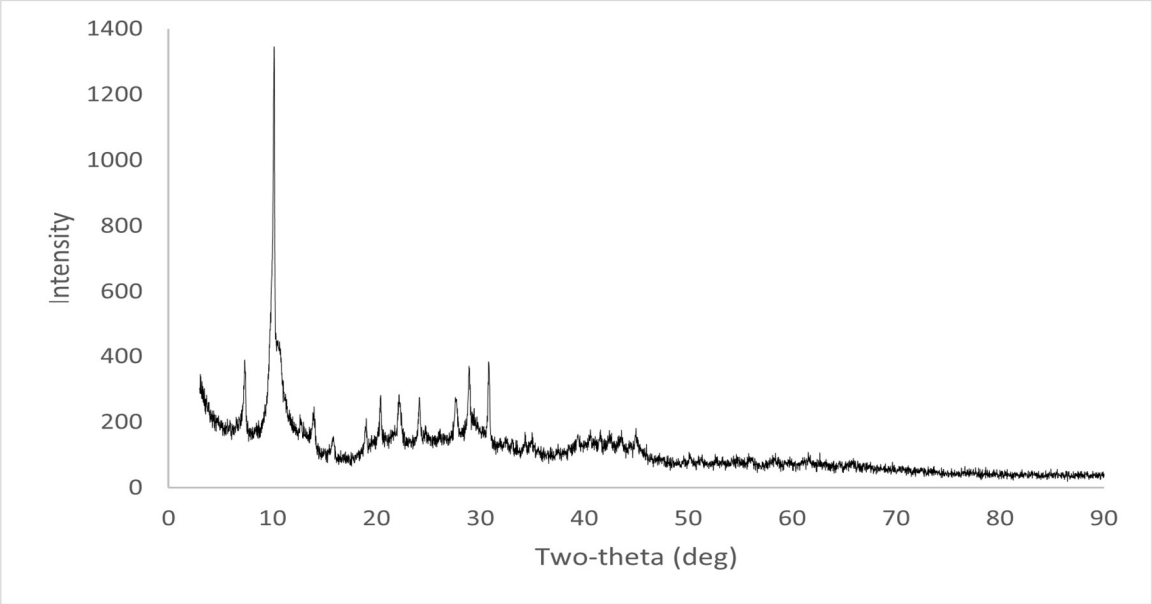

Figure 4.13. XRD pattern of $Fe^{III}(FA).H_2O$-5 with 10 mmol starting materials.

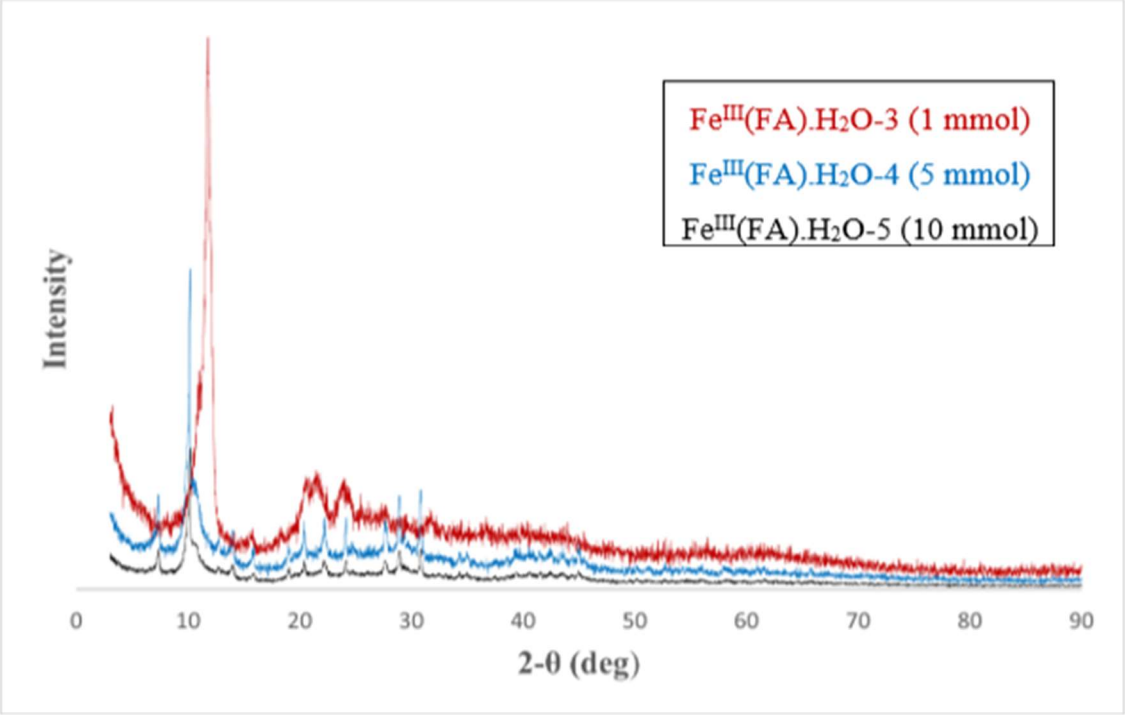

Figure 4.14. Comparison of XRD patterns for $Fe^{III}(FA).H_2O$-3 (1 mmol) in red, $Fe^{III}(FA).H_2O$-4 (5 mmol) in blue, $Fe^{III}(FA).H_2O$-5 (10 mmol) in black.

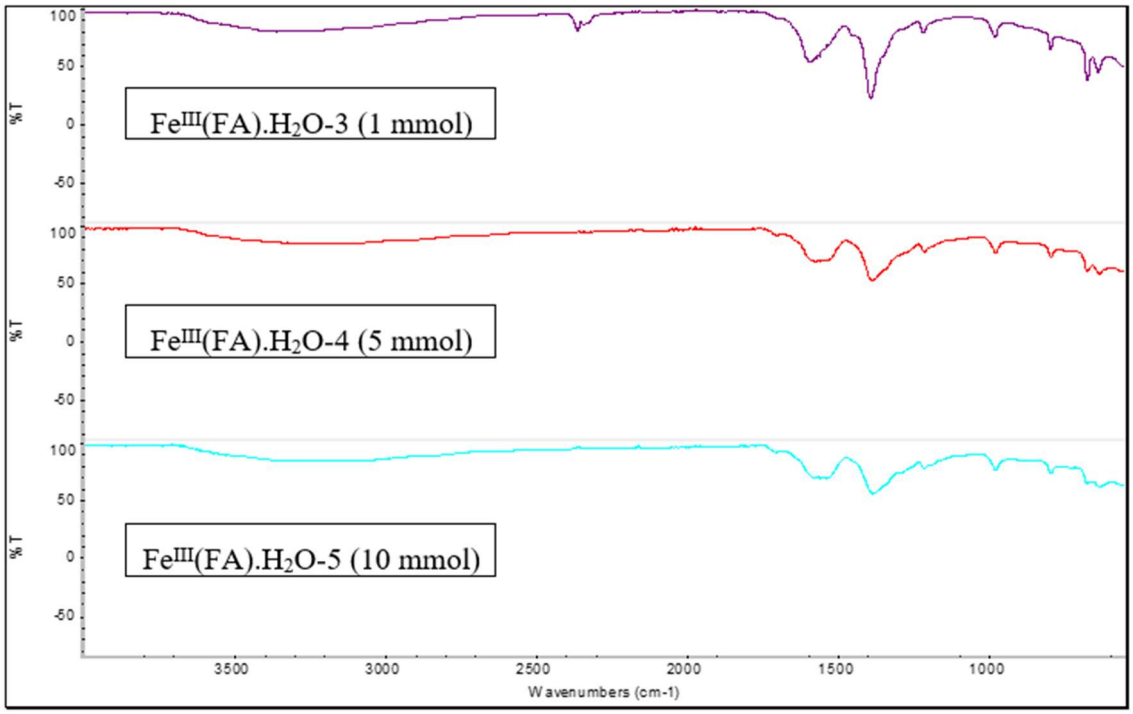

Figure 4.15. IR spectrums for Fe^{III}(FA).H$_2$O-3 (1 mmol) in purple, Fe^{III}(FA).H$_2$O-4 (5 mmol) in red, Fe^{III}(FA).H$_2$O-5 (10 mmol) in blue.

In conclusion of effect of concentration on Fe^{III}(FA).H$_2$O, fumaric acid was dissolved in water and ethanol mixture because of low solubility of fumaric acid in water. Uniform particle distribution was observed in Fe^{III}(FA).H$_2$O-3 that synthesized with 1 mmol starting materials, while it was not observed in Fe^{III}(FA).H$_2$O-4, and Fe^{III}(FA).H$_2$O-5 that were synthesized with 5 mmol and 10 mmol starting materials, respectively. Characteristic peaks of Fe-MOF (from iron (III) chloride hexahydride and fumaric acid) were present in all three XRD patterns. Crystallinity of the compound synthesized at the lowest concentration was found as highest. The cause of this situation could be that reaction possibility of metal ion with fumaric acid decreased with increasing concentration of starting materials.

4.2.3. Effect of pH on Fe^{III}(FA).H$_2$O

This part of the study was aimed that higher yields of the compounds were wanted to obtain with increasing pH of solution of fumaric acid by addition of NaOH because deprotonation of fumaric acid increased with increasing pH of the solution. Effect of

pH=natural (2.57) for $Fe^{III}(FA).H_2O$-3, pH=7 for $Fe^{III}(FA).H_2O$-6, and pH=10 for $Fe^{III}(FA).H_2O$-7 was investigated. $Fe^{III}(FA).H_2O$-3 was light brown coloured crystals and $Fe^{III}(FA).H_2O$-6 and $Fe^{III}(FA).H_2O$-7 were black coloured crystals. Yields were calculated as 44.7% for $Fe^{III}(FA).H_2O$-3, 38.2% for $Fe^{III}(FA).H_2O$-6 and 36.8% for $Fe^{III}(FA).H_2O$-7. When increase in yields with increasing pH of fumaric acid solution was expected, yields of the compounds decreased with increasing pH of the fumaric acid solution.

Figure 4.16. and Figure 4.17. showed SEM images of the compounds. According to SEM images of the compounds, nanoparticles were observed instead of MOF-compounds. It was possible due to the fact that iron ions in the reaction mixture were coated with deprotonated fumaric acid, and this caused formation of iron nanoparticles. Particle size of the nanoparticles was nearly 10 nm. In EDX analysis, C (8.8 w %), O (52.1 w %), and Fe (39.0 w %) for $Fe^{III}(FA).H_2O$-6, and C (3.3 w %), O (35.1 w %), and Fe (61.6 w %) for $Fe^{III}(FA).H_2O$-7 were detected. Result of EDX analysis was consisted with formation of iron nanoparticles.

XRD peaks (at 33.1º (2θ), 35.6º (2θ), 62.3º (2θ), and 63.9º (2θ) for $Fe^{III}(FA).H_2O$-6 and at 33.1º (2θ), 35.6º (2θ), 62.4º (2θ), and 63.9º (2θ) for $Fe^{III}(FA).H_2O$-7) were matched with iron oxide compound (JCPDS number: 89-0597) in database of Boğaziçi University Advanced Technologies Research and Development Center. (Figure 4.18. and Figure 4.19.). Peaks at 35.6º (2θ) and 63.9º (2θ) for $Fe^{III}(FA).H_2O$-6 and $Fe^{III}(FA).H_2O$-7 were labelled to (1 0 0) and (3 0 0), respectively. It was also consisted with literature for formation of iron oxide nanoparticles [111].

When results of SEM images and XRD pattern were compared with literature, similar SEM images and XRD patterns were obtained. Comparison of $Fe^{III}(FA).H_2O$-3, $Fe^{III}(FA).H_2O$-6, and $Fe^{III}(FA).H_2O$-7 was given in the Figure 4.20. to see difference in XRD patterns of MOF-compound and iron oxide nanoparticles.

In IR spectrum of $Fe^{III}(FA).H_2O$-6, there were O-H stretch of fumaric acid at between 3000 and 2500 cm^{-1} and C-OH bend at 1455 cm^{-1} (Figure 4.21.). The reason of this was considered as pH=7 was not enough to deprotonate all fumaric acid compounds in the solution. C=C stretching band was at 1557 cm^{-1} and C-O stretching band was at 1373 cm^{-1}. When pH increased to 10, O-H stretch of fumaric acid at between 3000 and 2500 cm^{-1} and C-OH bend at 1455 cm-1 were disappeared. Fumaric acid was fully deprotonated at pH=10.

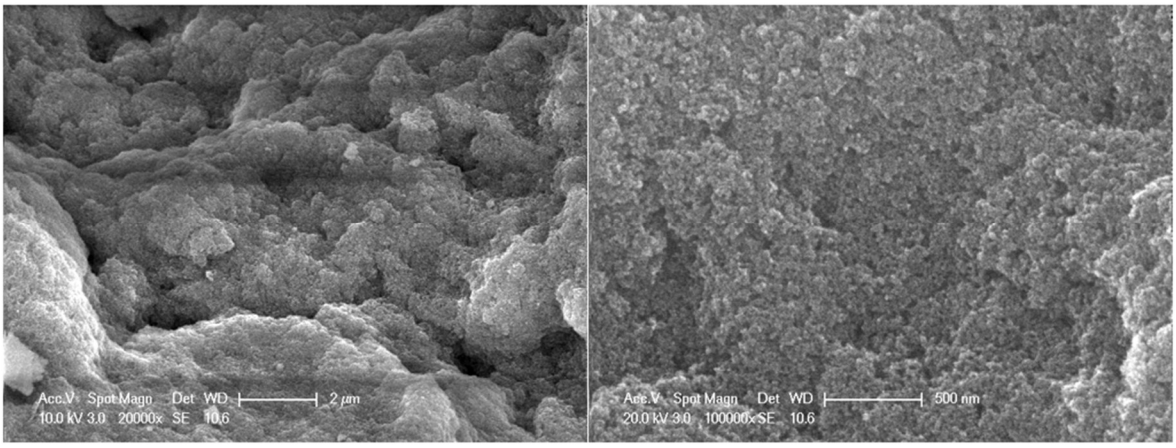

Figure 4.16. SEM images of $Fe^{III}(FA)H_2O$-6 at pH=7.

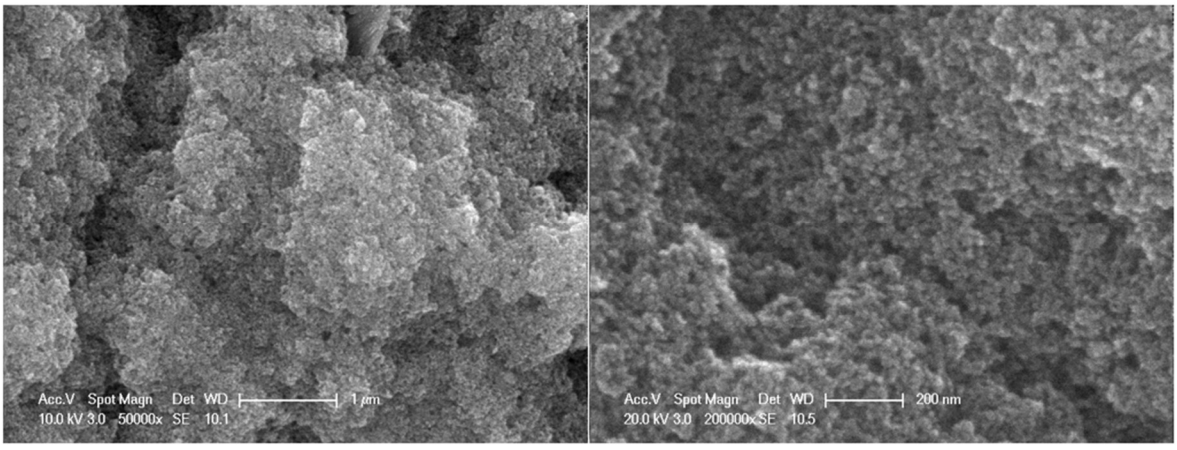

Figure 4.17. SEM images of $Fe^{III}(FA)H_2O$-7 at pH=10.

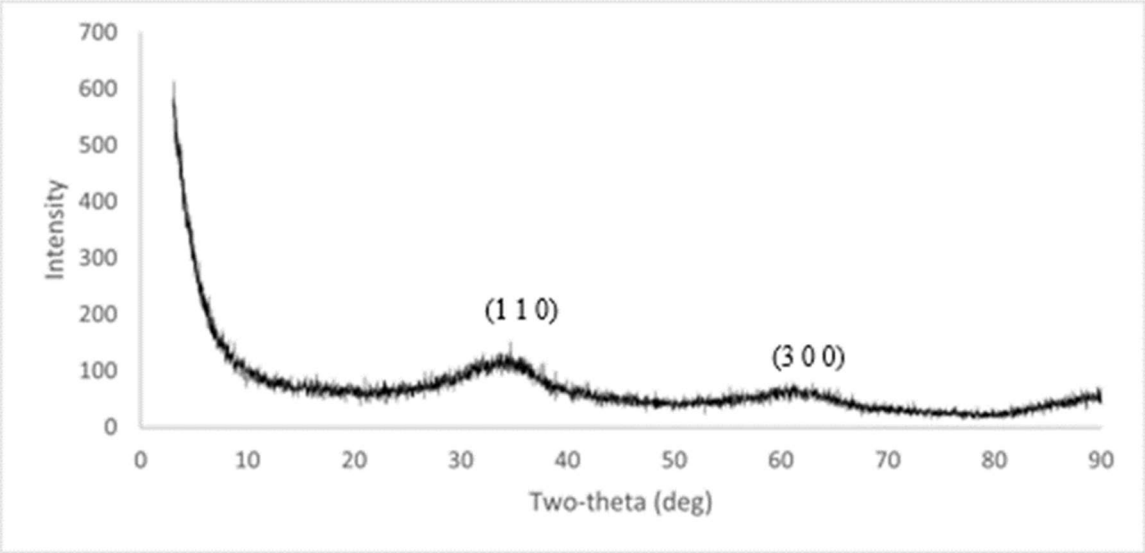

Figure 4.18. XRD pattern of $Fe^{III}(FA).H_2O$-6 at pH=7.

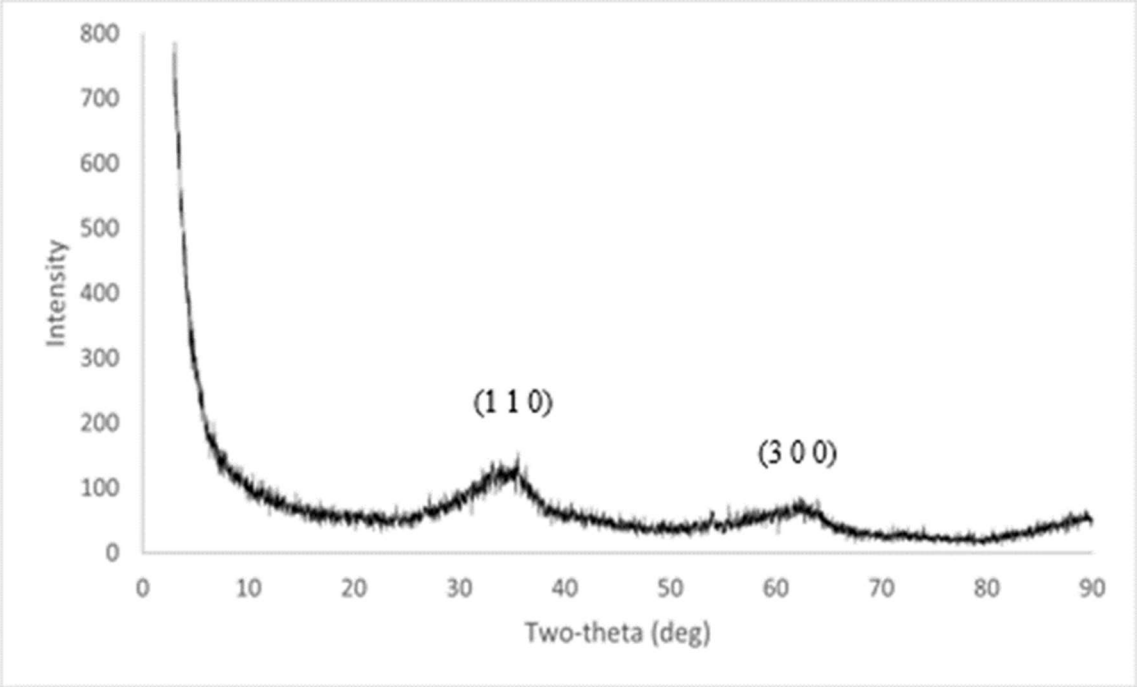

Figure 4.19. XRD pattern of $Fe^{III}(FA).H_2O$-7 at pH=10.

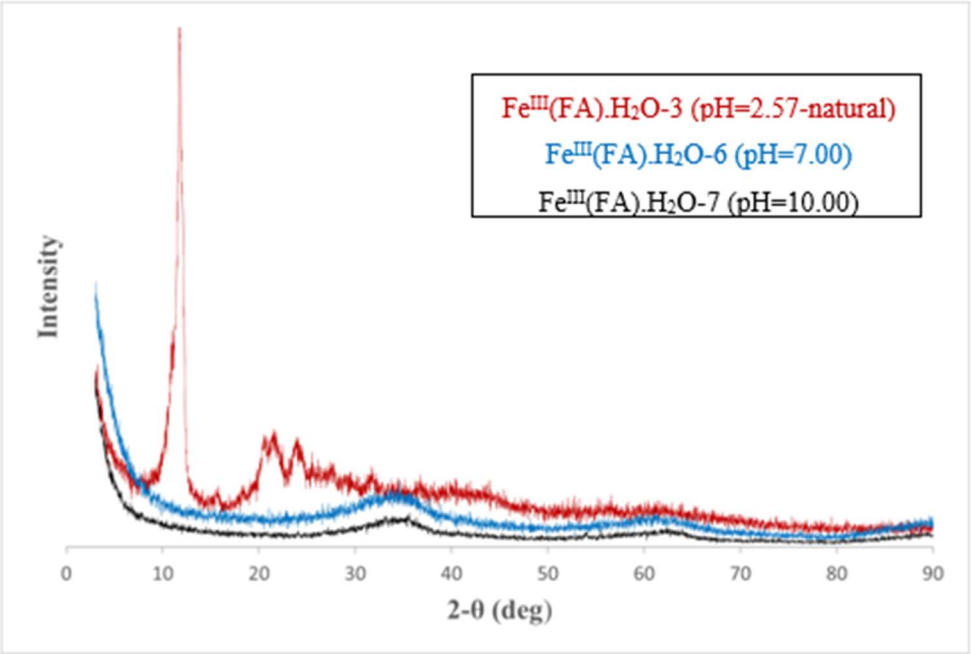

Figure 4.20. Comparison of XRD patterns for Fe^{III}(FA).H$_2$O-3 (pH=2.57-natural) in red, Fe^{III}(FA).H$_2$O-6 (pH=7.00) in blue, Fe^{III}(FA).H$_2$O-5 (pH=10.00) in black.

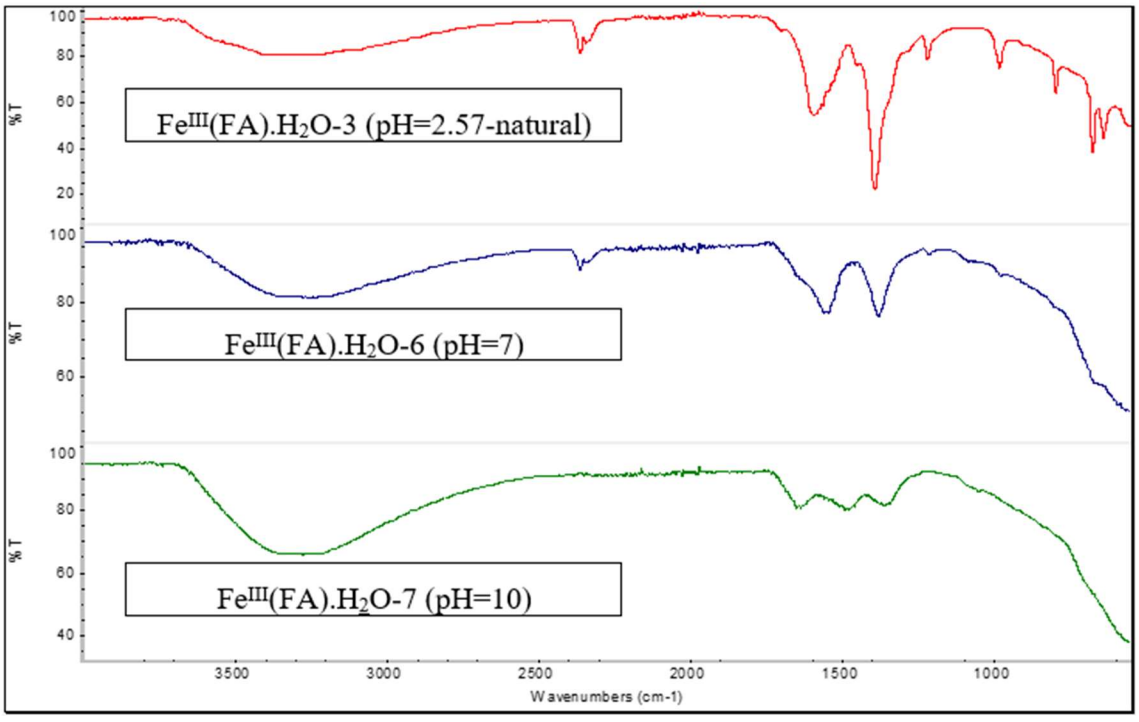

Figure 4.21. IR spectrums for Fe^{III}(FA).H$_2$O-3 (pH=2.57-neutral) in red, Fe^{III}(FA).H$_2$O-6 (pH=7) in blue, Fe^{III}(FA).H$_2$O-7 (pH=10) in green.

This part of the research was aimed to study the pH effect on MOF structures, but nanoparticle formation was observed instead of metal organic framework when pH was increased using sodium hydroxide. Formation of nanoparticles was confirmed with XRD analysis and SEM images of the compounds.

4.2.4. Effect of Metal Ion on M(TPA).DMF (M=Fe, Co, Ni, and Co/Ni)

Terephthalic acid was used as organic linker to synthesize iron, cobalt, nickel, and cobalt/nickel bimetallic MOFs. Since terephthalic acid had low solubility in water, DMF was used as solvent and triethanol amine (TEA) was used for deprotonating agent. All syntheses were performed at 75 ºC via sonochemical synthesis method. Colour of the compounds changed as metal ion changed. Dark orange coloured compound for Fe^{III}(TPA).DMF, light pink coloured compound for Co^{II}(TPA).DMF, light blue coloured compound for Ni^{II}(TPA).DMF, and light blue compound for Co^{II}/Ni^{II}(TPA).DMF were obtained.

SEM images of Fe^{III}(TPA).DMF showed particle size as nearly 10 nm (Figure 4.22.). Flower-like shapes were observed in SEM images of Co^{II}(TPA).DMF, particles of Ni^{II}(TPA).DMF had rectangular shape, and Co^{II}/Ni^{II}(TPA).DMF contained mixed shapes of Co^{II}(TPA).DMF and Ni^{II}(TPA).DMF (Figure 4.23., Figure 4.24., and Figure 4.25.). C (30.3 w %), O (30.2 w %), and Fe (32.1 w %) for Fe^{III}(TPA).DMF, C (55.6 w %), O (29.5 w %), and Co (14.9 w %) for Co^{II}(TPA).DMF, C (53.6 w %), O (33.6 w %), and Ni (12.8 w %) for Ni^{II}(TPA).DMF, and C (54.1 w %), O (25.3 w %), Co (9.2 w %), and Ni (6.5 w %) were found in EDX analysis.

No matched with database of Boğaziçi University Advanced Technologies Research and Development Center in XRD patterns of the compounds. Peaks at 6.42º and 13.6º (2θ) for Fe^{III}(TPA).DMF were consistent in the literature [112] (Figure 4.26.). Co^{II}(TPA).DMF, Ni^{II}(TPA).DMF and Co^{II}/Ni^{II}(TPA).DMF had similar XRD patterns, and this is consistent in the literature [107] (JCPDS number: 36-1451) and XRD patterns of these compounds are

seen in Figure 4.27., Figure 4.28., and Figure 4.29. Similarity of XRD pattern of these compounds was due to the fact that Co and Ni had $3d^{7-8}4s^2$ valence electron structures.

In IR spectrum of Fe^{III}(TPA).DMF, O-H stretch from terephthalic acid was not observed at between 3000 and 2500 cm^{-1}, and peaks at 1574 cm^{-1} and 1372 cm^{-1} came from aromatic ring. Terephthalic acid was deprotonated and included in the structure of the compound. In addition, peaks at 1557 cm^{-1} and 1372 cm^{-1} for Co^{II}(TPA).DMF, peaks at 1538 cm^{-1} and 1373 cm^{-1} for Ni^{II}(TPA).DMF, and peaks at 1538 cm^{-1} and 1373 cm^{-1} for Co^{II}/Ni^{II}(TPA).DMF were present in IR spectrums of the compounds. No peak was present at between 3000 and 2500 cm^{-1} in all three compounds (Figure 4.30.).

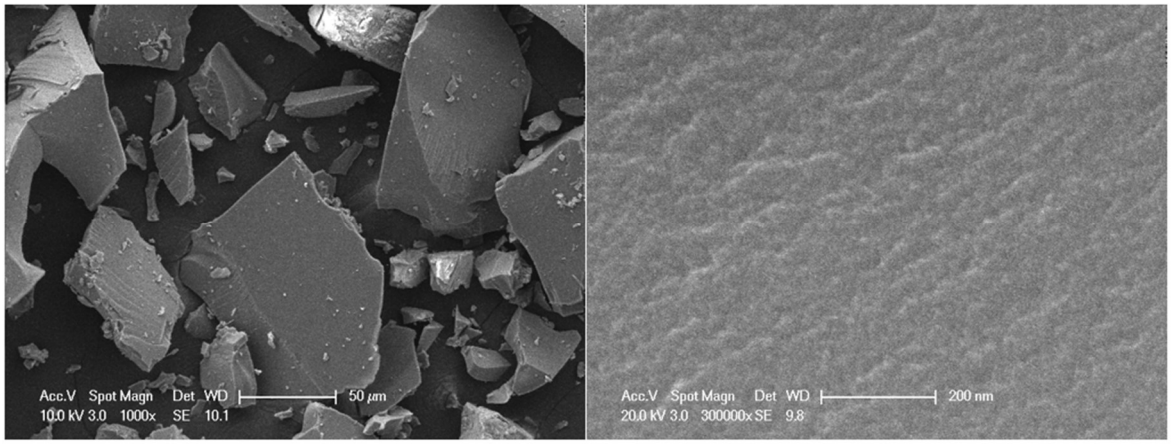

Figure 4.22. SEM images of Fe^{III}(TPA).DMF.

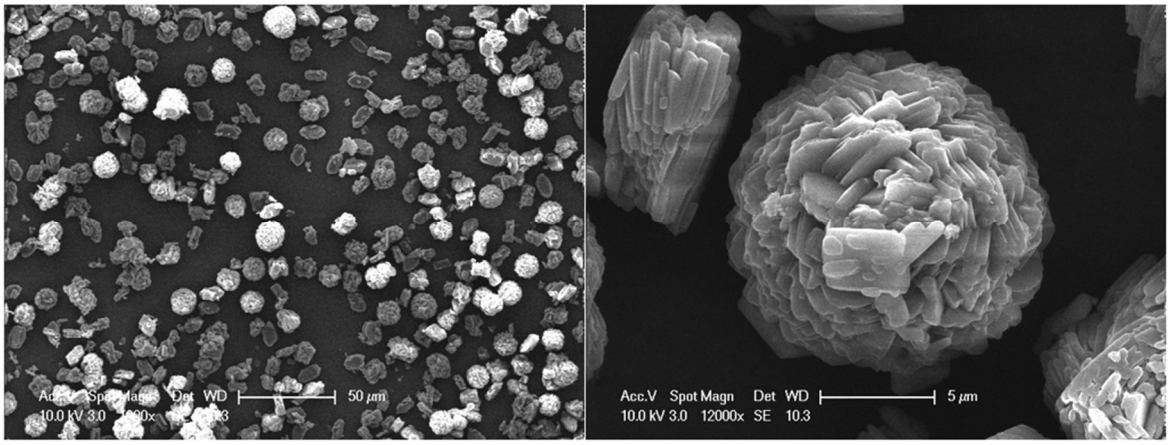

Figure 4.23. SEM images of Co^{II}(TPA).DMF.

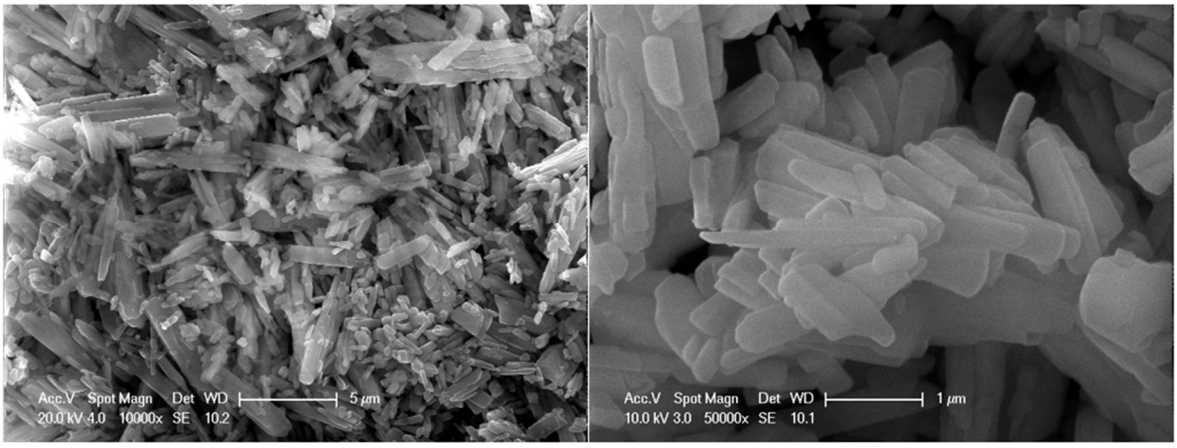

Figure 4.24. SEM images of Ni^{II}(TPA).DMF.

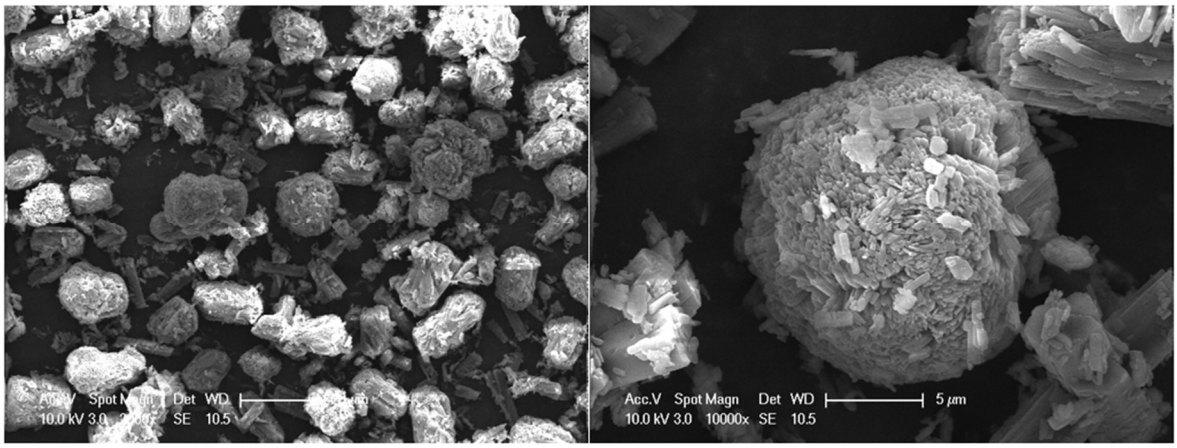

Figure 4.25. SEM images of Co^{II}/Ni^{II}(TPA).DMF.

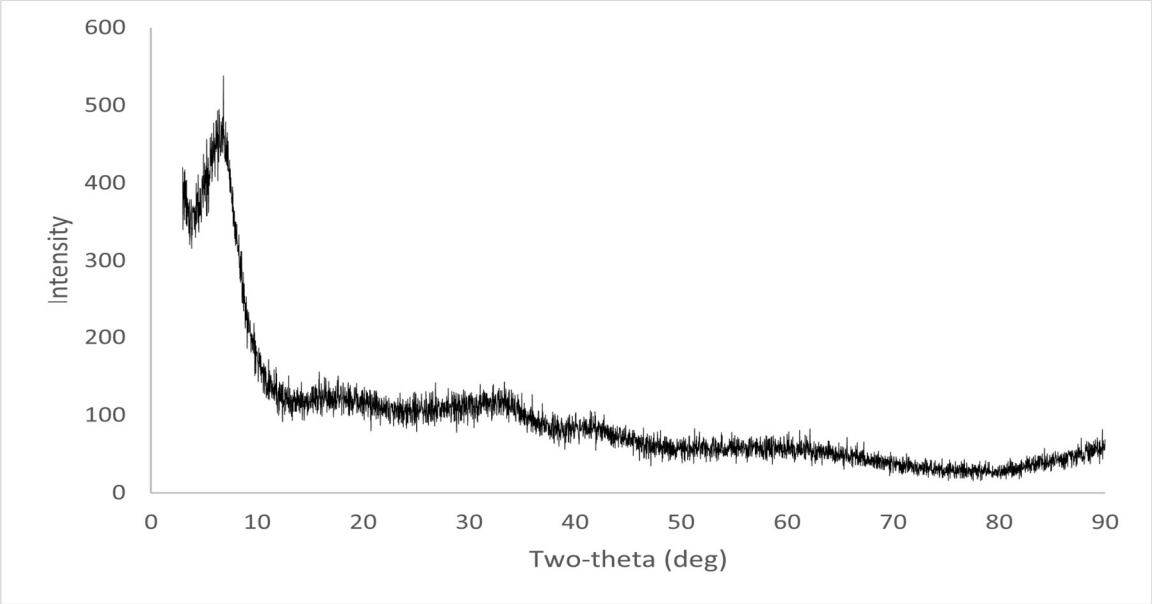

Figure 4.26. XRD pattern of Fe^{III}(TPA).DMF.

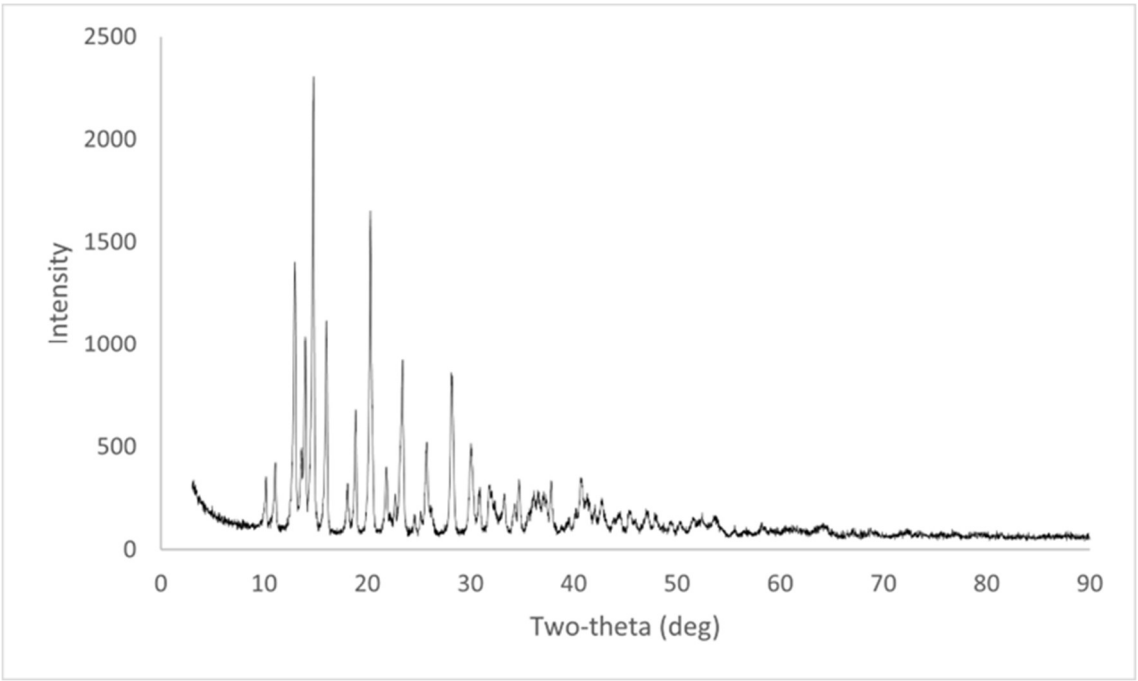

Figure 4.27. XRD pattern of Co^{II}(TPA).DMF.

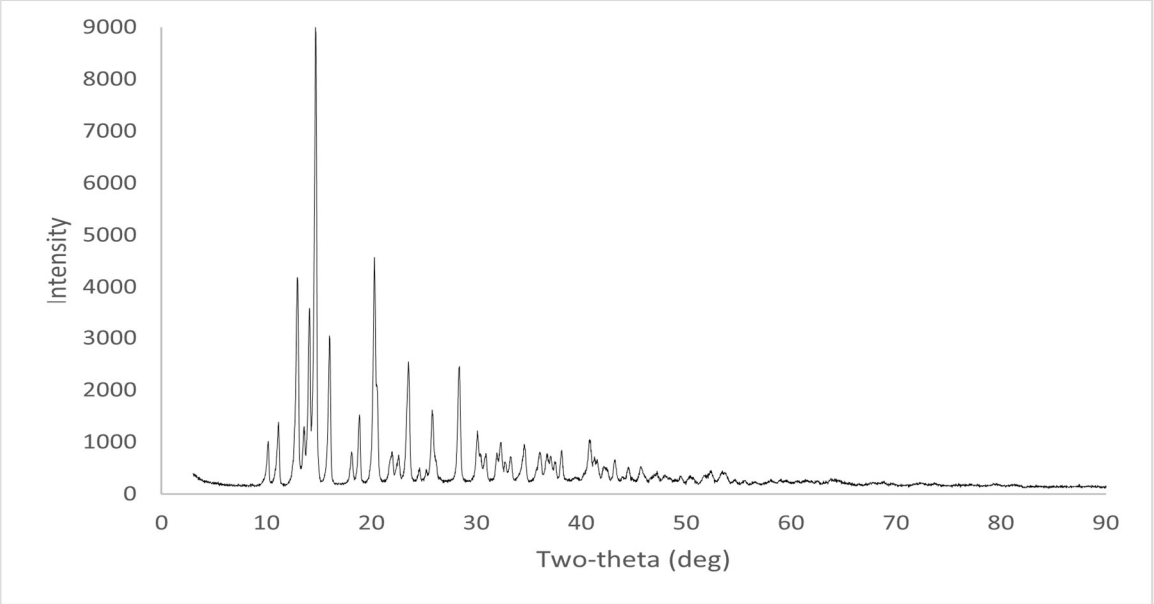

Figure 4.28. XRD pattern of Ni^{II}(TPA).DMF.

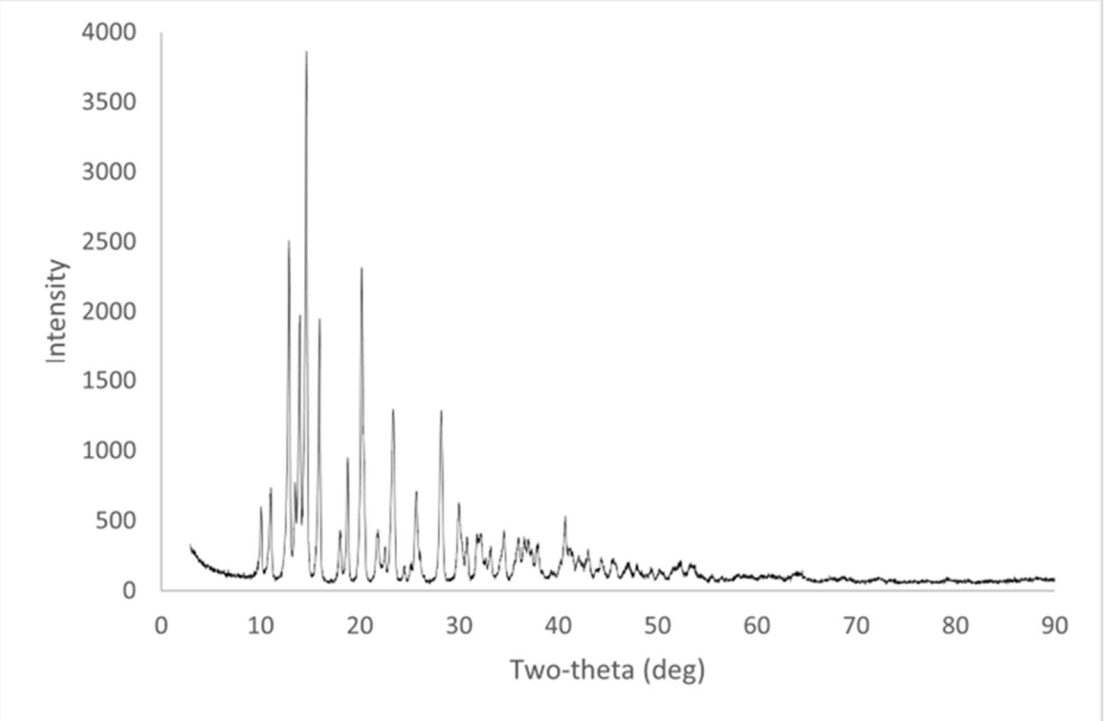

Figure 4.29. XRD pattern of Co^{II}/Ni^{II}(TPA).DMF.

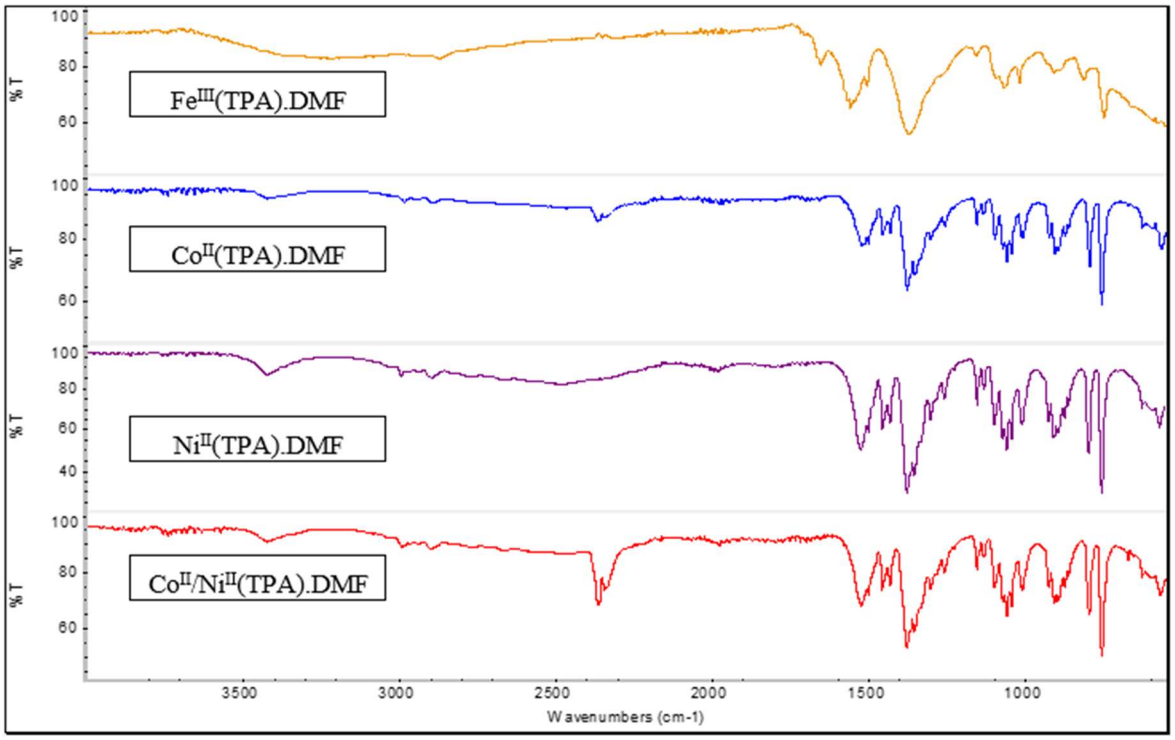

Figure 4.30. IR spectrums for Fe^{III}(TPA).DMF in yellow, Co^{II}(TPA).DMF in blue, Ni^{II}(TPA).DMF in purple, and Co^{II}/Ni^{II}(TPA).DMF in red.

As a result of these analysis, MOF structures were synthesized from ions of iron, cobalt, nickel metals and terephthalic acid via sonochemical synthesis method. Since Fe, Co, Ni had $3d^{6\text{-}8}4s^2$ valence electron structures, XRD patterns of the compounds were expected similar patterns. Co^{II}(TPA).DMF, Ni^{II}(TPA).DMF and Co^{II}/Ni^{II}(TPA).DMF had similar XRD patterns, and they were coherent with the literature. However, Fe^{III}(TPA).DMF had different XRD pattern, and it was also consistent with the literature. The reason of this case was considered as coordination of iron ion and terephthalic acid was different when compared to cobalt and nickel ions. As seen in the SEM images, the compounds had their own structures.

4.2.5. Effect of Solvent on M(TPA).H_2O (M=Fe, Co, Ni)

Aim of this part of the study was use of water as solvent instead of DMF because water is cheaper and cleaner solvent than DMF. Since terephthalic acid has low solubility in

water, pH of terephthalic acid solution was adjusted to pH=7 by addition of NaOH. When syntheses made with metal salts in ultrasonic bath at 75 ºC for 90 min only the experiment with iron (III) hexachloride hexahydride was give precipitate. Therefore, pH of terephthalic acid solution was adjusted to pH=10 for cobalt and nickel salts by addition of NaOH and no precipitate was observed for this case. Lastly, triethanol amine (TEA) was used as auxiliary base to increase deprotonation of terephthalic acid and precipitate of Co^{II}(TPA).H_2O and Ni^{II}(TPA).H_2O was obtained. The compounds were characterized with using SEM/EDX and XRD techniques.

SEM images were given in Figure 4.31, Figure 4.32, and Figure 4.33. Fe^{III}(TPA).H_2O had no specific structure and Co^{II}(TPA).H_2O and Ni^{II}(TPA).H_2O had spherical structures. According to EDX analysis, C (43.3 w %), O (35.8 w %), and Fe (20.53 w %) in Fe^{III}(TPA).H_2O, C (13.7 w %), O (23 w %), and Co (61.8 w %) in Co^{II}(TPA).H_2O, and C (14.7 w %), O (29.3 w %), and Ni (54 w %) in Ni^{II}(TPA).H_2O were found.

All peaks in XRD pattern of Fe^{III}(TPA).H_2O were matched with Fe_3O_4 (JCPDS number: 89-0951) and terephthalic acid (JCPDS number: 31-1916) and peaks at 17.3º and 28º (2θ) might be indexed to (1 1 0) and (2 0 0) from terephthalic acid and peak at 30º (2θ) might be indexed to (2 2 0) from magnetite. No characteristic peaks at 6.42º and 13.6º (2θ) for Fe^{III}(TPA).DMF were found (Figure 4.34.). According to SEM/EDX and XRD results of Fe^{III}(TPA).H_2O, the compound did not have structure of metal organic framework. XRD patterns of Co^{II}(TPA).H_2O and Ni^{II}(TPA).H_2O were very similar (Figure 4.35., Figure 4.36., and Figure 4.37.). Similarity was expected because of their $3d^{7\text{-}8}4s^2$ valence electron structures. However, XRD patterns of Co^{II}(TPA).H_2O and Ni^{II}(TPA).H_2O were not matched with XRD patterns at section 4.2.4. the patterns were matched with cobalt hydroxide and nickel hydroxide in the literature [113,114]. Reason of this case was considered as that cobalt and nickel ions first reacted hydroxide ion from NaOH and there was no free cobalt or nickel ions remained to react with deprotonated terephthalic acid.

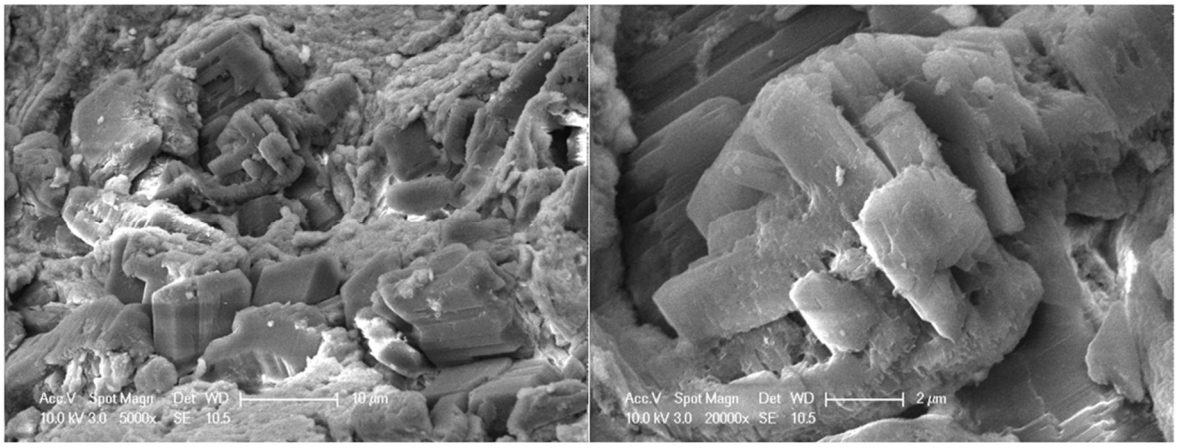

Figure 4.31. SEM images of $Fe^{III}(TPA).H_2O$.

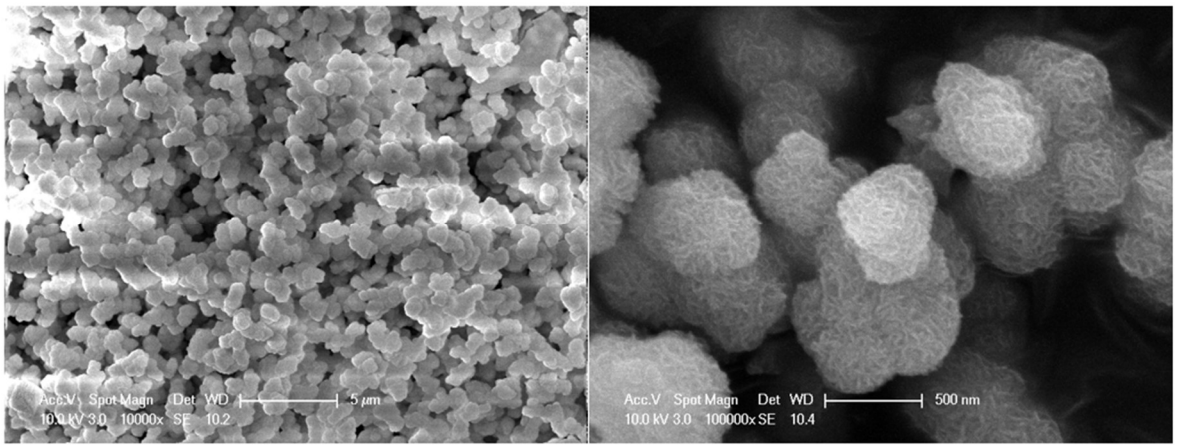

Figure 4.32. SEM images of $Co^{II}(TPA).H_2O$.

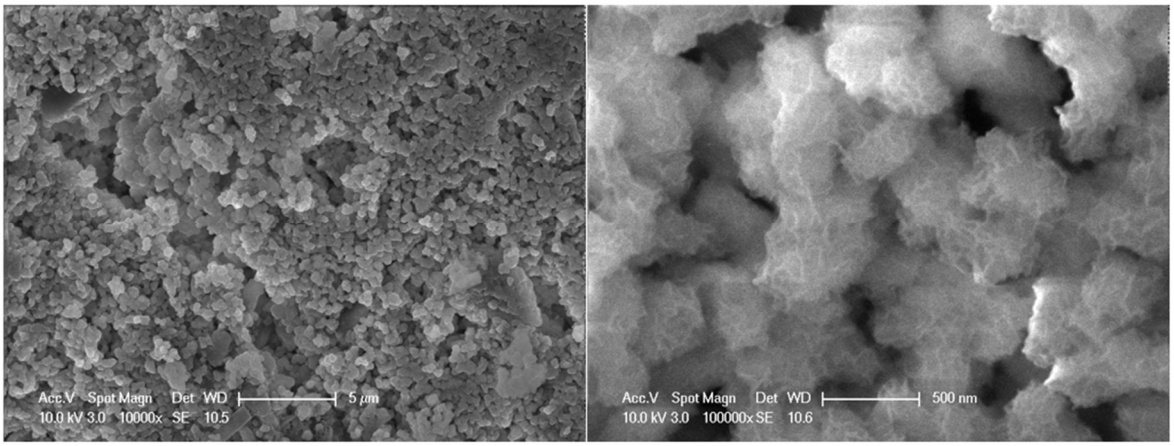

Figure 4.33. SEM images of $Ni^{II}(TPA).H_2O$.

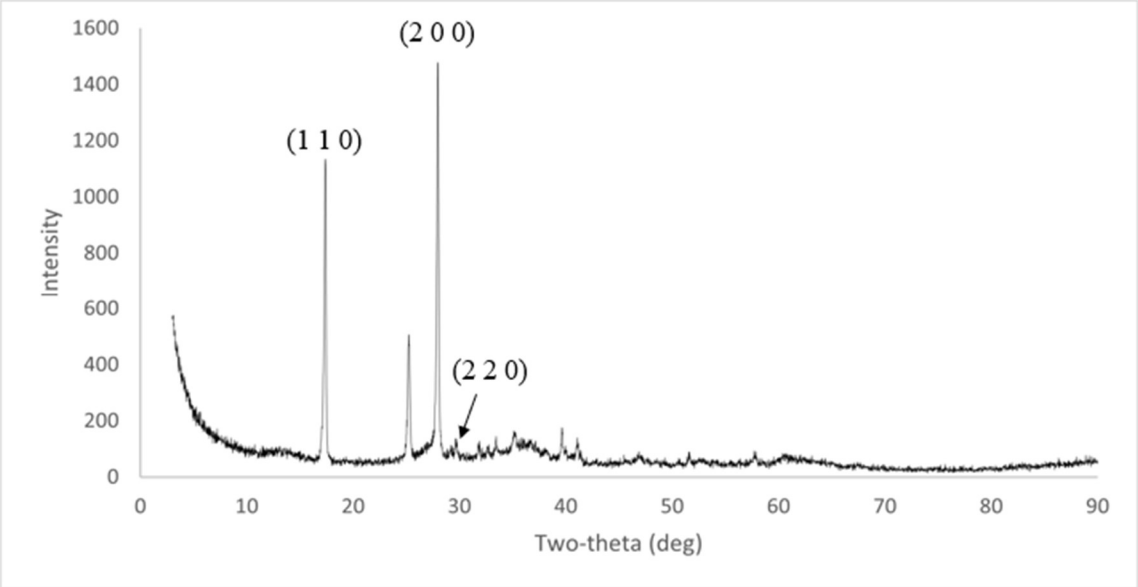

Figure 4.34. XRD pattern of $Fe^{III}(TPA).H_2O$.

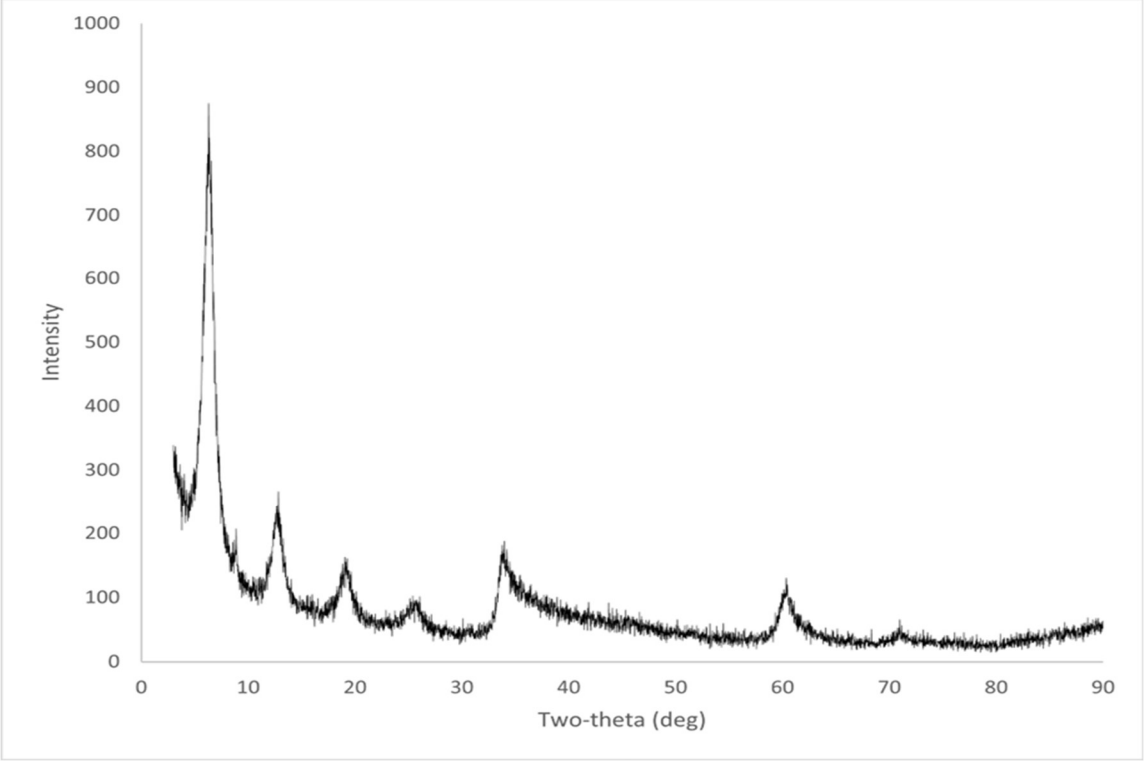

Figure 4.35. XRD pattern of $Co^{II}(TPA).H_2O$.

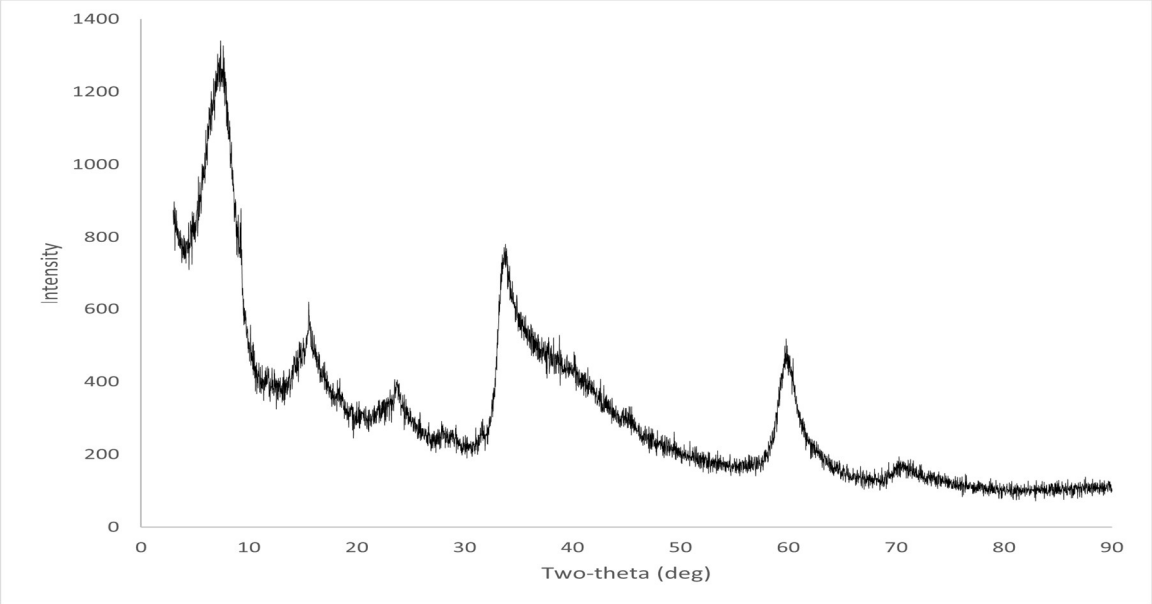

Figure 4.36. XRD pattern of $Ni^{II}(TPA).H_2O$.

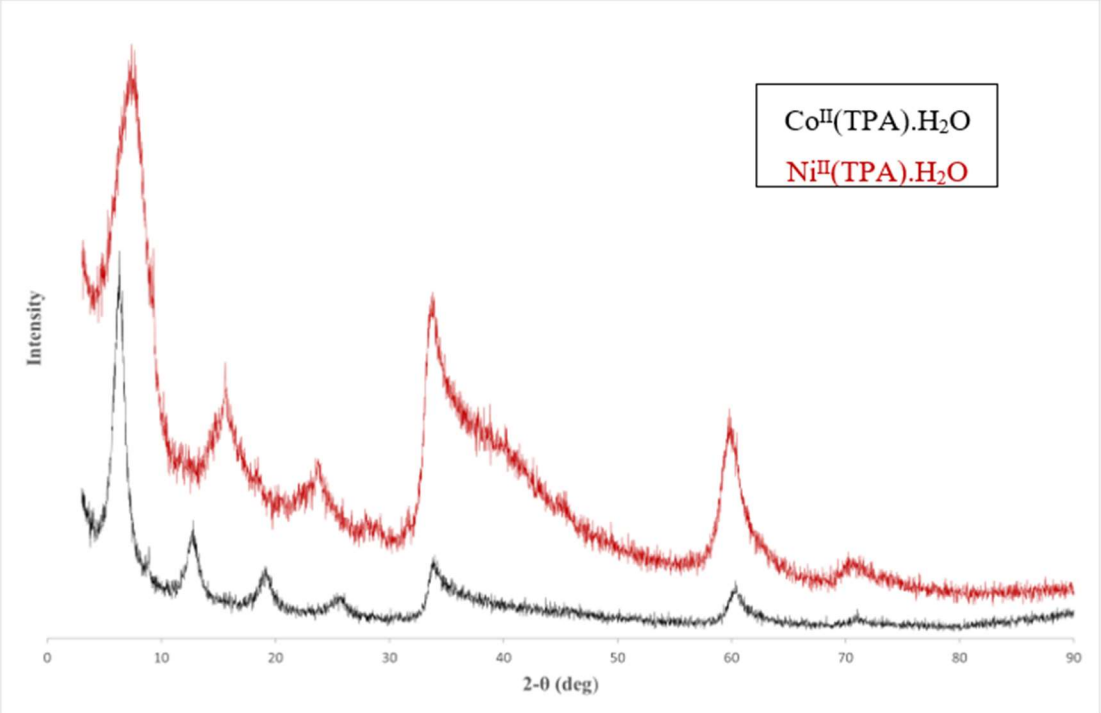

Figure 4.37. Comparison of XRD patterns for $Co^{II}(TPA).H_2O$ in black and $Ni^{II}(TPA).H_2O$ in red.

This study was aimed to use water instead of DMF. Since terephthalic acid has low solubility in water, pH=7 and 10 by addition of sodium hydroxide were studied in order to deprotonate TPA. Only iron gave precipitate at pH=7 and cobalt and nickel gave precipitate at pH=10 when using auxiliary base (TEA). Increase in pH caused formation of Fe_3O_4 for Fe^{III}(TPA).H_2O and cobalt hydroxide and nickel hydroxide for Co^{II}(TPA).H_2O and Ni^{II}(TPA).H_2O, respectively. As a conclusion of this study, changing solvent as water instead of DMF and increasing pH for deprotonation of terephthalic acid was not found as successful way to synthesize MOF structures.

5. CONCLUSION

This study is aimed to synthesize compounds that are Fe with fumaric acid-based MOFs and Fe, Co, and Ni with terephthalic acid-based MOFs in 90 minutes via sonochemical method for the first time and then, characterize these compounds by using XRD analysis, SEM/EDX images, and IR spectrums. The compounds were synthesized for the first time in 90 minutes via sonochemical synthesis method and synthesis time of MOF compounds were shorter when compared with conventional methods. Also, effects of temperature, concentration, pH, metal ion, and solvent on synthesis of these compounds were investigated for the first time.

Effect of temperature on $Fe^{III}(FA).H_2O$ material was found as increase in synthesis temperature leaded better crystallinity of the compound because motions of metal ions and organic linker increased with increasing temperature and their possibility of finding each other increased. As seen in SEM images of the compounds, they had hexagonal rod-like structures. Also, monodispersity of the compounds was increased with increasing temperature.

On the other hand, uniform particle distributions were not observed when concentration of starting materials was increased from 1 mmol to 5 mmol and 10 mmol. The all three compounds synthesized with 1 mmol, 5 mmol, and 10 mmol had characteristic iron-fumaric acid metal organic framework peaks in their XRD patterns and crystallinity of the compounds decreased with increasing the concentration of starting materials.

Main idea of studying higher pH was increasing yield of Fe-MOF materials and pH of fumaric acid solution was increased to 7 and 10 for better deprotonation of fumaric acid. Because reaction between metal ion and organic ligand was considered as faster when deprotonation rate of organic ligand increases. However, decrease in yield was obtained with increasing pH of fumaric acid solution and iron nanoparticles were formed instead of MOF

structures. It was probably due to the fact that iron ions in the synthesis mixture reacted with oxygen, and they were coated with deprotonated fumaric acid.

Fe, Co, Ni metals was chosen because of abundant and common metal salts and similar valence electron structures. When XRD patterns of Co^{II}(TPA).DMF, Ni^{II}(TPA).DMF, and Co^{II}/Ni^{II}(TPA).DMF had similar peaks, XRD pattern of Fe^{III}(TPA).DMF had different than the others. The reason for this case could be that coordination of Fe ion and terephthalic acid had different crystal structure than Co and Ni ions.

Lastly, we wanted to change solvent with water instead of DMF because water is abundant and easily removable solvent when compared to DMF. Since terephthalic acid has low solubility in water, the solution of TPA was adjusted to higher pH (7 and 10). However, iron oxides, cobalt (II) hydroxide, and nickel (II) hydroxide were obtained instead of MOF structures.

In conclusion, this study shows how temperature, concentration of starting materials, pH of organic ligand solution, using different metal salts, and solvent affect the synthesis of Fe, Co, Ni based metal organic frameworks via sonochemical synthesis method and analysis results of the compounds can be a library for future works.

6. FUTURE WORK

The surface area of metal organic frameworks (MOFs) synthesized in this study is needed to measure by using BET theory so that the potential of MOFs as a storage material for different gases such as hydrogen, methane, carbon dioxide and etc. However, the surface area measurements are not completed by good nitrogen adsorption-desorption isotherms. It may be due to shorter degassing time or lower degassing temperature. Therefore, BET surface area analysis can be repeated by extending the degassing time or raising the degassing temperature. Increase in temperature may damage the bonding between metal ions and organic linkers. This case should be considered.

JCPDS numbers of the compounds synthesized for this study were matched with database of research and development center in Boğaziçi University were given in related sections and XRD patterns of the compounds had no match were compared with XRD patterns of related compounds in literature. JCPDS or PDF file numbers for most MOF structured compounds were not given in articles. Therefore, further details in XRD patterns of the compounds are needed and detailed XRD analysis for these compounds will be completed in the near future.

Performance of synthesized metal organic frameworks should be tested in some applications such as gas adsorption and storage, catalysis, electrochemistry. Also, synthesized compounds can be calcinated at different temperatures and porous metal oxides can be obtained for appropriate applications.

In addition, since synthesis was made by sonochemical synthesis method, frequency or power of ultrasound can be changed, or ultrasonic probes can be used instead of ultrasonic bath because ultrasound hits the wall of a beaker and power of ultrasound decreases. Ultrasonic probes are put in reaction mixture, directly. Therefore, using ultrasonic probes

can be more efficient than ultrasonic baths. Effect of change in frequency or power of ultrasound on metal organic framework compounds can be investigated.

The syntheses of metal organic frameworks from cobalt and nickel salts and fumaric acid as an organic linker are tried via the same procedure of Fe^{III}(TPA).H_2O-3 synthesis. However, no precipitate was obtained. Therefore, these syntheses can be repeated with using more powerful ultrasonic baths, probes or different solvents or different synthesis method can be tried.

REFERENCES

1. Bennett, T. D., Coudert, F. X., James, S. L., and Cooper, A. I., "The Changing State of Porous Materials", *Nature Materials*, Vol. 20, Issue 9, pp. 1179–1187, 2021.

2. International Union of Pure and Applied Chemistry Physical Chemistry Division Commission on Colloid and Surface Chemistry, Subcommittee on Characterization of Porous Solids: "Recommendations for the Characterization of Porous solids (Technical Report)", *Pure Applied Chemistry*, Vol. 66 (8), pp. 1739–1758, 1994.

3. Brandon, N. P., and Brett, D. J., "Engineering Porous Materials for Fuel Cell Applications", *Philosophical Transactions of the Royal Society A: Mathematical, Physical and Engineering Sciences*, Vol. 364, pp. 147–159, 2005.

4. Chen, Y. Z., Cai, G., Wang, Y., Xu, Q., Yu, S. H., and Jiang, H. L., "Palladium Nanoparticles Stabilized with N-doped Porous Carbons Derived from Metal-Organic Frameworks for Selective Catalysis in Biofuel Upgrade: The Role of Catalyst Wettability", *Green Chemistry*, Vol. 18, No. 5, pp. 1212–1217, 2016.

5. Tan, H., Ma, C., Gao, L., Li, Q., Song, Y., Xu, F., Wang, T., and Wang, L., "Metal-Organic Framework-Derived Dopper Nanoparticle@carbon Nanocomposites as Peroxidase Mimics for Colorimetric Sensing of Ascorbic Acid", *Chemistry - A European Journal*, Vol. 20, pp. 16377–16383, 2014.

6. Chen, J., Jiang, L., Wang, W., Wang, P., Li, X., Ren, H., and Wang, Y., "Facile Construction of Highly Porous Carbon Materials Derived from Porous Aromatic Frameworks for Greenhouse Gas Adsorption and Separation", *Microporous and Mesoporous Materials*, Vol. 326, 111385, 2021.

7. Jarosz, R., Szerement, J., Gondek, K., and Mierzwa-Hersztek, M., "The Use of Zeolites as An Addition to Fertilisers – A Review", *Catena*, Vol. 213, 106125, 2022.

8. Noviello, M., Gattullo, C. E., Faccia, M., Paradiso, V. M., and Gambacorta, G., "Application of Natural and Synthetic Zeolites in the Oenological Field", *Food Research International*, Vol. 150, 110737, 2021.

9. Montalvo, S., Guerrero, L., Borja, R., Sánchez, E., Milán, Z., Cortés, I., and Angeles de la Rubia, M., "Application of Natural Zeolites in Anaerobic Digestion Processes: A Review", *Applied Clay Science*, Vol. *58*, pp. 125–133, 2012.

10. Villa, C. C., Valencia, G. A., López Córdoba, A., Ortega-Toro, R., Ahmed, S., and Gutiérrez, T. J., "Zeolites for Food Applications: A Review", *Food Bioscience*, Vol. 46, 101577, 2022.

11. Eroglu, N., Emekci, M., and Athanassiou, C. G., "Applications of Natural Zeolites on Agriculture and Food Production", *Journal of the Science of Food and Agriculture*, Vol. 97, No. 11, pp. 3487–3499, 2017.

12. Polat, E., Karaca, M., Demir, H., and Onus, A. N., "Use of Natural Zeolite (Clinoptilolite) in Agriculture", *Journal of Fruit and Ornamental Plant Research,* Vol. 12, pp. 183-189, 2004.

13. Manjaiah, K. M., Mukhopadhyay, R., Paul, R., Datta, S. C., Kumararaja, P., and Sarkar, B. (2019). Chapter 13 - Clay Minerals and Zeolites for Environmentally Sustainable Agriculture, Editors Mariano Mercurio, Binoy Sarkar, Alessio Langella, *Modified Clay and Zeolite Nanocomposite Materials: Environmental and Pharmaceutical Applications*. Elsevier, 309–329.

14. Nakhli, S. A. A., Delkash, M., Bakhshayesh, B. E., and Kazemian, H., "Application of Zeolites for Sustainable Agriculture: A Review on Water and Nutrient Retention", *Water, Air, and Soil Pollution,* Vol. 228, No.12, pp. 1–34, 2017.

15. Querol, X., Moreno, N., Umaa, J. C., Alastuey, A., Hernández, E., López-Soler, A., and Plana, F., "Synthesis of Zeolites from Coal Fly Ash: An Overview", *International Journal of Coal Geology*, Vol. 50, No.4, pp. 413–423, 2002.

16. Moshoeshoe, M., Silas Nadiye-Tabbiruka, M., and Obuseng, V. "A Review of the Chemistry, Structure, Properties and Applications of Zeolites", *American Journal of Materials Science*, Vol. 7, No. 5, pp. 196–221, 2017.

17. Illingworth, J. M., Rand, B., and Williams, P. T., "Non-woven Fabric Activated Carbon Produced from Fibrous Waste Biomass for Sulphur Dioxide Control", *Process Safety and Environmental Protection*, Vol. 122, pp. 209–220, 2019.

18. Malik, P. K., "Use of Activated Carbons Prepared from Sawdust and Rice-husk for Adsorption of Acid Dyes: A Case Study of Acid Yellow 36", *Dyes and Pigments*, Vol. 56 No. 3, pp. 239–249, 2003.

19. Nasrullah, A., Saad, B., Bhat, A. H., Khan, A. S., Danish, M., Isa, M. H., and Naeem, A. (2019). "Mangosteen Peel Waste as a Sustainable Precursor for High Surface Area Mesoporous Activated Carbon: Characterization and Application for Methylene Blue Removal", *Journal of Cleaner Production*, Vol. 211, pp. 1190–1200, 2019.

20. Tan, I. A. W., Hameed, B. H., and Ahmad, A. L., "Equilibrium and Kinetic Studies on Basic Dye Adsorption by Oil Palm Fibre Activated Carbon", *Chemical Engineering Journal*, Vol. 127, pp. 111–119, 2007.

21. Gurrath, M., Kuretzky, T., Boehm, H. P., Okhlopkova, L. B., Lisitsyn, A. S., and Likholobov, V. A., "Palladium Catalysts on Activated Carbon Supports Influence of Reduction Temperature, Origin of the Support and Pre-treatments of the Carbon Surface", *Carbon*, Vol. 38, pp. 1241-1255, 2000.

22. Mohamed, A. R., Lee, K. T., Noor, N. M., and Zainudin, N. F., "Oil Palm Ash/$Ca(OH)_2$/$CaSO_4$ Absorbent for Flue Gas Desulfurization", *Chemical Engineering and Technology*, Vol. 28, No. 8, pp. 939–945, 2005.

23. Wong, S., Ngadi, N., Inuwa, I. M., and Hassan, O., "Recent Advances in Applications of Activated Carbon from Biowaste for Wastewater Treatment: A Short Review", *Journal of Cleaner Production*, Vol. 175, pp. 361–375, 2018.

24. Baby R., Saifullah B., and Hussein M. Z., "Carbon Nanomaterials for the Treatment of Heavy Metal-Contaminated Water and Environmental Remediation", *Nanoscale Research Letters*, Vol. 14, No. 341, pp. 1-17, 2019.

25. Hoskins, B.F., and Robson, R. "Infinite Polymeric Frameworks Consisting of Three Dimensionally Linked Rod-like Segments", *Journal of the American Chemical Society,* Vol. 111, pp. 5962-5964, 1989.

26. Hoskins, B. F., and Robson, R., "Design and Construction of a New Class of Scaffolding-like Materials Comprising Infinite Polymeric Frameworks of 3D-Linked Molecular Rods. A Reappraisal of the $Zn(CN)_2$ and $Cd(CN)_2$ Structures and the Synthesis and Structure of the Diamond-Related Frameworks $[N(CH_3)_4][Cu^{I}Zn^{II}(CN)_4]$ and Cu^{I}[4,4',4″,4‴-tetracyanotetraphenylmethane]$BF_4 \cdot xC_6H_5NO_2$", *Journal of the American Chemical Society*, Vol. 112, No. 4, pp. 1546–1554, 1990.

27. Yaghi, O., Li, G., and Li, H., "Selective Binding and Removal of Guests in a Microporous Metal–Organic Framework", *Nature*, Vo., 378, pp. 703–706, 1995.

28. Kuppler, R. J., Timmons, D. J., Fang, Q. R., Li, J. R., Makal, T. A., Young, M. D., Yuan, D., Zhao, D., Zhuang, W., and Zhou, H. C., "Potential Applications of Metal-Organic Frameworks", *Coordination Chemistry Reviews*, Vol. 253, Issues 23–24, pp. 3042–3066, 2009.

29. Millward, A. R., and Yaghi, O. M., "Metal-Organic Frameworks with Exceptionally High Capacity for Storage of Carbon Dioxide at Room Temperature", *Journal of the American Chemical Society*, Vol. 127, No. 51, pp. 17998–17999, 2005.

30. Jeremias, F. *Synthesis and Characterization of Metal-Organic Frameworks for Heat Transformation Applications*. PhD. Heinreich Heine University Düsseldorf. 2015.

31. Janiak, C., and Vieth, J. K., "MOFs, MILs and more: Concepts, Properties, and Applications for Porous Coordination Networks (PCNs)", *New Journal of Chemistry*, Vol. 34, Issue 11, pp. 2366–2388, 2012.

32. Millange, F., Serre, C., and Férey, G., "Synthesis, Structure Determination and Properties of MIL-53 as and MIL-53ht: the First Cr^{III} Hybrid Inorganic–Organic Microporous Solids: $Cr^{III}(OH)\cdot\{O_2C–C_6H_4–CO_2\}\cdot\{HO_2C–C_6H_4–CO_2H\}x$", *Chemical Communications*, Vol. 2, No. 8, pp. 822–823, 2002.

33. Dinh Du, P., and Ngoc Hoai, P., "Synthesis of MIL-53(Fe) Metal-Organic Framework Material and Its Application as a Catalyst for Fenton-Type Oxidation of Organic Pollutants", *Advances in Materials Science and Engineering*, Vol. 2021, 5540344, 2021.

34. Naeimi, S., and Faghihian, H., "Application of Novel Metal Organic Framework, MIL-53(Fe) and Its Magnetic Hybrid: For Removal of Pollutant, Doxycycline from Aqueous Solutions", *Environmental Toxicology and Pharmacology*, Vol. 53, pp. 121–132, 2017.

35. Ahadi, N., Askari, S., Fouladitajar, A., and Akbari, I., "Facile Synthesis of Hierarchically Structured MIL-53(Al) with Superior Properties Using an Environmentally Friendly Ultrasonic Method for Separating Lead Ions from Aqueous Solutions", *Scientific Reports*, Vol. 12, Issue 2649, pp. 1-17, 2022.

36. Barthelet, K., Adil, K., Millange, F., Serre, C., Riou, D., and Férey, G., "Synthesis, Structure Determination and Magnetic Behaviour of the First Porous Hybrid Oxyfluorinated Vanado(III)carboxylate: MIL-71 or $V^{III}_2(OH_2F_2(O_2C\text{-}C\ 6H_4\text{-}CO_2)\cdot H_2O$", *Journal of Materials Chemistry*, Vol. 13, No. 9, pp. 2208–2212, 2003.

37. Guillou, N., Livage, C., van Beek, W., Noguõs, M., Fÿrey, G., and van Beek, W. (2003). "A Layered Nickel Succinate with Unprecedented Hexanickel Units: Structure Elucidation from Powder-Diffraction Data, and Magnetic and Sorption Properties", *Angewandte Chemie International Edition,* Vol. 42, Issue 6, pp. 643-646, 2003.

38. Férey, G., “Hybrid Porous Solids: Past, Present, Future”, *Chemical Society Reviews*, Vol. 37, No. 1, pp. 191–214, 2008.

39. Batten, S. R., Champness, N. R., Chen, X. M., Garcia-Martinez, J., Kitagawa, S., Öhrström, L., O’Keeffe, M., Suh, M. P., and Reedijk, J. (2012). “Coordination Polymers, Metal-Organic Frameworks and the Need for Terminology Guidelines”, *Crystal Engineering Community*, Vol. 14, No. 9, pp. 3001–3004, 2012.

40. Bedia, J., Muelas-Ramos, V., Peñas-Garzón, M., Gómez-Avilés, A., Rodríguez, J. J., and Belver, C., “A Review on the Synthesis and Characterization of Metal Organic Frameworks for Photocatalytic Water Purification”, *Catalysts*, Vol. 9, Issue 1, pp. 1-43, 2019.

41. Safaei, M., Foroughi, M. M., Ebrahimpoor, N., Jahani, S., Omidi, A., and Khatami, M., “A Review on Metal-Organic Frameworks: Synthesis and Applications”, *Trends in Analytical Chemistry,* Vol. 118, pp. 401–425, 2019.

42. Maina, J. W., Gonzalo, C. P., Merenda, A., Kong, L., Schütz, J. A., and Dumée, L. F., “The Growth of High-Density Network of MOF Nano-Crystals Across Macroporous Metal Substrates – Solvothermal Synthesis Versus Rapid Thermal Deposition”, *Applied Surface Science*, Vol. 427, pp. 401–408, 2018.

43. Farha, O. K., and Hupp, J. T., “Rational Design, Synthesis, Purification, and Activation of Metal-Organic Framework Materials”, *Accounts of Chemical Research*, Vol. 43, No. 8, pp. 1166–1175, 2010.

44. Liu, C., Wang, J., Wan, J., and Yu, C., “MOF-on-MOF Hybrids: Synthesis and Applications”, *Coordination Chemistry Reviews*, Vol. 432, 213743, 2021.

45. Lee, Y. R., Kim, J., and Ahn, W. S., “Synthesis of Metal-Organic Frameworks: A Mini Review”, *Korean Journal of Chemical Engineering,* Vol. 30, No. 9, pp. 1667–1680, 2013.

46. Remya, V. R., and Kurian, M., “Synthesis and Catalytic Applications of Metal–Organic Frameworks: A Review on Recent Literature”, *International Nano Letters,* Vol. 9, No. 1, pp. 17–29, 2018.

47. Mueller U., Puetter H., Hesse M., Schubert M., Huff J., and Guzmann M., “Method for Electrochemical Production of a Crystalline Porous Metal, Organic Skeleton Material”, Patent no. US7968739B2, 2005.

48. Martinez Joaristi, A., Juan-Alcañiz, J., Serra-Crespo, P., Kapteijn, F., and Gascon, J., “Electrochemical Synthesis of Some Archetypical Zn^{2+}, Cu^{2+}, and Al^{3+} Metal Organic Frameworks”, *Crystal Growth and Design*, Vol. 12, No. 7, pp. 3489–3498, 2012.

49. Aniruddha, R., Sreedhar, I., and Reddy, B. M., “MOFs in Carbon Capture-Past, Present and Future”, *Journal of CO2 Utilization*, Vol. 42, 101297, 2020.

50. Beldon, P. J., Fábián, L., Stein, R. S., Thirumurugan, A., Cheetham, A. K., and Friščić, T., “Rapid Room-Temperature Synthesis of Zeolitic Imidazolate Frameworks by Using Mechanochemistry”, *Angewandte Chemie - International Edition*, Vol. 49, No. 50, pp. 9640–9643, 2010.

51. Pichon, A., Lazuen-Garay, A., and James, S. L., “Solvent-Free Synthesis of A Microporous Metal-Organic Framework”, *Crystal Engineering Community*, Vol. 8 No. 3, pp. 211–214, 2006.

52. Yang, H., Orefuwa, S., and Goudy, A., “Study of Mechanochemical Synthesis in the Formation of the Metal-Organic Framework $Cu_3(BTC)_2$ for Hydrogen Storage”, *Microporous and Mesoporous Materials*, Vol. 143, No. 1, pp. 37–45, 2011.

53. Chen, Y., Ni, D., Yang, X., Liu, C., Yin, J., and Cai, K., “Microwave-Assisted Synthesis of Honeycomblike Hierarchical Spherical Zn-doped Ni-MOF as a High-Performance Battery-type Supercapacitor Electrode Material”, *Electrochimica Acta*, Vol. 278, pp. 114–123, 2018.

54. Lidström, P., Tierney J., Wathey B., and Westman J., "Microwave Assisted Organic Synthesis – A Review", *Tetrahedron,* Vol. 57, pp. 9225-9283, 2001.

55. Jhung S. H., Lee J.H., and Chang J. S., "Microwave Synthesis of a Nanoporous Hybrid Material, Chromium Trimesate", *Bulletin of the Korean Chemical Society,* Vol. 26, No. 6, pp. 880-881, 2005.

56. Choi, J. S., Son, W. J., Kim, J., and Ahn, W. S., "Metal-Organic Framework MOF-5 Prepared by Microwave Heating: Factors to Be Considered", *Microporous and Mesoporous Materials*, Vol. 116, Issues 1–3, pp. 727–731, 2008.

57. Gedanken, A., "Using Sonochemistry for the Fabrication of Nanomaterials", *Ultrasonics Sonochemistry,* Vol. 11, Issue 2, pp. 47–55, 2004.

58. Suslick K. S., Choe S. B., Cichowlas A. A., and Grinstaff M. W., "Sonochemical Synthesis of Amorphous Iron", *Nature,* Vol. 353, pp. 414-416, 1991.

59. Bang, J. H., and Suslick, K. S., "Applications of Ultrasound to the Synthesis of Nanostructured Materials", *Advanced Materials,* Vol. 22, pp. 1309-1059, 2010.

60. Safarifard, V., and Morsali, A., "Applications of Ultrasound to the Synthesis of Nanoscale Metal-Organic Coordination Polymers" *Coordination Chemistry Reviews,* Vol. 292, pp. 1–14, 2015.

61. Haque, E., and Jhung, S. H., "Synthesis of Isostructural Metal-Organic Frameworks, CPO-27s, with Ultrasound, Microwave, and Conventional Heating: Effect of Synthesis Methods and Metal ions", *Chemical Engineering Journal*, Vol. 173, No. 3, pp. 866–872, 2011.

62. Kumari, B., Tiwari, B. K., Hossain, M. B., Brunton, N. P., and Rai, D. K., "Recent Advances on Application of Ultrasound and Pulsed Electric Field Technologies in the Extraction of Bioactives from Agro-Industrial By-product", *Food and Bioprocess Technology*, Vol. 11, No. 2, pp. 223–241, 2018.

63. Li, Z. Q., Qiu, L. G., Xu, T., Wu, Y., Wang, W., Wu, Z. Y., and Jiang, X. "Ultrasonic Synthesis of the Microporous Metal-Organic Framework Cu3(BTC)2 at Ambient Temperature and Pressure: An Efficient and Environmentally Friendly Method", *Materials Letters*, Vol. 63, No. 1, pp. 78–80, 2009.

64. Son, W. J., Kim, J., Kim, J., and Ahn, W. S., "Sonochemical Synthesis of MOF-5", *Chemical Communications*, Vol. 47, pp. 6336–6338, 2008.

65. Chalati, T., Horcajada, P., Gref, R., Couvreur, P., and Serre, C., "Optimisation of the Synthesis of MOF Nanoparticles Made of Flexible Porous Iron Fumarate MIL-88A" *Journal of Materials Chemistry*, Vol. 21, No. 7, pp. 2220–2227, 2011.

66. Seetharaj, R., Vandana, P. v., Arya, P., and Mathew, S., "Dependence of Solvents, pH, Molar Ratio and Temperature in Tuning Metal Organic Framework Architecture", *Arabian Journal of Chemistry*, Vol. 12, No. 3, pp. 295–315, 2019.

67. Soni S., Bajpai P. K., and Arora C., "A Review on Metal-Organic Framework: Synthesis, Properties and Application", *Characterization and Application of Nanomaterials*, Vol. 2, No. 2, pp. 1-20, 2018.

68. Cheng, M., Lai, C., Liu, Y., Zeng, G., Huang, D., Zhang, C., Qin, L., Hu, L., Zhou, C., and Xiong, W., "Metal-Organic Frameworks for Highly Efficient Heterogeneous Fenton-like Catalysis", *Coordination Chemistry Reviews,* Vol. 368, pp. 80–92, 2018.

69. Huang, W. H., Yang, G. P., Chen, J., Chen, X., Zhang, C. P., Wang, Y. Y., and Shi, Q. Z., "Solvent Influence on Sizes of Channels in Three New Co(II) Complexes, Exhibiting an Active Replaceable Coordinated Site", *Crystal Growth and Design*, Vol. 13, No. 1, pp. 66–73, 2013.

70. Luo, L., Lv, G. C., Wang, P., Liu, Q., Chen, K., and Sun, W. Y., "pH-Dependent Cobalt(II) Frameworks with Mixed 3,3′,5,5′- tetra(1H-imidazol-1-yl)-1,1′-biphenyl and 1,3,5-benzenetricarboxylate Ligands: Synthesis, Structure and Sorption Property", *Crystal Engineering Community*, Vol. 15, No. 45, pp. 9537–9543, 2013.

71. Chen, W. X., Wu, S. T., Long, L. S., Huang, R. bin, and Zheng, L. S., "Construction of a Three-fold Parallel Interpenetration Network and Bilayer Structure Based on Copper(II) and Trimesic acid", *Crystal Growth and Design*, Vol. 7, No. 6, pp. 1171–1175, 2007.

72. Wang, H. N., Yang, G. S., Wang, X. L., and Su, Z. M. "pH-Induced Different Crystalline Behaviors in Extended Metal-Organic Frameworks Based on the Same Reactants", *Dalton Transactions*, Vol. 42, No. 18, pp. 6294–6297, 2013.

73. Forster, P. M., Burbank, A. R., Livage, C., Férey, G., and Cheetham, A. K., "The Role of Temperature in the Synthesis of Hybrid Inorganic–Organic Materials: The Example of Cobalt Succinates" *Chemical Communications*, Vol. 4, No. 4, pp. 368–369, 2004.

74. Deng, L., Qu, H., Zhang, Y., Jiao, S., Zhang, X., Liu, K., Zhang, Z., Wang, L., Feng, S., Deng, L., Qu, H., Zhang, Y., Jiao, S., Zhang, X., Liu, K., Zhang, Z., Wang, L., and Feng, S., "Temperature Effect on the Synthesis of Two Ni-MOFs with Distinct Performance in Supercapacitor", *Journal of Solid-State Chemistry,* Vol. 281, 121026, 2020.

75. Langmi, H. W., Ren, J., North, B., Mathe, M., and Bessarabov, D., "Hydrogen Storage in Metal-Organic Frameworks: A Review", *Electrochimica Acta*, Vol. 128, pp. 368–392, 2014.

76. Rosi, N. L., Eckert, J., Eddaoudi, M., Vodak, D. T., Kim, J., O'Keeffe, M., and Yaghi, O. M., "Hydrogen Storage in Microporous Metal-Organic Frameworks" *Science (New York.)*, Vol. 300, Issue 5622, pp. 1127–1129, 2003.

77. Furukawa, H., Ko, N., Go, Y. B., Aratani, N., Choi, S. B., Choi, E., Yazaydin, A. Ö., Snurr, R. Q., O'Keeffe, M., Kim, J., and Yaghi, O. M., "Ultrahigh Porosity in Metal-Organic Frameworks", *Science*, Vol. 329, Issue 5990, pp. 424–428, 2012.

78. He, Y., Zhou, W., Qian, G., and Chen, B., "Methane Storage in Metal-Organic Frameworks", *Chemical Society Reviews*, Vol. 43, No. 16, pp. 5657–5678, 2014.

79. Arnold, L., Averlant, G., Marx, S., Weickert, M., Müller, U., Mertel, J., Horch, C., Peksa, M., and Stallmach, F., "Metal Organic Frameworks for Natural Gas Storage in Vehicles", *Chemie-Ingenieur-Technik*, Vol. 85, No. 11, pp. 1726–1733, 2013.

80. Kondo M., Yoshitomi T., Seki K., Matsuzaka H., and Kitagawa S., "Three-Dimensional Framework with Channeling Cavities for Small Molecules: {[M_2(4,4'-bpy)$_3$(NO_3)$_4$].xH_2O}n (M = Co, Ni, Zn)", *Angewandte Chemistry International Edition,* Vol. 36, No. 16, pp. 1725-1727, 1997.

81. Guo, Z., Wu, H., Srinivas, G., Zhou, Y., Xiang, S., Chen, Z., Yang, Y., Zhou, W., O'Keeffe, M., and Chen, B., "A Metal-Organic Framework with Optimized Open Metal Sites and Pore Spaces for High Methane Storage at Room Temperature", *Angewandte Chemie - International Edition*, Vol. 54, No. 14, pp. 3178–3181, 2011.

82. Diederich F., Stang P. J., and Tykwinski R. R. (2005). Chapter 1 – Theoretical Studies on Acetylenic Scaffolds. Editors François Diederich, Peter J. Stang, and Rik R. Tykwinski. *Acetylene Chemistry: Chemistry, Biology and Material Science*. Wiley, 1-50.

83. Matsuda, R., Kitaura, R., Kitagawa, S., Kubota, Y., Belosludov, R. v., Kobayashi, T. C., Sakamoto, H., Chiba, T., Takata, M., Kawazoe, Y., and Mita, Y., "Highly Controlled Acetylene Accommodation in a Metal–Organic Microporous Material", *Nature*, Vol. 436, Issue 7048, pp. 238–241, 2005.

84. Xiang, S., Zhou, W., Gallegos, J. M., Liu, Y., and Chen, B., "Exceptionally High Acetylene Uptake in a Microporous Metal-Organic Framework with Open Metal Sites", *Journal of the American Chemical Society*, Vol. 131, No. 34, pp. 12415–12419, 2009.

85. Sumida, K., Rogow, D. L., Mason, J. A., Mcdonald, T. M., Bloch, E. D., Herm, Z. R., Bae, T.-H., and Long, J. R., "Carbon Dioxide Capture in Metal-Organic Frameworks", *Chemical Rev*iews, Vol. 112, pp. 724–781, 2012.

86. Millward, A. R., and Yaghi, O. M., "Metal-Organic Frameworks with Exceptionally High Capacity for Storage of Carbon Dioxide at Room Temperature", *Journal of the American Society*, Vol. 127, pp. 17998–17999, 2005.

87. Kim, H. R., Yoon, T. U., Kim, S. I., An, J., Bae, Y. S., and Lee, C. Y., " Beyond Pristine MOFs: Carbon Dioxide Capture by Metal-Organic Frameworks (MOFs)-Derived Porous Carbon Materials", *RSC Advances*, Vol. 7, No. 3, pp. 1266–1270, 2017.

88. Jiao, L., Wang, Y., Jiang, H. L., and Xu, Q., "Metal–Organic Frameworks as Platforms for Catalytic Applications", *Advanced Materials*, Vol. 30, Issue 37, 2018.

89. Dhakshinamoorthy, A., Asiri, A. M., and Garcia, H., "Metal-Organic Frameworks Catalyzed C-C and C-heteroatom Coupling Reactions." *Chemical Society Reviews,* Vol. 44, Issue 7, pp. 1922–1947, 2015.

90. Fujita, M., Jung Kwon, Y., Washizu, S., and Ogura, K., "Preparation, Clathration Ability, and Catalysis of a Two-Dimensional Square Network Material Composed of Cadmium(II) and 4,4'-Bipyridine", *Journal of the American Chemical Society*, Vol. 116, pp. 1151-1152, 1994.

91. Liang, R., Jing, F., Shen, L., Qin, N., and Wu, L., "MIL-53(Fe) as a Highly Efficient Bifunctional Photocatalyst for the Simultaneous Reduction of Cr(VI) and Oxidation of Dyes", *Journal of Hazardous Materials*, Vol. 287, pp. 364–372, 2015.

92. Lu, Y., Tonigold, M., Bredenkötter, B., Volkmer, D., Hitzbleck, J., and Langstein, G., "A Cobalt(II)-Containing Metal-Organic Framework Showing Catalytic Activity in Oxidation reactions", *Zeitschrift Fur Anorganische Und Allgemeine Chemie*, Vol. 634, pp. 2411–2417, 2008.

93. Zheng, S., Li, X., Yan, B., Hu, Q., Xu, Y., Xiao, X., Xue, H., and Pang, H., "Transition-Metal (Fe, Co, Ni) Based Metal-Organic Frameworks for Electrochemical Energy Storage", *Advanced Energy Materials*, Vol. 7, Issue 18, pp. 1-27, 2017.

94. Mehtab, T., Yasin, G., Arif, M., Shakeel, M., Korai, R. M., Nadeem, M., Muhammad, N., and Lu, X., "Metal-organic Frameworks for Energy Storage Devices: Batteries and Supercapacitors", *Journal of Energy Storage*, Vol. 21, pp. 632–646, 2019.

95. Wang, L., Han, Y., Feng, X., Zhou, J., Qi, P., and Wang, B., "Metal-Organic Frameworks for Energy Storage: Batteries and Supercapacitors", *Coordination Chemistry Reviews*, Vol. 307, pp. 361–381, 2016.

96. Simon, P., and Gogotsi, Y., "Materials for Electrochemical Capacitors", *Nature Materials,* Vol. 7, No. 11, pp. 845–854, 2008.

97. Lee, D. Y., Yoon, S. J., Shrestha, N. K., Lee, S. H., Ahn, H., and Han, S. H., "Unusual Energy Storage and Charge Retention in Co-based Metal-Organic-Frameworks" *Microporous and Mesoporous Materials*, Vol. 153, pp. 163–165, 2012.

98. Meng, W., Chen, W., Zhao, L., Huang, Y., Zhu, M., Huang, Y., Fu, Y., Geng, F., Yu, J., Chen, X., and Zhi, C., "Porous Fe_3O_4/carbon Composite Electrode Material Prepared from Metal-Organic Framework Template and Effect of Temperature on its Capacitance", *Nano Energy*, Vol. 8, pp. 133–140, 2014.

99. Zhao, Y., Song, Z., Li, X., Sun, Q., Cheng, N., Lawes, S., and Sun, X., "Metal Organic Frameworks for Energy Storage and Conversion" *Energy Storage Materials*, Vol. 2, pp. 35–62, 2016.

100. Férey, G., Millange, F., Morcrette, M., Serre, C., Doublet, M. L., Grenèche, J. M., and Tarascon, J. M., "Mixed-Valence Li/Fe-based Metal-Organic Frameworks with Both Reversible Redox and Sorption Properties", *Angewandte Chemie - International Edition*, Vol. 46, No. 18, pp. 3259–3263, 2007.

101. An, T., Wang, Y., Tang, J., Wang, Y., Zhang, L., and Zheng, G., "A Flexible Ligand-Based Wavy Layered Metal-Organic Framework for Lithium-ion Storage", *Journal of Colloid and Interface Science*, Vol. 445, pp. 320–325, 2015.

102. Hu, X., Hu, H., Li, C., Li, T., Lou, X., Chen, Q., and Hu, B., "Cobalt-based Organic Framework with Superior Lithium Anodic Performance", *Journal of Solid-State Chemistry*, Vol. 242, pp. 71–76, 2016.

103. Liu, J., Zhang, L., Li, H., Zhao, P., Ren, P., Shi, W., and Cheng, P., "Facile Construction of Two-dimensional Coordination Polymers with a Well-designed Redox-active Organic Linker for Improved Lithium-ion Battery Performance", *Science China Chemistry*, Vol. 62, No. 5, pp. 602–608, 2019.

104. Abbasi, A., Tarighi, S., and Badiei, A., "A Three-dimensional Highly Stable Cobalt(II) Metal-Organic Framework Based on Terephthalic Acid: Synthesis, Crystal Structure, Thermal and Physical Properties", *Transition Metal Chemistry*, Vol. 37, No. 7, pp. 679–685, 2012.

105. Taylan, E. (2017). Chapter 13 – Addition Reactions of Alkenes 1- Geometric Isomerization of Maleic Acid. Editor Ediz Taylan. *Experimental Organic Chemistry*. Boğaziçi University Printing House. 85-87.

106. Zhang Y., Yin X., Jiang H., Hao J., Wang J., Yu J., Li D., Liu Y., and Li J., "Cobalt Nanoparticles Embedded in Nitrogen-Doped Carbon Nanotubes for Efficient Catalysis of Oxygen Reduction Reaction", *Journal of Iranian Chemical Society*, Vol. 16, pp. 2575-2585, 2019.

107. Ionashiro, E. Y., Caires, F. J., Siqueira, A. B., Lima, L. S., and Carvalho, C. T., "Thermal Behaviour of Fumaric Acid, Sodium Fumarate and Its Compounds with Light Trivalent Lanthanides in Air Atmosphere", *Journal of Thermal Analysis and Calorimetry*, Vol. 108, No. 3, pp. 1183–1188, 2012.

108. Nájera, J. J., Percival, C. J., and Horn, A. B., "Infrared Spectroscopic Studies of the Heterogeneous Reaction of Ozone with Dry Maleic and Fumaric Acid Aerosol Particles", *Physical Chemistry Chemical Physics*, Vol. 11, No. 40, pp. 9093–9103, 2009.

109. Larkin, P.J. (2011). Chapter 6 – IR and Raman Spectra-Structure Correlations: Characteristic Group Frequencies. Editor Peter J. Larkin. *Infrared and Raman Spectroscopy*. Elsevier, 73-115.

110. Wang l., Zhang Y., Li X., Xie Y., He J., Yu J., and Song Y., "The MIL-88A-Derived Fe_2O_3-Carbon Hierarchical Nanocomposites for Electrochemical Sensing", *Scientific Reports,* Vol 5., Issue 14341, pp. 1-12, 2015.

111. Predescu A. M., Matei E., Berbecaru A. C., Pantilimon C., Dragan C., Vidu R., Predescu C., and Kuncser V., "Synthesis and Characterization of Dextran-Coated Iron Oxide Nanoparticles", *Royal Society Open Science*, Vol. 5, 171525, 2018.

112. Horcajada P., Salles F., Wuttke S., Devic T., Heurtaux D., Maurin G., Vimont A., Daturi M., David O., Magnier E., Stock N., Filinchuk Y., Popov D., Reikel C., Ferey G., and Serre C., "How Linker's Modification Controls Swelling Properties of Highly Flexible Iron (III) Dicarboxylates MIL-88", *Journal of the American Chemical Society*, Vol. 133, pp. 17839-17847, 2011.

113. Wang M., Ma J., Chen C., Zheng X., Du Z., and Xu J., "Preparation of Self-Assembled Cobalt Hydroxide Nanoflowers and the Catalytic Decomposition of Cyclohexyl Hydroperoxide", *Journal of Materials Chemistry*, Vol. 21, pp. 12609-12612, 2011.

114. Mohammadyani D., Hosseini S.A., and Sadrnezhaad S.K., "Characterization of Nickel Oxide Nanoparticles Synthesized via Rapid Microwave-Assisted Route", *International Journal of Modern Physics: Conference Series*, Vol. 5, pp. 270-276, 2012.

APPENDIX A: COPYRIGHT NOTICES

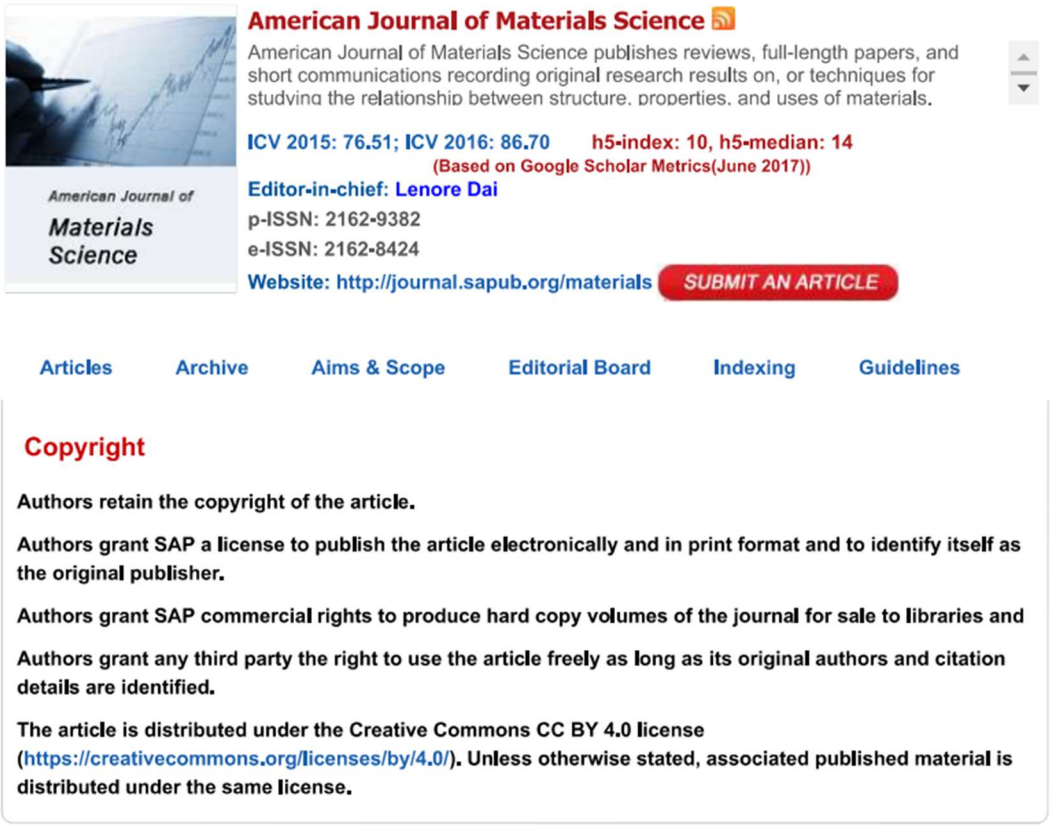

Figure A.1. Copyright notice for Figure 1.1.

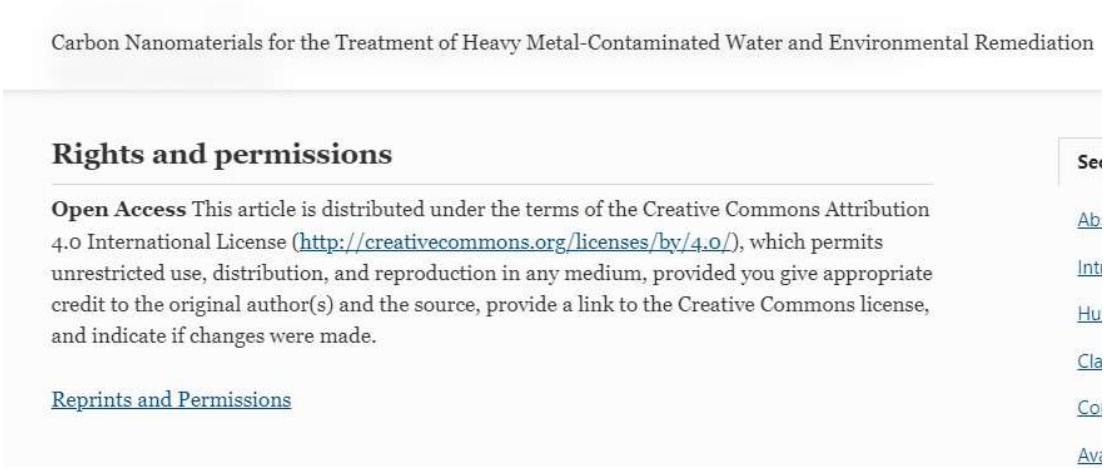

Figure A.2. Copyright notice for Figure 1.2.

CCC Marketplace™

This is a License Agreement between Çağla Galın ("User") and Copyright Clearance Center, Inc. ("CCC") on behalf of the Rightsholder identified in the order details below. The license consists of the order details, the Marketplace Order General Terms and Conditions below, and any Rightsholder Terms and Conditions which are included below.

All payments must be made in full to CCC in accordance with the Marketplace Order General Terms and Conditions below.

Order Date	13-Aug-2022	Type of Use	Republish in a thesis/dissertation
Order License ID	1257610-1		
ISSN	1369-9261	Publisher	ROYAL SOCIETY OF CHEMISTRY
		Portion	Chart/graph/table/figure

LICENSED CONTENT

Publication Title	New journal of chemistry	Rightsholder	Royal Society of Chemistry
Article Title	MOFs, MILs and more: concepts, properties and applications for porous coordination networks (PCNs)This article is part of a themed issue on Coordination polymers: structure and function.	Publication Type	e-Journal
		Start Page	2366
		Issue	11
		Volume	34
		URL	http://www.rsc.org/njc
Author/Editor	Royal Society of Chemistry (Great Britain), Centre national de la recherche scientifique (France)		
Date	01/01/1987		
Language	English		
Country	United Kingdom of Great Britain and Northern Ireland		

REQUEST DETAILS

Portion Type	Chart/graph/table/figure	Distribution	Worldwide
Number of charts / graphs / tables / figures requested	1	Translation	Original language of publication
		Copies for the disabled?	No
Format (select all that apply)	Print, Electronic	Minor editing privileges?	No
Who will republish the content?	Academic institution	Incidental promotional use?	No
		Currency	USD
Duration of Use	Life of current edition		
Lifetime Unit Quantity	Up to 499		
Rights Requested	Main product		

NEW WORK DETAILS

Title	Synthesis and Characterization of Fe (Iron), Co (Cobalt), and Ni (Nickel) Containing Metal Organic Frameworks	Institution name	Boğaziçi University
		Expected presentation date	2022-08-19

Figure A.3. Copyright notice for Figure 1.4.

CCC Marketplace™

This is a License Agreement between Çağla Galın ("User") and Copyright Clearance Center, Inc. ("CCC") on behalf of the Rightsholder identified in the order details below. The license consists of the order details, the Marketplace Order General Terms and Conditions below, and any Rightsholder Terms and Conditions which are included below.

All payments must be made in full to CCC in accordance with the Marketplace Order General Terms and Conditions below.

Order Date	13-Aug-2022	Type of Use	Republish in a thesis/dissertation
Order License ID	1257611-1	Publisher	ROYAL SOCIETY OF CHEMISTRY
ISSN	1460-4744	Portion	Chart/graph/table/figure

LICENSED CONTENT

Publication Title	Chemical Society reviews	Publication Type	e-Journal
Article Title	Hybrid porous solids: past, present, future.	Start Page	191
		End Page	214
Author/Editor	Royal Society of Chemistry (Great Britain)	Issue	1
		Volume	37
Date	01/01/1972	URL	http://www.rsc.org/csr
Language	English		
Country	United Kingdom of Great Britain and Northern Ireland		
Rightsholder	Royal Society of Chemistry		

REQUEST DETAILS

Portion Type	Chart/graph/table/figure	Distribution	Worldwide
Number of charts / graphs / tables / figures requested	1	Translation	Original language of publication
		Copies for the disabled?	No
Format (select all that apply)	Print, Electronic	Minor editing privileges?	No
Who will republish the content?	Academic institution	Incidental promotional use?	No
		Currency	USD
Duration of Use	Life of current edition		
Lifetime Unit Quantity	Up to 499		
Rights Requested	Main product		

NEW WORK DETAILS

Title	Synthesis and Characterization of Fe (Iron), Co (Cobalt), and Ni (Nickel) Containing Metal Organic Frameworks	Institution name	Boğaziçi University
		Expected presentation date	2022-08-19
Instructor name	Assoc. Prof. Oktay Demircan		

Figure A.4. Copyright notice for Figure 1.5.

SPRINGER NATURE LICENSE
TERMS AND CONDITIONS

Aug 12, 2022

This Agreement between Çağla Galın ("You") and Springer Nature ("Springer Nature") consists of your license details and the terms and conditions provided by Springer Nature and Copyright Clearance Center.

License Number	5366680899205
License date	Aug 12, 2022
Licensed Content Publisher	Springer Nature
Licensed Content Publication	Korean Journal of Chemical Engineering
Licensed Content Title	Synthesis of metal-organic frameworks: A mini review
Licensed Content Author	Yu-Ri Lee et al
Licensed Content Date	Aug 17, 2013
Type of Use	Thesis/Dissertation
Requestor type	non-commercial (non-profit)
Format	print and electronic
Portion	figures/tables/illustrations
Number of figures/tables/illustrations	5
Will you be translating?	no

Figure A.5. Copyright notice for Figure 1.7., Figure 1.8., Figure 1.9., Figure 1.10., and Figure 1.12.

SPRINGER NATURE LICENSE
TERMS AND CONDITIONS

Aug 12, 2022

This Agreement between Çağla Galın ("You") and Springer Nature ("Springer Nature") consists of your license details and the terms and conditions provided by Springer Nature and Copyright Clearance Center.

License Number	5366691264627
License date	Aug 12, 2022
Licensed Content Publisher	Springer Nature
Licensed Content Publication	Food and Bioprocess Technology
Licensed Content Title	Recent Advances on Application of Ultrasound and Pulsed Electric Field Technologies in the Extraction of Bioactives from Agro-Industrial By-products
Licensed Content Author	Bibha Kumari et al
Licensed Content Date	Jul 22, 2017
Type of Use	Thesis/Dissertation
Requestor type	non-commercial (non-profit)
Format	print and electronic
Portion	figures/tables/illustrations
Number of figures/tables/illustrations	1
Will you be translating?	no

Figure A.6. Copyright notice for Figure 1.11.

ELSEVIER LICENSE
TERMS AND CONDITIONS

Aug 12, 2022

This Agreement between Çağla Galın ("You") and Elsevier ("Elsevier") consists of your license details and the terms and conditions provided by Elsevier and Copyright Clearance Center.

License Number	5366691427459
License date	Aug 12, 2022
Licensed Content Publisher	Elsevier
Licensed Content Publication	Coordination Chemistry Reviews
Licensed Content Title	Metal–organic frameworks for energy storage: Batteries and supercapacitors
Licensed Content Author	Lu Wang,Yuzhen Han,Xiao Feng,Junwen Zhou,Pengfei Qi,Bo Wang
Licensed Content Date	Jan 15, 2016
Licensed Content Volume	307
Licensed Content Issue	n/a
Licensed Content Pages	21
Start Page	361
End Page	381
Type of Use	reuse in a thesis/dissertation

Figure A.7. Copyright notice for Figure 1.13.